


2016

Deposition and characterization studies of boron carbon nitride (BCN) thin films prepared by dual target sputtering

Adithya Prakash
University of Central Florida

 Part of the [Electrical and Computer Engineering Commons](#)
Find similar works at: <https://stars.library.ucf.edu/etd>
University of Central Florida Libraries <http://library.ucf.edu>

This Doctoral Dissertation (Open Access) is brought to you for free and open access by STARS. It has been accepted for inclusion in Electronic Theses and Dissertations, 2004-2019 by an authorized administrator of STARS. For more information, please contact STARS@ucf.edu.

STARS Citation

Prakash, Adithya, "Deposition and characterization studies of boron carbon nitride (BCN) thin films prepared by dual target sputtering" (2016). *Electronic Theses and Dissertations, 2004-2019*. 5088.
<https://stars.library.ucf.edu/etd/5088>

**DEPOSITION AND CHARACTERIZATION STUDIES OF BORON
CARBON NITRIDE (BCN) FILMS PREPARED BY DUAL TARGET
SPUTTERING**

by

ADITHYA PRAKASH

B.E. Visvesvaraya Technological University, 2011
M.S.E.E University of Central Florida, 2013

A dissertation submitted in partial fulfillment of the requirements
for the degree of Doctor of Philosophy
in the Department of Electrical Engineering and Computer Science
in the College of Engineering and Computer Science
at the University of Central Florida
Orlando, Florida

Summer Term
2016

Major Professor: Kalpathy B Sundaram

© 2016 Adithya Prakash

ABSTRACT

As complementary metal-oxide semiconductor (CMOS) devices shrink to smaller size, the problems related to circuit performance such as critical path signal delay are becoming a pressing issue. These delays are a result of resistance and capacitance product (RC time constant) of the interconnect circuit. A novel material with reduced dielectric constants may compromise both the thermal and mechanical properties that can lead to die cracking during package and other reliability issues. Boron carbon nitride (BCN) compounds have been expected to combine the excellent properties of boron carbide (B_4C), boron nitride (BN) and carbon nitride (C_3N_4), with their properties adjustable, depending on composition and structure. BCN thin film is a good candidate for being hard, dense, pore-free, low-k dielectric with values in the range of 1.9 to 2.1. Excellent mechanical properties such as adhesion, high hardness and good wear resistance have been reported in the case of sputtered BCN thin films. Problems posed by high hardness materials such as diamonds in high cutting applications and the comparatively lower hardness of c-BN gave rise to the idea of a mixed phase that can overcome these problems with a minimum compromise in its properties. A hybrid between semi-metallic graphite and insulating h-BN may show adjusted semiconductor properties. BCN exhibits the potential to control optical bandgap (band gap engineering) by atomic composition, hence making it a good candidate for electronic and photonic devices. Due to tremendous bandgap engineering capability and refractive index variability in BCN thin film, it is feasible to develop filters and mirrors for use in ultra violet (UV) wavelength region. It is of prime importance to understand process integration challenges like deposition rates, curing, and etching, cleaning and polishing during characterization of low-k films. The sputtering

technique provides unique advantages over other techniques such as freedom to choose the substrate material and a uniform deposition over relatively large area. BCN films are prepared by dual target reactive magnetron sputtering from a B_4C and BN targets using DC and RF powers respectively. In this work, an investigation of mechanical, optical, chemical, surface and device characterizations is undertaken. These holistic and thorough studies, will provide the insight into the capability of BCN being a hard, chemically inert, low-k, wideband gap material, as a potential leader in semiconductor and optics industry.

To my family, friends and humanity

ACKNOWLEDGMENTS

I would like to thank my advisor, Dr. Kalpathy B Sundaram, for his continuous commitment to help and support me through my graduate career. His advice, technical and otherwise, has been valuable to my experience as a graduate student and as a person. I would also like to thank my committee members, Dr. Vikram J Kapoor, Dr. Jiann S Yuan, Dr. Yier Jin, and Dr. Louis Chow, for their support throughout my years at UCF.

My heartfelt gratitude goes out to all of my previous and present colleagues at the lab Giji Skaria, Victor Velez, Ashwin Kumar Saikumar, Ritika Oswal, and Shraddha Nehate. A special thanks to Prabhu Doss Mani, who was instrumental in helping me in various situations in the clean room and other technical difficulties with his experience in this domain. I would like to thank Shashank Saraf and Sweta Barkam for their continued support through research and career advises. A special thanks to Namita Varudkar, who has been a great and unconditional support throughout this journey. At last, I would like to thank my study buddies and great friends Shreyas Somashekara and Tushar Deshapande for their ever readiness to pull an all nighter during technical writing sessions.

I would like to thank my father Mr. H Prakash and my mother Mrs. Asha Prakash for their constant motivation and for boosting my confidence at every step and in every walks of my life. Also I would like to thank my sister Ms. Ananya Prakash for her love and support. And last but not the least, I would like to thank my grandparents, relatives and friends who stood by my side during ups and downs of my academic life here.

TABLE OF CONTENTS

LIST OF FIGURES	ix
LIST OF TABLES	xiii
LIST OF ACRONYMS/ABBREVIATIONS	xiv
CHAPTER 1: INTRODUCTION	1
1.1: Overview	7
CHAPTER 2: LITERATURE REVIEW	10
2.1: Boron Carbide	10
2.2: Boron Nitride	13
2.3: Boron carbon Nitride.....	16
2.4: Carbon nitride.....	20
CHAPTER 3: METHODOLOGY	23
3.1: Fabrication of MIM devices.....	25
3.1.1: Preparation of the base Al electrodes	25
3.1.2: Deposition of BCN thin films.....	26
3.2: Mechanical Characterization.....	28
3.3: Optical Characterization.....	28
3.3.1: UV-Visible Spectroscopy	28
3.4: Surface characterization	29

3.4.1: X-ray photoelectron spectroscopy (XPS).....	29
3.4.2: Secondary Ion Mass Spectroscopy (SIMS).....	31
3.4.3: Fourier Transmission Infrared Spectroscopy (FTIR)	32
3.4.4: X-ray diffraction spectroscopy (XRD).....	33
3.4.5: X-ray reflectivity (XRR)	34
3.4.6: Photoluminescence	35
3.5: Etching studies of BCN thin films	36
CHAPTER 4: RESULTS AND DISCUSSION.....	39
4.1: Mechanical Properties of BCN thin films	39
4.2: Deposition and XPS studies of dual sputtered BCN thin films	47
4.3: Feasibility of etching studies on BCN thin films	61
4.4: Study of Copper diffusion in RF magnetron sputtered BCN thin films	72
4.5: Optical studies of BCN thin films by co-sputtering of B ₄ C and BN targets.....	79
4.6: Photoluminescence studies on BCN thin films synthesized by RF magnetron sputtering ..	93
4.7: Boron carbon nitride based Metal-Insulator-Metal UV detectors for harsh environment applications.....	102
CONCLUSION.....	108
FUTURE WORK.....	112
LIST OF REFERENCES	113

LIST OF FIGURES

Figure 1.1: A CMOS device	1
Figure 1.2: A typical interconnect element. LG and LL refer to the line-to-line and line-to-ground contributions	2
Figure 1.3: Relationship between the dielectric constant and mechanical strength, as represented by modulus of a representative ILD material.	3
Figure 1.4: Schematic representation of current density through a dielectric as a function of the applied field.	5
Figure 1.5: A log-log plot of the dielectric breakdown field (or field strengths), as a function of dielectric constant of dielectric.	6
Figure 1.6: Ternary Triangle	9
Figure 2.1: Icosahedron shape of unit cell of boron carbide.....	11
Figure 2.2: β -BN sphalerite structure	16
Figure 2.3: h-BN hexagonal (graphite like)	16
Figure 2.4: Crystal structure of carbon nitride.....	21
Figure 3.1: Sputtering Process Cartoon	24
Figure 3.2: MIM structures (Al-BCN-Al) on a glass substrate	25
Figure 3.3: An XPS system setup.	30
Figure 3.4: An example of an FTIR spectrometer with attenuated total reflectance (ATR) attachment.	33
Figure 3.5: XRR specular reflectivity	34

Figure 4.1: FTIR spectra for BCN films sputter deposited at room temperature using C and BN targets and various N ₂ /Ar gas ratios.....	41
Figure 4.2: FTIR spectra for BCN films sputter deposited at room temperature using B ₄ C and BN targets and various N ₂ /Ar gas ratios.....	42
Figure 4.3: Nanoindentation Young's modulus as a function of indentation depth (h _c) for two BCN films sputter deposited using C and BN targets with and without N ₂ working gas.....	43
Figure 4.5: Nanoindentation Young's modulus and hardness as a function of N ₂ /(N ₂ +Ar) gas ratio for BCN films sputter deposited using B ₄ C and BN targets.	45
Figure 4.6: a) Deposition rate as a function of RF target power to BN target, 100W DC power to BC target and b) Deposition rate as a function of DC target power to B ₄ C target, 100W RF power to BN target.....	48
Figure 4.7: Deposition rate as a function of substrate deposition temperature at Ar = 20sccm and 200W power for both the targets.	49
Figure 4.8: Deposition rate as a function of various gas flow ratios at 20W DC	52
Figure 4.9: Deposition rate as a function of various gas flow ratios at 40W DC	54
Figure 4.10: XPS narrow scan of N1s for BCN thin films deposited at 20W DC and N ₂ /Ar = a) 0.25, b) 0.5, c) 0.75 d) 1; 40W DC and N ₂ /Ar = e) 0.25, f) 0.5, g) 0.75, h) 1.	56
Figure 4.11: XPS narrow scan of N1s for BCN thin films deposited at 20W DC and N ₂ /Ar = a) 0.25, b) 0.5, c) 0.75 d) 1; 40W DC and N ₂ /Ar = e) 0.25, f) 0.5, g) 0.75, h) 1.	58
Figure 4.12: XPS narrow scan of B1s for BCN thin films deposited at 20W DC and N ₂ /Ar = a) 0.25, b) 0.5, c) 0.75 d) 1; 40W DC and N ₂ /Ar = e) 0.25, f) 0.5, g) 0.75, h) 1.	60
Figure 4.13: Etch rate as a function of N ₂ /Ar gas flow ratio at various etching temperatures for	

films deposited at a.) Room temperature, b.) 200°C, c.) 300°C.....	64
Figure 4.14: Arrhenius plot of films deposited at a.) Room temperature, b.) 200°C, c.) 300°C. .	68
Figure 4.15: Activation energy as a function of N ₂ /Ar gas flow ratios at various substrate deposition temperatures.	71
Figure 4.16. SIMS data plot showing inter-diffusion of B, C, N and Cu at (a) N ₂ /Ar = 0.25 and (b) N ₂ /Ar = 0.5 for as-deposited BCN films on copper.	74
Figure. 4.17 SIMS data plotted for Cu diffusion in the BCN deposited at (a) N ₂ /Ar = 0.25, (b) N ₂ /Ar = 0.5 at different annealing periods at 200°C and 300°C.	76
Figure 4.18 SIMS data plot showing inter-diffusion of B, C, N and Cu at N ₂ /Ar = 0.25, for copper deposited on the as-deposited BCN films and annealed at 400°C for 30 minutes.....	78
Figure 4.19: Percentage elemental compositions of B, C and N for BCN thin films deposited at a) 20W B ₄ C and b) 40W B ₄ C.....	80
Figure 4.20: B1s spectra of BCN thin films deposited at a) 20W B ₄ C and N ₂ /Ar = 0.25, b) 20W B ₄ C and N ₂ /Ar = 1, c) 40W B ₄ C and N ₂ /Ar = 0.25, d) 40W B ₄ C and N ₂ /Ar = 1	85
Figure 4.21: N1s spectra of BCN thin films deposited at a) 20W B ₄ C and N ₂ /Ar = 0.25, b) 20W B ₄ C and N ₂ /Ar = 1, c) 40W B ₄ C and N ₂ /Ar = 0.25, d) 40W B ₄ C and N ₂ /Ar = 1	84
Figure 4.22: C1s spectra of BCN thin films deposited at a) 20W B ₄ C and N ₂ /Ar = 0.25, b) 20W B ₄ C and N ₂ /Ar = 1, c) 40W B ₄ C and N ₂ /Ar = 0.25, d) 40W B ₄ C and N ₂ /Ar = 1	86
Figure 4.23: a) % Transmission for various gas ratios at 20W DC power to B ₄ C; b) % Transmission for various gas ratios at 40W DC power to B ₄ C.	88
Figure 4.24: Tauc plot of BCN thin films deposited at 20W power to B ₄ C	90
Figure 4.25: a) Optical band gap as a function of gas flow ratio at 20W DC; b) Optical band gap	

as a function of gas flow ratio at 40W DC.....	92
Figure 4.26: X-ray diffraction patterns for BCN thin films deposited at (a) room temperature, (b) 200°C, and (c) 400°C.	94
Figure 4.27: FTIR transmission spectra of BCN thin films deposited at room temperature, 200°C and 400 °C.	96
Figure 4.28. Photoluminescence measurements of BCN thin films deposited at different substrate deposition temperatures.	99
Figure 4.29. Photoluminescence at room temperature and 77K, for BCN thin films deposited at different substrate deposition temperatures.	101
Figure 4.30: FTIR spectra of BCN thin films deposited at gas flow ratio of $N_2/Ar = 1$ and at 200°C deposition temperature.....	103
Figure 4.31: UV-Vis transmission spectra of BCN thin film deposited at 200°C.	104
Figure 4.32: Tauc plot for bandgap extraction.....	104
Figure 4.33. PL spectra of BCN thin films deposited at gas flow ratio of $N_2/Ar = 1$ and at 200°C deposition temperature.....	105
Figure 4.34: IV characteristics of Al-BCN-Au MIM devices showing dark and UV photocurrent	106

LIST OF TABLES

Table 1.1: Defining ILD characteristics.....	2
Table 2.1: General properties of boron carbide [[14], 17].....	12
Table 2.2: Comparison of various properties of BN with those of other semiconductors [100]..	15
Table 4.1: XPS elemental composition, mass density, and dielectric constant for BCN thin films sputter deposited using C and BN targets and different N ₂ /Ar gas flow ratios. NM = not measured due to high leakage currents.	40
Table 4.2: XPS elemental composition, mass density, and dielectric constant for BCN thin films sputter deposited using B ₄ C and BN targets and different N ₂ /Ar gas flow ratios	40
Table 4.3: XPS elemental composition and nanoindentation Young's modulus and hardness for BCN thin films sputter deposited using B ₄ C and BN targets and varying DC and RF biases.	46
Table 4.4: The percentage composition of B, C and N in the BCN thin film deposited at various N ₂ /Ar gas flow ratio at 20W DC power with constant RF power of 250W calculated from XPS data.....	51
Table 4.5: The percentage composition of B, C and N in the BCN thin film deposited at various N ₂ /Ar gas flow ratio at 40W DC power with constant RF power of 250W calculated by XPS...	53
Table 4.6: Percentage elemental compositions of B, C and N at various N ₂ /Ar gas flow ratios and substrate deposition temperatures.	62
Table 4.7: Activation energy and pre-exponential factor of BCN thin films deposited at various gas flow ratios and substrate deposition temperatures.....	69
Table 4.8: XPS percentage compositions of B, C and N of BCN thin films deposited at various substrate deposition temperatures.	97

LIST OF ACRONYMS/ABBREVIATIONS

ARC	Anti-reflection coatings
BC	Boron Carbide
BCN	Boron Carbon Nitride
BN	Boron Nitride
CMOS	Complementary Metal Oxide Semiconductor
CMP	Chemical Mechanical Polishing
CVD	Chemical Vapor Deposition
IDL	Inter Dielectric Layer
<i>DC</i>	Direct Current
<i>E_g</i>	Band gap
<i>LCR</i>	Inductance capacitance and resistance

MIM	Metal-Insulator- Metal
PACVD	Plasma Assisted Chemical Vapor Deposition
PECVD	Plasma Enhanced Chemical Vapor Deposition
PVD	Physical Vapor Deposition
RF	Radio Frequency
<i>RPLA</i>	Reactive Pulsed laser ablation
rpm	Rotations per minute
sccm	Standard cubic centimeter per minute
ULSI	Ultra Large Scale Integration
VLSI	Very Large Scale integration

CHAPTER 1: INTRODUCTION

The horizontal and vertical conducting segments of transistors and other active parts of the semiconductor are connected by metallic lines. That serve as the gate metallization, contacts and metal interconnects that may consist of an adhesion promoter/diffusion barrier under and over the main current carrier metal as shown in the figure 1.1 and some processors contain nearly 10 levels of metallizations [1].

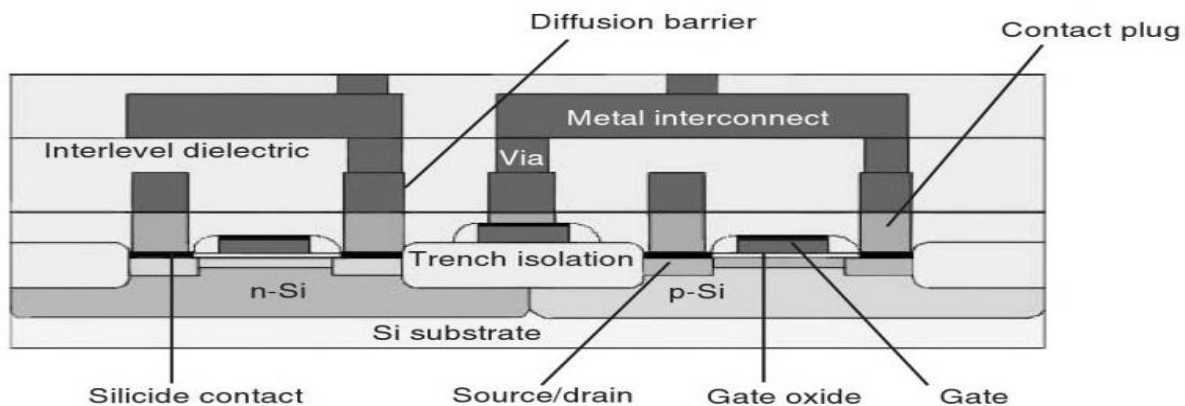


Figure 1.1: A CMOS device

Inter layer dielectrics (ILD) are divided into three groups

- (i) The active dielectric layers
- (ii) Layers only for Device processing.
- (iii) Insulating layers

The first group is used for storage of charges and other kind of active operation. Examples are gate oxide and dielectric capacitor in memory devices. The second group comprises of films

which are used for device processing like (a) anti-reflection coatings (ARC) in lithography step; (b) etch stop layers and for chemical mechanical polishing (CMP) and (c) as masks.

The third group is used as insulation in microelectronic devices. The isolation between metal lines of same level is called inter-metal dielectric, and that between two metal levels is called inter level dielectric. Both are called interlayer dielectrics (ILDs). The effective speed of the devices is also due to the speed of signal propagation to and from the device through the metal interconnects. These are capacitively coupled to the insulating dielectrics surrounding them, ILDs, leading to RC time delay.

An interconnects equivalent model is given in figure 1.2, where ‘P’ is line pitch, ‘W’ the line width, ‘S’ the line spacing, ‘T’ the line thickness, and the ILD line thickness above and below is equal. The RC delay is given by:

$$RC = 2\rho\kappa\epsilon_0 [(4L^2/P^2) + (L^2/T^2)] \quad (1)$$

Where ρ is the metal resistivity, ϵ_0 the vacuum permittivity, κ the relative dielectric constant of the ILD, and L is the line length. For devices smaller than $0.25\mu\text{m}$, the RC time delay controls the overall on-chip cycle time [2].

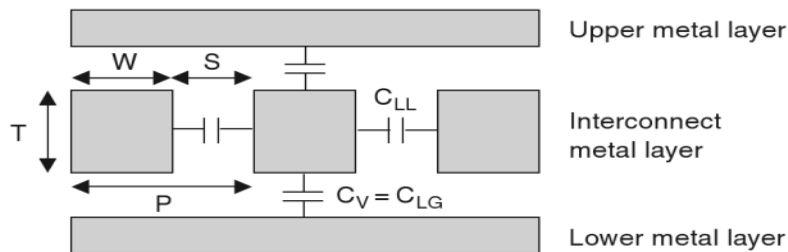


Figure 1.2: A typical interconnect element. LG and LL refer to the line-to-line and line-to-ground contributions. [2]

The power dissipation is also caused by parasitic capacitance as given by the following equation
$$P = (1/2) f_d C V^2 f \quad (2)$$

Where C is the total on-capacitance, V the supply voltage, f the operational frequency, and f_d the fraction of gates that switch during a clock period. Thus by reducing κ , the value of 'C' will also be reduced making circuits faster, hence also more portable.

In this work the electrical properties of proposed ILD material is investigated. These all relate to electrical conduction through the dielectric and polarization that lead to interaction with electrons, as a result of applied field on the conductor in contact with dielectric. Some desired electrical properties in an ILD are high electrical bulk and surface resistivity, extremely low leakage, high electric field strength, low leakage, low charge trapping, dielectric constant, low dissipation and high reliability. The table below specifies all the electrical properties desired in a dielectric material of constant lower than 3.

Table 1.1: Defining ILD characteristics

Dielectric constant at 1 MHz	1.5 - 3
Dissipation factor	<0.005
Anisotropy	Undesirable
Breakdown strength	$\geq 1\text{MV/cm}$
Bulk resistivity	$\geq 10^{15} \Omega\text{cm}$
Surface resistivity	$\geq 10^{15} \Omega\text{cm}$

The list of the requirements of the low- κ material is as given below;

- 1) Dielectric constant < 3.0
- 2) Chemical compatibility with Si
- 3) Highly insulating
- 4) Good thermal stability (up to 400°C)
- 5) High resistance to environmental degradation
- 6) Low hydrogen/moisture content
- 7) Compatibility with planarization, lithographic and etching processes
- 8) Low diffusivity for metallic impurities
- 9) High breakdown voltage
- 10) Low dissipation factor
- 11) Compositional uniformity
- 12) Low void/crack/defect density
- 13) Low compressive stress
- 14) Conformal deposition
- 15) Good adhesion
- 16) Low deposition temperature

- 17) Thickness uniformity over large areas
- 18) Low particle density
- 19) High elastic modulus
- 20) Low shrinkage
- 21) Low thermal expansion

However, the main technology limiter was not the ability to develop low- κ ILD materials but rather two fundamentally difficult problems associated with this category of materials. Firstly, is the inherent weak mechanical strength of low- κ ILD which seriously limits the ability to package chips made with such ILDs. Moreover, the lower the dielectric constant, the weaker the ILD gets as shown in Fig 1.3. The second problem is the degradation of the dielectric constant of the low- κ materials during processing. Typical processing steps used in the CMOS technology includes photo resist removal, dry and wet etch and metal cleans. All these steps extract carbon from the materials and render them to a higher dielectric constant.

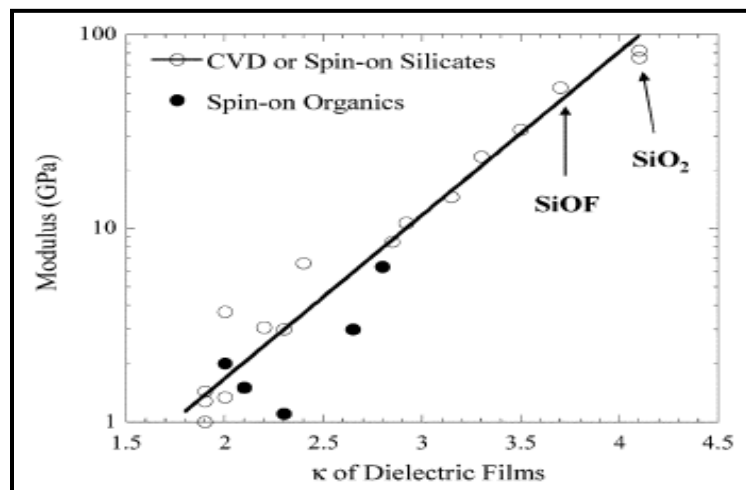


Figure 1.3: Relationship between the dielectric constant and mechanical strength, as represented by modulus of a representative ILD material.

While the existence of a low dielectric constant is a critical requirement for any new low κ dielectric material, it is far being the only requirement. It is equally important that the new material be chemically stable and compatible with Si microelectronics processing. As this work deals with the electrical properties of the BCN thin films. The desired electrical properties of an ideal dielectric material are discussed in the following section.

The need of good ILD material is in terms of high electrical bulk and surface resistivity, extremely low charge trapping, dielectric constant and its anisotropy, low dissipation and high reliability. Some of the desired ILD characteristics are dielectric constant at 1MHz may be from 1.5 – 3, dissipation factor could be less than 0.005, undesirable anisotropy, Breakdown strength should be greater than 1MV/Cm and the surface resistivity should be greater than $10^{15}\Omega\text{cm}$.

The resistivity determines the voltage-induced current through the material. Dielectrics are subjected to very high electrical fields up to 10^7 volt/cm. Thus a very high resistivity material is chosen of the order of $10^{14}\Omega\text{-cm}$. Besides the bulk resistivity the surface resistivity also plays an important role in determining the dielectric feasibility. In surface resistivity the surfaces are defected and provide fast charge diffusion paths leading to less resistivity compared to bulk. As dielectric films become thinner the surface to volume ratio increases which in turn leads to surface and interface electrical conduction mechanisms. Similarly interface between two metal layers and metal surfaces lead to increase in gross total resistance[3].

Coming to Bulk resistivity, it is seem to be influenced by:

- (1) impurities, mostly by easily ionizable under bias ones like water, H^+ , OH^- , Na^+ etc.;
- (2) defects like point, line, area and volume are due to lower bulk resistivity

- (3) stress affecting the band gap of the material.
- (4) non-stoichiometry in some inorganic dielectrics will lead to higher vacancies.
- (5) the ionic dielectrics generally have lower electrical resistance than covalently bonded.
- (6) some ionizable covalent polymers due to the metal interface.

The leakage current capability is defined in terms of the maximum voltage (or the electric field which is voltage per unit thickness of the dielectric) that an ILD can sustain without leading to runaway currents (Current per unit area A/cm^2) called dielectric strength defined in the unit of volt/cm. For ILD application the dielectric strength of 2-5 MV/cm is considered as feasible. Figure 1.4 shows the schematic of current density vs. Electric field [1]

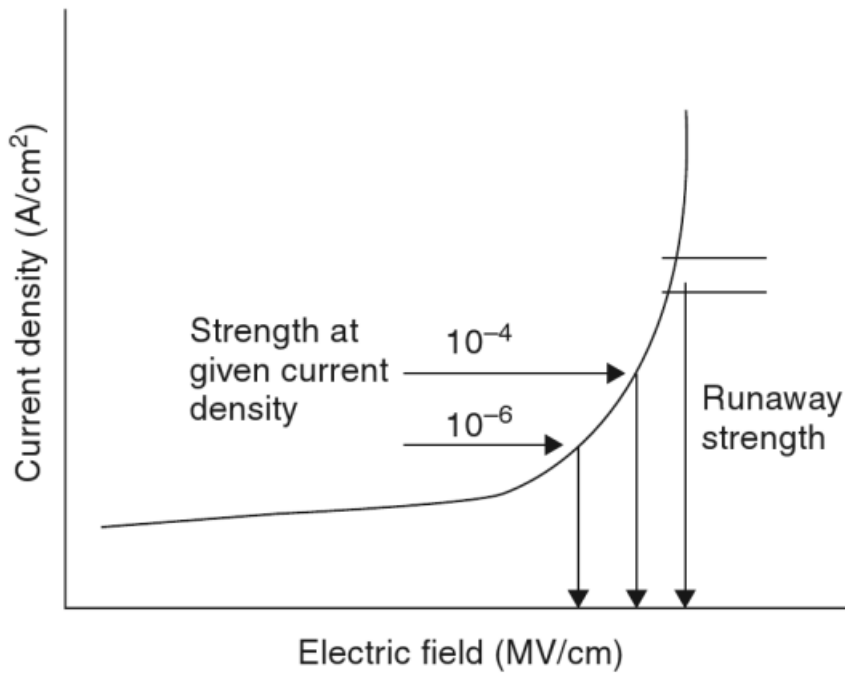


Figure 1.4: Schematic representation of current density through a dielectric as a function of the applied field.

Dielectric strength is related to the dielectric constant. The Dielectric constant of the

inorganic dielectrics is shown in figure 1.5 [4]. It shows that lowest the dielectric constant higher is the field strength of a given dielectric.

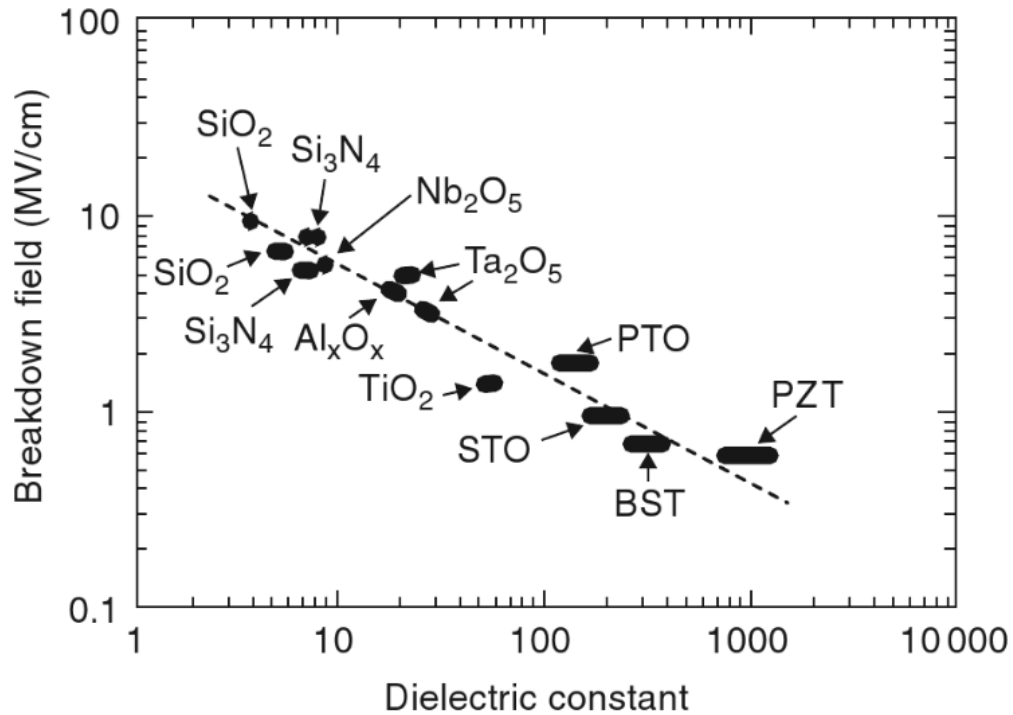


Figure 1.5: A log-log plot of the dielectric breakdown field (or field strengths), as a function of dielectric constant of dielectric.

Finally, it is noted that the dielectric breakdown field strength has dielectric-thickness dependence and decreases with the thickness. The lowering of the field strength at higher thickness is due to defects and also may be because of low thermal conductivities of the dielectric, the heating effectively raising the temperature more in thicker dielectrics than in thinner ones. Higher the temperature lower is the field strength and drop in the field strength at high temperatures could be very large.

In a regular dielectric capacitor, the voltage lags current by 90° but practically it lags by $(90^\circ - \delta)$ where δ is dielectric loss angle which leads to power loss in the form of heat. The dissipation of energy is defined now as follows.

(a) Dissipation factor = $\tan \delta$

(b) Dielectric loss factor = $k \tan \delta$.

$$\text{Power loss (watt)} = 5.56 \times 10^{-11} E^2 f v k \tan \delta \quad (8)$$

Where E is the applied field strength in volts per meter, f the frequency in hertz and v the volume. Therefore to reduce the energy dissipation from a given material, we have to find lowest δ . Under AC conditions it should be noted that

(a) Polarizations and loss are frequency dependent

(b) Electronic polarizations dominate at higher frequencies ($>10^{12}$ Hz)

(c) Amorphous dielectric materials polarize at higher frequencies than the crystalline materials of same composition.

1.1: Overview

There exist atomic bonding similarities amongst boron, carbon, and nitrogen that allow the formation of compounds with a wide compositional range. BCN compounds have been expected to combine the excellent properties of B_4C , BN and C_3N_4 , with their properties adjustable, depending on composition and structure [5]. As graphite is semi metallic and h-BN is insulating (band gap $>3.8\text{eV}$), it is expected that such a hybrid between semi metallic graphite and insulating h-BN may show adjusted semiconductor properties [6]. Moreover, recent efforts have been devoted to develop a low dielectric constant BCN film in order to reduce the stray capacitance

induced signal delay of interconnections in Si ultra large scale integrated circuits (ULSI). Dense (pore-free) BCN films with a low dielectric constant in the range of 1.9 to 2.1 have been successfully demonstrated [7]. The use of BCN films in the CMOS back end technology is really very interesting and promising. A material with a low dielectric constant and with high mechanical hardness is a perfect match for inter layer dielectrics. Several methods of preparing boron carbon nitride films have been reported, such as chemical vapor deposition (CVD), plasma assisted CVD, pulsed laser ablation, ion beam deposition, and sputtering. Also, shock wave compression or high pressure/high temperature techniques (HP/HT) have been used. The limitations in composition arise and are due to experimental restrictions like target composition or precursor mixing, so that one element is always incorporated in approximately the same while other two can be varied over a greater range.

The sputtering technique provides unique advantages over other techniques such as freedom to choose the substrate material and a uniform deposition over relatively large area. Furthermore, it is possible to control the deposition parameters to prepare BCN films of various compositions. According to the chemical properties of the B, C and N during the depositing process of the BCN films, B and C can exist both as elements and as compounds reacting with N or each other, while N could be existed in the films only as compounds by reacting with B or C. Therefore, the process of N deposited into the films and the reciprocity among B, C, and N during the deposition of films becomes the main factors, which affect the composition and properties of films.

For low carbon content the h-BN is preserved in boron carbonitride compounds. By increasing the carbon content towards BCN stoichiometry ($1 < x < 2$) the hexagonal stacking

sequence tends into a fullerene-like structure. Increasing the carbon content to the composition BC_4N , the sample exhibits an amorphous structure. A ternary compound of boron carbonitride (BCN) has gained increased attention due to its potential applications in electronic, optoelectronic and luminescent devices. The boron-carbon-nitrogen phase diagram contains interesting phases, such as diamond, graphite, fullerene, cubic-BN, B_4C and there is also a hypothetical C_3N_4 as shown in Figure 1.6.

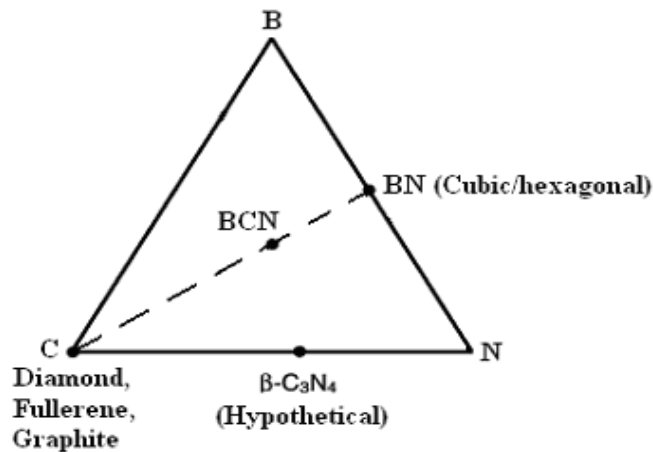


Figure 1.6: Ternary Triangle [8] [34]

Carbon nitride (C-N) thin films are predicted to have hardness comparable to diamond due to the small bond length and low ionicity of this material. The focus of this work was to synthesize the boron carbon nitrogen (BCN) through Rf sputtering and investigating its electrical properties and access its feasibility to use as a low- κ material in the CMOS back end technology.

CHAPTER 2: LITERATURE REVIEW

2.1: Boron Carbide

Boron carbide (B_4C) is an extremely hard boron–carbon ceramic material used in tank armor, bulletproof vests, and numerous industrial applications. With a Mohs hardness of about 9.497, it is one of the hardest materials known, behind cubic boron nitride and diamond [7]. The ability of boron carbide to absorb neutrons makes it an absorbent for neutron radiation arising in nuclear power plants. Nuclear applications of boron carbide include shielding, control rod and shut down pellets. Within control rods, boron carbide is often powdered, to increase its surface area. Electrically, boron carbide is p-type semiconductor material at even high temperatures which suggests is thermally very stable. In thin film form too, this material finds applications as hard and protective coatings, hard disk drives and other corrosion-resistance applications [9]. Sputtering techniques have been commercialized more successfully in big manufacturing fabs because of their high film deposition rate and low temperature features.

The chemical formula of boron carbide is B_4C . But some time there exist a deficiency in Carbon. Hence the formula is somewhere between $B_{12}C_3$ and $B_{12}C_2$. Boron carbide has a complex crystal structure typical of icosahedron-based borides as shown in figure 2.1 [10]

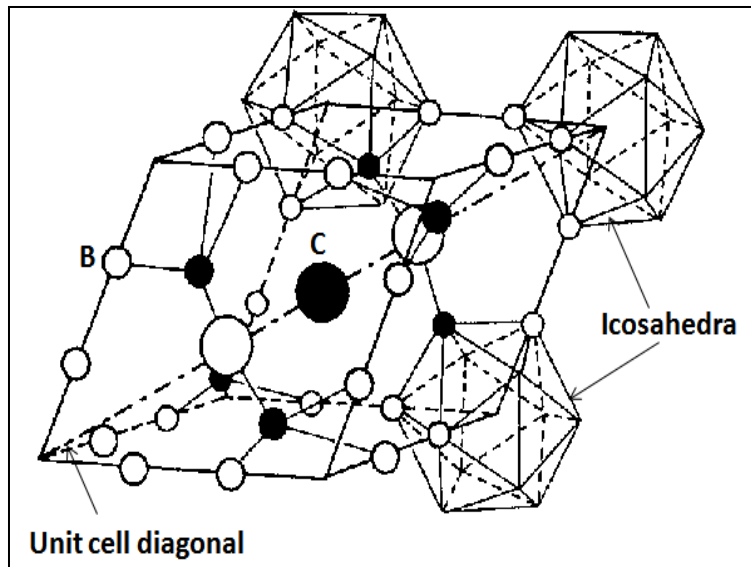


Figure 2.1: Icosahedron shape of unit cell of boron carbide [11]

Boron carbide has the band gap of 1.2-1.8 eV [11]. But according to the literature it is given that the conductivity of Boron carbide is highest at 13% carbon percentage in the Boron carbide and later it decreases as and when the carbon content increases in the composition [10]. All sputter deposited thin films of boron carbide reported in the literature are amorphous. The boron carbide is very stable at high temperature as it has very high melting point and hence it is desired to be used at high temperatures in the form of an electronic device at inhospitable situations. In some work it is reported that amorphous hydrogenated boron carbide thin films with boron concentrations varying from 0 through 18 % by plasma decomposition of a feedstock of diborane and methane. They found out that boron acts like a dopant with increase in boron concentrations which leads to increase in acceptor densities. Similar work on amorphous hydrogenated carbon doped with boron was first done by Jones and Stewart and they reported an increase by a factor of ten in conductivity [12]. The electrical conductivity was measured for boron carbide films that had

boron to carbon ratio from 4.7 to 19.0, for temperatures from room temperature to 100⁰C. The electrical conductivity found to vary exponentially with reciprocal temperature. This shows that there is a little variation in conductivity as a function of Carbon composition. Hence it has been concluded that the electrical conductivity depends in the sample purity and preparation and the number of free carbon present in a given composition [13].

Table 2.1: General properties of boron carbide [[14], 17].

Properties of boron carbide	
Molecular weight (g/mol)	55.26
Density (g/cm ³)	2.52 for B ₄ C
Melting Point (°C)	~ 2400
Specific Heat (Cal/mol K at 300 K)	12.7
Thermal conductivity (W/cm K)	0.35-0.16 (25-800°C)
Thermal expansion (1/K)	4-8 E ⁻⁶ (25-800°C)
Electrical Resistivity (Ω-cm)	5 (at 298K)
Electrical conductivity (1/ Ω-cm)	~10 ³
Band Gap (eV)	0.77-1.80
Dielectric Constant	5
Seeback coefficient (μV/K)	200-300
Vickers Hardness (GPa)	27.4-40
Young's Modulus (GPa)	290-460
Shear Modulus (GPa)	158-200
Bulk Modulus (GPa)	190-250
Tensile Strength (N/mm ²)	155 (980°C) 162 (1425°C)

Properties of boron carbide	
Poisson's Ratio	0.14-0.18
Flexural Strength (MPa)	323-430
Lattice constant (nm)	c=1.207 a=0.561
Oxidation resistance	in air up to 600°C
Chemical resistance	Excellent. Reacts with halogens at high temperature.

2.2: Boron Nitride

Boron nitride is very similar to diamond and can be used to make crystals that are as hard as diamond. Boron nitride is an excellent conductor of heat in spite being an insulator electrically. Boron nitride is mostly found in cubic (c-BN or β -BN) and hexagonal (h-BN) phases. BN in general is not found naturally. Cubic BN has properties close to diamond and is known to be the second hardest material after diamond. Also, c-BN can be made either n or p type conductivity for electronic applications. On the other hand h-BN is a soft material with insulating properties and has a band gap of 5 eV. Cubic boron nitride is one of the physical forms of boron nitride and is made of tetrahedral bonded light elements. BN is also known as c-BN, β -BN or z-BN. The application of powdered form of c-BN in industrial abrasive and boron nitride deposits are used to minimize friction and wear. Techniques used to prepare cubic boron nitride are physical vapor deposition (PVD), plasma enhanced chemical vapor deposition (PECVD), pulsed laser deposition, DC and RF magnetron sputtering from conductive and non-conductive targets (h-BN, boron, B₄C composite).

Also, c-BN can easily be doped n-type using Si and p-type using Be and Mg. This is something that cannot be achieved with diamond. Lastly, c-BN does not react with foreign materials at high altitudes and in harsh environments [15]. It has a very large indirect energy band gap E_g varying between 5.4 and 7.0 eV at room temperature. Hexagonal boron nitride (h-BN) or α -BN or g-BN (graphite BN) is used at both very low temperature and at high temperature as a lubricant and in situations where the electrical conductivity or chemical reactivity would be problematic. Boron nitride lubricants can be used even in vacuum for space applications as the lubricity mechanism does not contain water molecules which will be trapped between the layers. h-BN can be included in ceramics, alloys, resins, plastics, rubbers and other materials, giving them self-lubricating properties. Hexagonal boron nitride is stable at temperatures up to 1000 °C in air, 1400 °C in vacuum and 2800 °C in inert gas thus is a material which has one of the best thermal conductivities of all electric insulators. Another important characteristic of h-BN is that it is fairly chemically inert and is not wetted by many melted materials (e.g. aluminum, copper, zinc and steels, germanium, silicon, glass and halide salts). Because of its excellent dielectric and thermal properties, BN is used in electronics as a substrate for semiconductors, microwave-transparent windows, and as a structural material for seals [16]. Thin films of boron nitride can be obtained by chemical vapor deposition from boron trichloride and nitrogen precursors

Table 2.2: Comparison of various properties of BN with those of other semiconductors [100].

Parameter	c-BN	h-BN	Diamond	3C-SiC	GaAs	Si
Lattice Constant (Å)	3.615	a=2.504	3.567	4.358	5.65	5.43
Thermal expansion Coefficient	3.5	2.7, 3.7	1.1	4.7	5.9	2.6
Density (gm/cm ³)	3.487	2.28	3.515	3.216	-	2.328
Melting Point (°C)	>2973	-	3800	2540	1238	1420
Energy bandgap (eV)	6.4	5.2	5.45	3.0	1.43	1.12
Electron mobility (cm ² /Vs)	-	-	2200	400	8500	1500
Hole mobility (cm ² /Vs)	-	-	1600	50	400	600
Dielectric constant	7.1	5.06	5.5	9.7	12.5	11.8
Breakdown(x10 ⁵ Vcm ⁻¹)	~80	~80	100	40	60	3
Resistivity (Ω-cm)	10 ¹⁶	10 ¹⁰	10 ¹³	150	10 ⁸	10 ³
Thermal conductivity	13	-	20	5	0.46	1.5
Absorption edge (μm)	0.205	0.212	0.20	0.40	-	1.40
Refractive index	2.117	1.700	2.42	2.65	3.4	3.5
Hardness (kg/mm)	9000	-	10,000	3500	600	1000

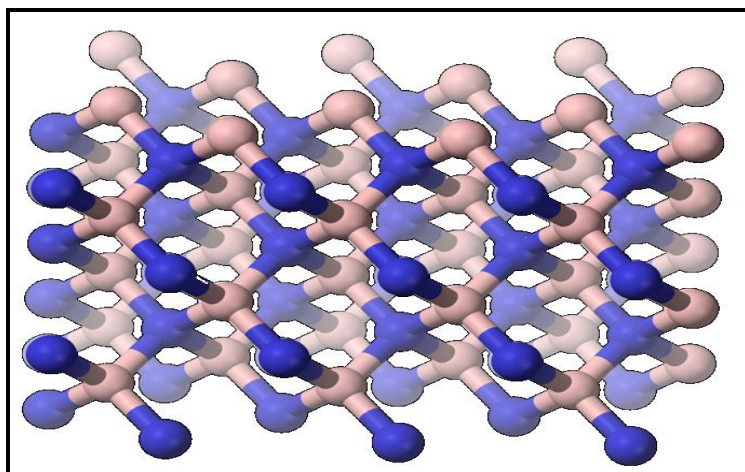


Figure 2.2: β -BN sphalerite structure

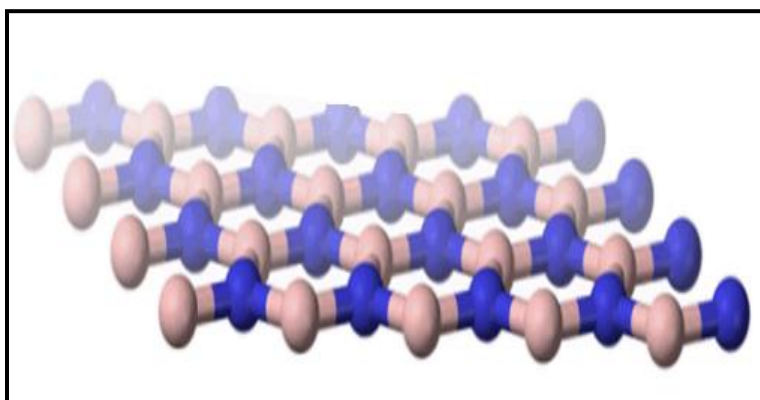


Figure 2.3: h-BN hexagonal (graphite like)

2.3: Boron carbon Nitride

The atomic sizes of boron, carbon and nitrogen are similar, also structures of carbon and boron nitride polymorphs are similar, it suggests that it is possible to produce diamond-like phase containing all three elements. Beginning in 1990, a great interest has been put in studying the possibility to synthesize dense B-C-N phases. They are expected to be thermally and chemically

more stable than diamond, and harder than c-BN, and hence it would be used as materials for high speed cutting and polishing of ferrous alloys. These characteristic properties are because of diamond-like structure combined with the sp^3 σ -bonds among carbon and the heteroatoms. BC_xN_y thin films were synthesized by chemical vapor deposition in 1972. It is unclear whether the synthesis products are diamond-like solid solutions between carbon and boron nitride or just mechanical mixtures of highly dispersed diamond and c-BN. Ternary B–C–N phases can also be made using shock-compression synthesis. It was further suggested to extend the B–C–N system to quaternary compounds with silicon included. The phase diagram of the B-C-N is showed in Figure 1.6. One of the characteristic features of the materials in the BCN ternary phase system is that they have short bond lengths and thus expected to combine the specific properties of diamond, cubic boron nitride (c-BN), hexagonal boron nitride (h-BN) and boron carbide (B_4C).

The boron-carbon-nitrogen phase diagram contains interesting phases, such as diamond, graphite, fullerene, cubic-BN, B_4C and there is also a hypothetical C_3N_4 . Also, the ability to control the band gap (E_g) by changing the atomic composition and structure makes them suitable for the application in electronic and photonic devices [14]. Different deposition techniques have been reported for depositing BCN thin films, including chemical vapor deposition (CVD), ion beam assisted deposition, cathodic arc plasma deposition, pulsed laser deposition, DC and RF magnetron sputtering. The experimental investigations reported above focuses mainly on the synthesis, characterization and mechanical properties. A group deposited BCN films by plasma-assisted chemical vapor deposition and studied the optical and electrical properties. They concur that the carbon composition had a good dependence on the optical and electrical properties of the BCN films. The band gap of the film decreased from 5.3 to 3.4 eV with increase in Carbon composition

ratio from 9 to 30%. The electrical resistivity of the BCN film decreases from 1×10^{12} to 3.4×10^9 Ω -cm as the carbon content in the films increased from 9 to 30% [7]. The electrical properties of BC₂N thin films with respect to temperature were found out and it was reported that there was a dependence of resistivity and Hall Effect measurements. The resistivity and Hall Effect measurements results indicated that BC₂N thin films are p-type semiconductors and the acceptor levels were between 7.5 and 23 meV. They also studied the dependency of type of substrate and found that the quality of thin film is better on Ni substrates than on quartz [17]. Other group reported the growth of c-BCN thin films by reactive pulsed laser ablation (RPLA). They used a rotating target consisted of two semi disks wherein one of h-BN and other one of graphite and this deposition was done at room temperature. They observed crystalline BCN films with the formation of c-BCN, h-BCN and h-BN. The films were hard, adherent and transparent. BCN films were also prepared by pulsed laser deposition from a sintered B₄C target. The films prepared were found to be smooth and adhered well to the substrate. They also observed that with the help of reactive nitrogen plasma they can incorporate more amounts of nitrogen in the films.

BCN thin films deposited using sputtering and the work on it is discussed from now on. One of the work reports that they prepared BCN films by RF reactive sputtering from a hexagonal h-BN target in an Ar-CH₄ discharge. They made different films with different carbon contents by varying the CH₄ partial pressure. Under optimum processing conditions they observed polycrystalline BC₂N and the calculated activation energy was approximately 0.8 eV [17]. BCN films were also deposited by RF magnetron sputtering using a composite target consisting of h-BN and graphite in an Ar-N₂ atmosphere. They studied the effect of sputtering power on the composition of BCN films and found that the films deposited at 80W and 130W are close to the

BC₂N stoichiometry and the sample deposited at 110 W is close to the stoichiometry of BCN.

Lastly the samples deposited at 100W and 120W have the chemical composition of BC₂N. Thus they were able to achieve the BCN films with different compositions by varying the power to the composite target [18]. Dual cathode magnetron sputtering was used to deposit BCN films by Kusano et al. and they sputtered from graphite and boron targets. They varied the power to the sputtering targets and concentration of nitrogen gas in the sputtering chamber. They observed the variation of deposition rate with reactive gas and the BCN films deposited at pure nitrogen exhibited a higher content of sp and sp² carbon and had lower durability in friction tests as compared to other BCN films. Another group reported that BCN thin films near B₄C composition deposited by radio frequency magnetron sputtering from a sintered B₄C target. They observed the increase in nitrogen incorporation in the films from 0 to 40 at. % while the relative atomic composition of B/C was relatively constant at 4 thus the films structure changed from B₄C to a mixture of h-BN and amorphous carbon. Same group of researchers characterized BCN films by their micromechanical and micro tribological behavior. They evaluated the adhesion and friction coefficient against diamond by micro scratch and also characterized their wear behavior at the nano metric scale. They found that the hardness is higher in the films with lower nitrogen concentration and the least hard films had nitrogen content of around 20 at.% [19].

Some work on dielectric constant studies was also performed by many groups. Takashi et al the dielectric constant of BCN is found to decrease with decrease in growth temperature. The dielectric Constant is estimated from the accumulation region of capacitance–voltage (C–V) characteristics of Au/BCN/p-Si samples. Reduction in the crystal grain size and increase of the amorphous region of The BCN films are observed with decreasing growth temperature. Here the Polycrystalline

boron carbon nitride (BCN) films are synthesized at various temperatures by plasma-assisted chemical-vapor deposition [20]. Also it has been reported by Sugino et al that boron nitride films with a dielectric constant as low as 2.2 can be synthesized by plasma-assisted chemical-vapor deposition (PACVD)[21]. It has been reported that the addition of C atoms to BN films is effective in reducing the dielectric constant.

2.4: Carbon nitride

Liu and Cohen made theoretical prediction that β -C₃N₄ which is isomorphic with β -Si₃N₄ might have a bulk modulus which can exceed that of diamond [22]. Figure 2.4 shows the structure of the carbon nitride. This has triggered a lot of research work in the development of C₃N₄ over the past two decades. C-N material along with high hardness also is expected to possess wide band gap, high thermal conductivity, high strength, high decomposition temperature and excellent resistance to corrosion and wear. Carbon Nitride possesses applications for insulator devices in III-V metal-insulator-semiconductor structures. C-N is a preferred material over Si₃N₄ for such applications because it doesn't introduce any shallow impurities.

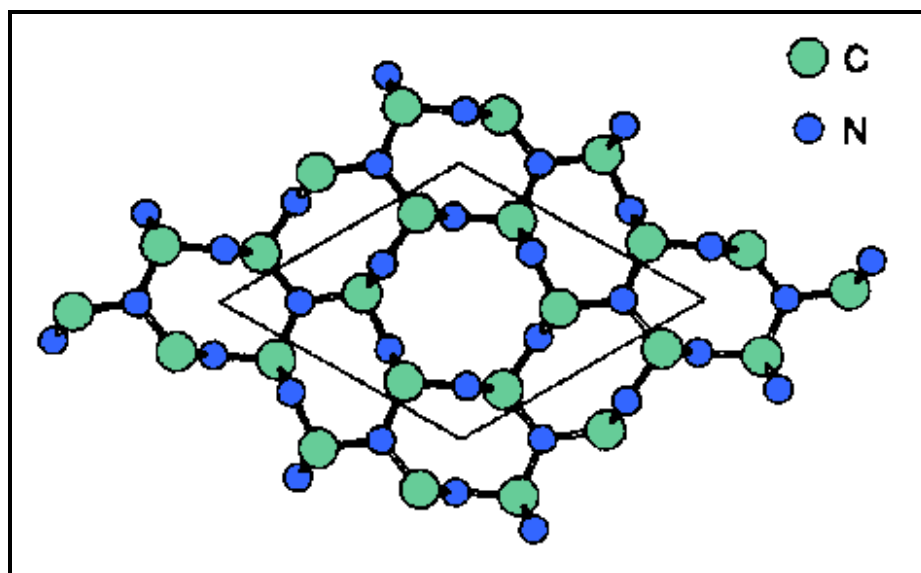


Figure 2.4: Crystal structure of carbon nitride

There have been many research reported on the deposition of C-N films such as reactive sputtering, plasma chemical vapor deposition (CVD), laser ablation, ion-assisted deposition and metal-organic chemical vapor deposition (MOCVD). The incorporation of nitrogen in the C-N films was around 40% which is lesser than that expected for stoichiometric β -C₃N₄ (57 at %) in all the work reported above. Higher amounts of nitrogen (50-57 at. %) has been reported in the hydrogenated C-N films prepared by plasma CVD and the CN films obtained by dual ion beam sputtering, laser ablation of graphite using a low-wavelength excimer laser and by using the MOCVD technique[23]. The sputtering being the most commonly used method of deposition in the industry results in relatively low nitrogen content in the carbon nitride films [24]. One group performed reactive sputtering and observed the effect of nitrogen incorporation on the growth kinetics, composition, structure and type on bonding. They noticed that the incorporation of N₂ in the plasma leads to an increase in the growth rate and that the growth kinetics and N content in the

films is dependent on physical and chemical sputtering. The alteration in growth kinetics influenced the chemical, structural and optical properties. Another group also deposited C-N films by reactive sputtering and premised that by decreasing the target power and at high nitrogen pressure results in higher N₂ contents in the film. They were able to gain equal amounts of carbon and boron for a wide range of sputtering pressures at low temperatures and the structure of the film obtained was graphite-like.

CHAPTER 3: METHODOLOGY

In this chapter, the techniques and procedure for fabricating BCN devices for characterization and measurement purposes are conducted. This chapter also elucidates various materials and electrical characterization techniques used to study the thin film samples. Also it outlines briefly about different electrical measurements like I-V Characteristics, Capacitance measurements, Breakdown voltage measurements.

Sputter deposition technique was used to deposit thin film samples. Sputter deposition is a physical vapor deposition (PVD) method of depositing thin films by eroding material from a source, which in turn is deposited onto a substrate. The advantage of sputtering is that the deposited films have the same composition as the source material. The similitude of the film and target stoichiometry will be maintained because the sputter yield depends on the atomic weight of the atoms in the target. Magnetron sputtering was instrumental in getting strong electric and magnetic fields to trap electrons close to the surface of the target. Insulating targets can cause buildup of charges that is why biasing was varied in the anode and cathode with a radio frequency (rf) power source. Sputter deposition sources (also called sputter “guns”) creates low pressure plasma by the excitation of an inert gas (typically argon) contained at 1 to 30 mTorr in a vacuum chamber. This process extracts energetic ions which accelerate toward the cathode target, striking it with kinetic energy up to several hundred electron volts. It then ejects material from the target with approximately 90% leaving as neutral atoms and 10% as ions as a result of energy transfer. Gas phase collisions between target atoms and argon atoms scatter the ejected material into a distributed cloud. As the cloud migrates towards the substrate, the random approach angles result

in deposition of a uniform film, even on surfaces that have micron-sized vertical structures.

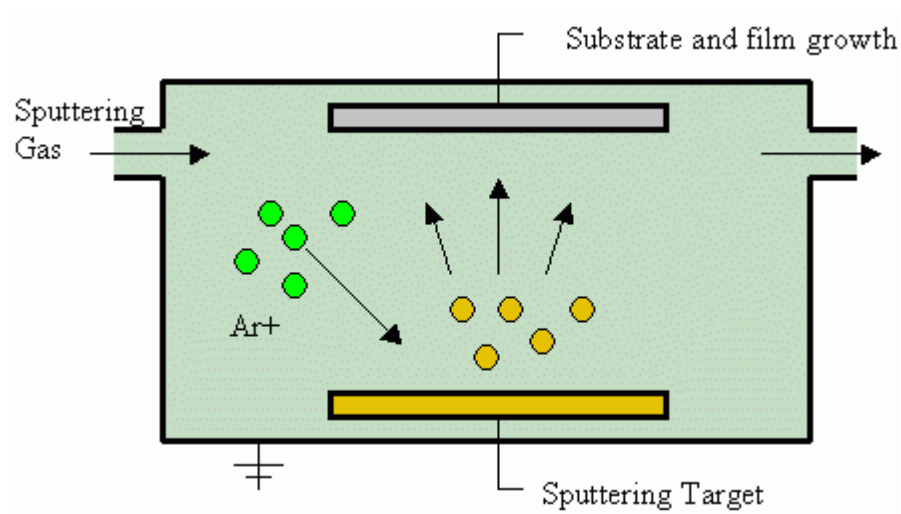


Figure 3.1: Sputtering Process Cartoon

Thin films of BCN were deposited by reactive RF magnetron sputtering in an Ultra High Vacuum system. Three inches, powder pressed, B_4C target with a purity of 99.5% was used. The system base pressure was approximately 1×10^{-7} Torr and the purity of the process gas were maintained by a hot reactive metal getter. Reactive sputtering was used where the deposited film is formed by chemical reaction between the target material and a gas which is introduced into the vacuum chamber. Oxide and nitride films are fabricated using this technique. The composition of the film is controlled by changing gas flow ratios of inert and reactive gases. In this case nitrogen was used as the reactive gas and, the N_2 to Ar ratio was varied from 0.25 to 1, in steps of 0.25 by changing the individual gas flow rate, while total gas flow was kept constant at 20 sccm and the deposition pressures were varied between 2 mTorr and 5 mTorr. And for each ratio the deposition temperature was varied. The deposition temperatures used are room temperature, 200°C, 300°C, 400°C, 500°C.

3.1: Fabrication of MIM devices

MIM stands for Metal-Insulator-Metal devices. The Corning glass was used as substrate to fabricate the MIM structure. The standard cleaning procedure was followed to clean the substrate that includes rinsing with acetone, methanol and DI (De-ionized) water. The substrate was then rinsed thoroughly with DI water, dried with Nitrogen gas jet and was loaded in to the sputtering chamber for subsequent BCN deposition. It is always good to make sure that there is no surface oxide before depositing the insulating film. The surface oxide if present will add an additional parasitic capacitance which may hinder the total capacitance value of the device.

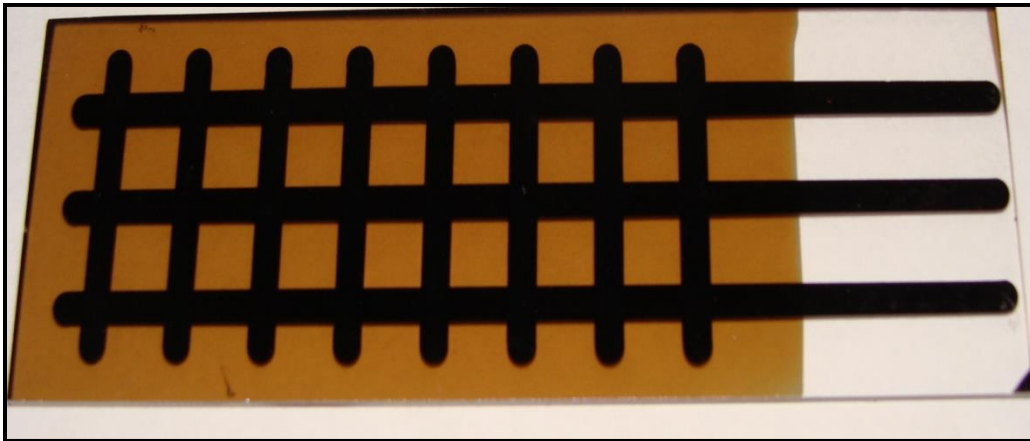


Figure 3.2: MIM structures (Al-BCN-Al) on a glass substrate

3.1.1: Preparation of the base Al electrodes

The aluminum electrodes of 3mm wide were deposited using a mechanical mask in a vacuum thermal evaporation system. During the deposition of aluminum, the thermal evaporation chamber was first roughed from atmosphere pressure to the pressure of 50 mTorr with the help of a mechanical pump (Backup pump). Then by closing the mechanical pump, the foreline pump's valve is opened. Here we have used the cryo pump as the foreline pump. This cryo pump helps in

pumping down the system from 50 mTorr chamber pressure to 1×10^{-5} Torr. It was found out from the earlier experiments that to get the high quality films with fewer defects, the pressure around 1×10^{-5} Torr would be required. The aluminum strips were dangled on the tungsten filament in the chamber. The cleaned substrates were attached to the holder from the lid and it is closed and it is made sure that the substrates are facing the filament forming a minimal distance between the substrates and Al strips. The initial roughing is done to the chamber to achieve the pressure of 50 mTorr and then the cryo pump is used to bring down the pressure to 1×10^{-5} Torr. Then the high current is passed from an induction coil current source by slowly incrementing the current from 0A to 35A. 35A is maintained for a minute for proper uniform deposition of Al on the substrate. After that another minute is left for degassing.

3.1.2: Deposition of BCN thin films

BCN film is sputter deposited on a glass substrate in a sputtering chamber. These were deposited from a 3 inch B_4C target. The reactive sputtering was used to deposit BCN films. The base pressure of the chamber was achieved in the range of 2×10^{-7} Torr. The N_2/Ar gas flow ratio was varied in the steps of 0.25 from 0.25 to 1, keeping the total gas flow in the sputtering chamber constant at 20 sccm. The R.F power of 200W to the B_4C target was kept constant. The depositions were done at 2 mTorr and 5 mTorr partial pressures (Plasma pressure). The time for deposition was 1 hour for all the samples. The thickness of the BCN film was measured by α -step Profilometer. The BCN thicknesses ranged from 900 Å - 2000 Å. The samples were deposited at a range of deposition temperatures from room temperature, 200°C, 300°C, 400°C, 500°C.

Thermocouple attached to the substrate holder was used to measure the temperature of the substrate. The temperature was noted in steady state condition. The rotation speed of the substrate was set around 20 rpm. There are two steps for achieving the base pressure of 1×10^{-7} Torr. The samples are loaded into the load lock system attached to a substrate holder and it is pumped down (roughing) from atmospheric pressure to 5×10^{-5} Torr. Then the samples are introduced to the main chamber from the load lock system by opening the valve between them and the substrate holder with the samples are placed to a pre-set distance from the target. The target is placed facing the substrate holder at an angle of 45° . When the samples are positioned accordingly, RF power is started from 0W to 200W in small incremental steps and made sure the plasma is sustained for the rest of the sputtering process. The desired N_2/Ar flow ratio is maintained and also the partial pressure in the chamber and the desired temperature is maintained as required. Now the sputtering is started in the chamber by opening the lid covering the target and it is left open for an hour of sputtering.

Lastly, aluminum electrodes of 3 mm width each running all through the length were deposited on the BCN layer to form the top layer electrode of the MIM structures using the Vacuum thermal evaporation method as explained previously. The substrates are dealt with same cleaning procedures before all three kinds of depositions.

3.2: Mechanical Characterization

Nanoindentation tests were performed with a Hysitron Triboindenter and a Berkovich diamond tip with a load range of 4 mN [25]. Each sample was tested at ten locations. Depth-dependent properties were collected by performing multiple load/unload cycles. At different indentation loads, hardness (H) and indentation modulus (I) were calculated. Young's modulus was then calculated assuming a Poisson's ratio of 0.25 and using the depth-dependent apparent modulus via linear extrapolation [26].

3.3: Optical Characterization

Optical properties of thin films can be instrumental in finding the application prospects in the electronic devices. Ultra violet (UV) through the visible and infrared to the millimeter wavelength range have significant power to examine various aspects of solids, especially semiconductors such as; lattice structure and the electronic band gap. Optical transmission, absorption, reflectance and band gap studies are considered in these studies. For optical transmission studies, BCN was deposited on quartz substrates.

3.3.1: UV-Visible Spectroscopy

UV-Visible spectrophotometer is used for the optical transmission characterization of the deposited BCN films. Optical density and absorption coefficient (α) are calculated from the % transmission values and the thickness of the film deposited. With the help of Tauc plot, the optical band gap (E_g) is obtained. These E_g values are plotted against various gas flow ratios at different

substrate deposition temperatures to study the variation with respect to the amount of nitrogen incorporation in the film. A Cary 5E high resolution spectrophotometer which is a double beam instrument controlled by a microprocessor and has a measurement range of 800-200 nm, was used to study the optical properties of BCN thin films. The ratio of transmitted light to that of incident light (%T) and absorption data were collected. Base line correction which was obtained using blank substrate was applied prior to collection of spectral data.

3.4: Surface characterization

Surface characterization is a significant part of thin film analyses. Various characterization techniques can provide us information ranging from morphology, roughness to chemical nature and bonding structure of the thin film material. Tools used in correlation with achieved properties can help correlate characteristics, thereby explaining some uniquely observed phenomena. Some of the surface characterization tools used in this study are X-ray photoelectron spectroscopy (XPS), Secondary Ion Mass Spectroscopy (SIMS), Fourier Transmission Infrared Spectroscopy (FTIR), X-ray diffraction spectroscopy (XRD).

3.4.1: X-ray photoelectron spectroscopy (XPS)

X-ray photoelectron spectroscopy (XPS) is a surface quantitative technique which measures the elemental composition, empirical formula, chemical and electronic states of the elements that exist within a material. The spectra are obtained by irradiating a material with a beam of X-rays while measuring the kinetic energy and number of electrons that escape away from the top 10 nm of the

film. Surface chemistry of a material in its as-received state, or after some treatment XPS can be analyzed by XPS. Elemental composition and chemical bonding of BCN films can be investigated. The XPS measurements were performed ex-situ transfer in a VG Theta 300 XPS system, which has a hemispherical analyzer and a mono-chromated Al anode x-ray source (1486.6 eV). Using a 2 keV Ar⁺ ion sputtering beam, surface contamination was removed and depth profiling was performed. A pass energy of 20 eV was utilized for collecting high resolution scans of the B1s, N1s, C1s, and O1s core levels as the Ar⁺ beam sputtered through a portion of the film.

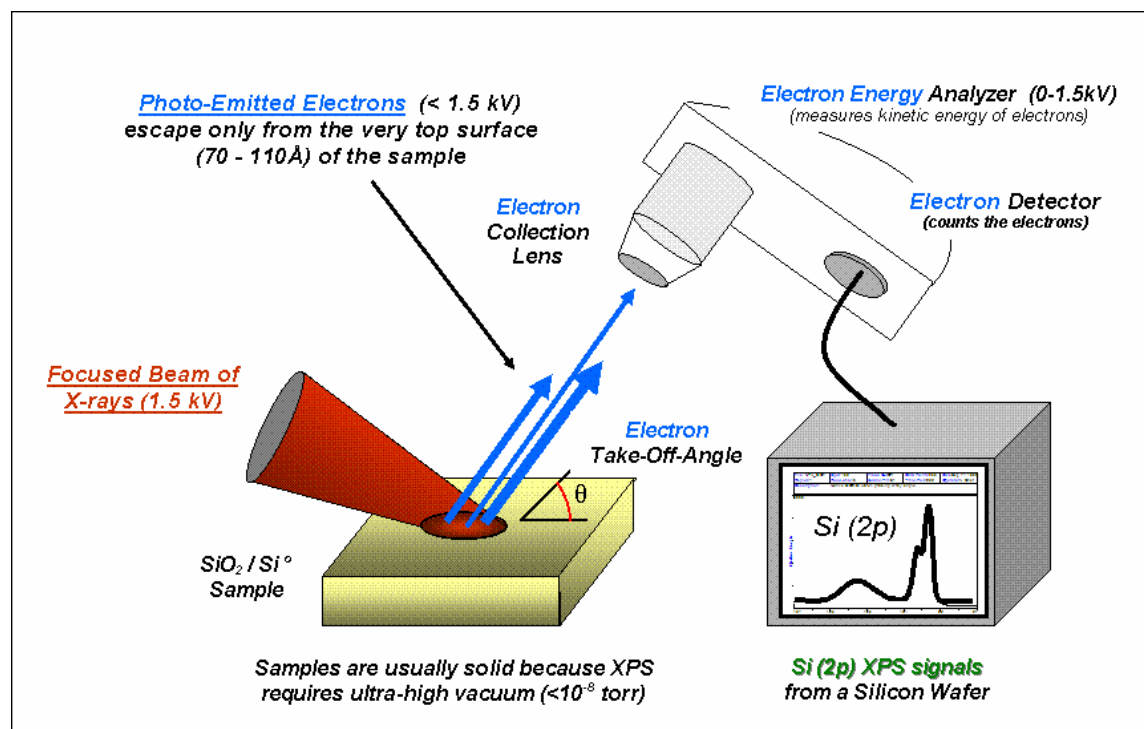


Figure 3.3: An XPS system setup.

3.4.2: Secondary Ion Mass Spectroscopy (SIMS)

Secondary ion mass spectroscopy (SIMS) is a technique for the characterization of solid surfaces and thin films. It uses the process of ion formation by bombarding the surface to be tested with a highly collimated beam of primary ions. The surface then emits material through a sputtering process - only a fraction of these emitted particles is ionized. These secondary ions are measured with a mass spectrometer to determine the quantitative elemental, isotopic or molecular composition of the surface.

The SIMS technique requires high vacuum to ensure undisturbed movement of secondary ions to the detector. The primary ion beam used (often Cs^+ , O_2^- , Ga^+ or Bi clusters like Bi_3^{2-}) determines the detection limits of the instrument. Two surface analysis modes are static and dynamic. Static SIMS is the process involved in surface atomic monolayer analysis, usually with a pulsed ion beam and a time of flight mass spectrometer, while Dynamic SIMS is the process involved in bulk analysis, closely related to the sputtering process, using a DC primary ion beam and a magnetic sector or quadrupole mass spectrometer.

SIMS analysis was performed using a PHI Adept 1010 Dynamic quadrupole SIMS system capable of depth resolution up to 1nm. A cesium (Cs^+) ion source operated at 3 kV and 25nA was used so that oxygen detection can be possible. For depth profile the depth scale was quantified by measuring the analysis craters with a stylus profilometer.

3.4.3: Fourier Transmission Infrared Spectroscopy (FTIR)

Fourier transform infrared spectroscopy (FTIR) is a technique which is used to obtain an infrared spectrum of absorption or emission of a solid, liquid or gas. An FTIR spectrometer simultaneously collects high spectral resolution data over a wide spectral range. This confers a significant advantage over a dispersive spectrometer which measures intensity over a narrow range of wavelengths at a time[27]. The goal FTIR is to measure how well a sample absorbs light at each wavelength. The most straightforward way to do this, the "dispersive spectroscopy" technique, is to shine a monochromatic light beam at a sample, measure how much of the light is absorbed, and repeat for each different wavelength. (This is how UV-Vis spectrometers work, for example.) Fourier transform spectroscopy is a less intuitive way to obtain the same information. Rather than shining a monochromatic beam of light at the sample, this technique shines a beam containing many frequencies of light at once, and measures how much of that beam is absorbed by the sample. Next, the beam is modified to contain a different combination of frequencies, giving a second data point. This process is repeated many times. Afterwards, a computer takes all these data and works backwards to infer what the absorption is at each wavelength. FTIR measurements were performed in both transmission and reflection mode. The transmission FTIR measurements were performed with a Nicolet-Magna-IR 860 spectrometer [28]. The reflection FTIR measurements were performed with the same spectrometer in combination with a Ge attenuated reflection (ATR) cell from Harrick Scientific[29]. Both transmission and reflection FTIR spectra were collected from 400–4000 cm^{-1} with a resolution of 4 cm^{-1} .



Figure 3.4: An example of an FTIR spectrometer with attenuated total reflectance (ATR) attachment.

(Courtesy: https://en.wikipedia.org/w/index.php?title=Fourier_transform_infrared_spectroscopy&oldid=723747621)

3.4.4: X-ray diffraction spectroscopy (XRD)

Crystals are regular arrays of atoms, and X-rays can be considered waves of electromagnetic radiation. Atoms scatter X-ray waves, primarily through the atoms' electrons. Just as an ocean wave striking a lighthouse produces secondary circular waves emanating from the lighthouse, so an X-ray striking an electron produces secondary spherical waves emanating from the electron. This phenomenon is known as elastic scattering, and the electron (or lighthouse) is known as the scatterer. A regular array of scatters produces a regular array of spherical waves. Although these waves cancel one another out in most directions through destructive interference, they add constructively in a few specific directions, determined by Bragg's law:

$$2d \sin\theta = n\lambda$$

Here d is the spacing between diffracting planes, θ is the incident angle, n is any integer, and λ is the wavelength of the beam. These specific directions appear as spots on the diffraction

pattern called reflections. Thus, X-ray diffraction results from an electromagnetic wave (the X-ray) impinging on a regular array of scatterers (the repeating arrangement of atoms within the crystal).

The X-ray diffraction measurements were performed using Panalytical Empyrean with copper X-ray source, operated at 45 kV and 40 mA and the subsequent analysis was performed using Jade 7.5. Incident optics consisted of Bragg Brentano HD fixture with 1/8 degree slit and 1/2 degree anti scatter slit. For detection optics, a pixel 3D detector with 7.5 mm anti scatter slit was used. A depth profile was performed by fixing the sample tilt (ω) relative to the incident beam, and scanning the detector (2θ).

3.4.5: X-ray reflectivity (XRR)

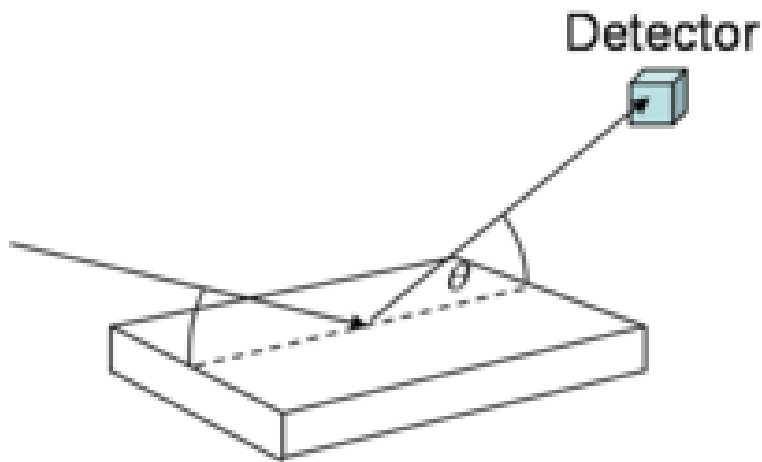


Figure 3.5: XRR specular reflectivity

(Courtesy: https://en.wikipedia.org/w/index.php?title=X-ray_reflectivity&oldid=726048688)

The basic idea behind the technique is to reflect a beam of x-rays from a flat surface and to then measure the intensity of x-rays reflected in the specular direction (reflected angle equal to incident angle). If the interface is not perfectly sharp and smooth then the reflected intensity will deviate from that predicted by the law of Fresnel reflectivity. The deviations can then be analyzed to obtain the density profile of the interface normal to the surface.

The mass density (ρ) of the films was measured by X-ray reflectivity (XRR) using a Siemens D5000 equipped with a Cu line source and graphite monochromator. The data was collected in the range of 0 to 9000–15,000 arc sec with approximately 20 arc sec steps. The XRR spectra were fitted using the REFS software package (version 4.0, Bede). For the simulations, the thickness was fixed at the value determined by ellipsometry and the mass density was adjusted to fit the XRR spectra [30].

3.4.6: Photoluminescence

Photoluminescence (abbreviated as PL) is light emission from any form of matter after the absorption of photons (electromagnetic radiation). It is one of many forms of luminescence (light emission) and is initiated by photoexcitation (excitation by photons), hence the prefix photo- [1]. Following excitation various relaxation processes typically occur in which other photons are re-radiated. Time periods between absorption and emission may vary: ranging from short femtosecond-regime for emission involving free-carrier plasma in inorganic semiconductors [2] up to milliseconds for phosphorescent processes in molecular systems; and under special circumstances delay of emission may even span to minutes or hours.

Observation of photoluminescence at a certain energy can be viewed as indication that excitation populated an excited state associated with this transition energy. While this is generally true in atoms and similar systems, correlations and other more complex phenomena also act as sources for photoluminescence in many-body systems such as semiconductors. A theoretical approach to handle this is given by the semiconductor luminescence equations.

The photoluminescence measurements were performed using a FluoroMax-3 (Horiba Jobin Yvon, Edison, NJ). A 450W xenon arc source was used. The gratings of 1200 grooves/mm in the single excitation and emission monochromators were blazed at 330 and 500 nm respectively. Their reciprocal linear dispersion was equal to 4.25 nm/mm. As a detector, uncooled photomultiplier tube (Hamamatsu, Model R928) was operated in the photon-counting mode. Commercial software (DataMax, version 2.20, Horiba Jobin Yvon) was used for automated scanning and fluorescence data acquisition. The PL measurements were done in both the room temperature and at a low-temperature of 77K. The low-temperature measurements were performed by immersing the sample holding capsule into the liquid nitrogen and the PL excitation and emission characteristics were collected.

3.5: Etching studies of BCN thin films

Based on the limited knowledge of different etching techniques of BN and B₄C thin films, further investigation of BCN etching is conducted. Various dry etching techniques have been employed like using C₄F₆ gas to etch methyl-BCN [31]. Samuel et.al reports advancements in dry etching techniques like inductively coupled plasma using SF₆ on h-BN films [32]. Nguyen et.al demonstrated the magnetron enhanced reactive ion etching (MRIE) system using Freon/Oxygen

(CF_4/O_2) and found out that the etch rate increases with increase in CF_4 gas flows [33]. Dry plasma etching technique like reactive ion etching (RIE) is highly anisotropic and furthermore it can cause surface damage by ion-bombardment [34] [35]. While fluorinated plasma etching is still the mainstay for plasma etching for patterning applications in the semiconductor industry, sometimes wet chemical etching complements dry etching for processes like cleaning and complete removal of deposited BCN on undesirable places. Further, for some specific applications where large line width patterning is required, the wet etching process may be more viable and inexpensive. Watanabe et al. studied the influence of wet chemicals which are used for interconnection integration on BCN. They studied the effects of various chemicals used for post CMP processing and cleaning after dry etching like oxalic acid, dilute hydrofluoric acid ((HF), trimethylammonium hydroxide (TMAH) and ammonium hydroxide on BCN thin films with different oxide concentration [36]. However, they did not focus holistically on the wet chemical etching techniques for BCN films. As BCN thin film wet etching studies are seldom reported elsewhere, the present work reports a detailed analysis on wet etching of BCN thin films.

As BCN thin films are not so reactive, a very good oxidizing agent with better standard reduction potential (SRP) should be considered. The etchant candidate should be such that it should seldom interfere with other components of fabrication like silicon, silicon dioxide or silicon nitride. One of the good candidates would be the common Piranha etch, which is comprised of sulfuric acid (H_2SO_4) and hydrogen peroxide (H_2O_2) in the ratio of 7:3 respectively. Our group tried using freshly prepared Piranha etch at 50°C, 60°C and 70°C and found that it barely etched BCN even for 15-20 minutes duration. Also, the preparation of Piranha etch is highly exothermic which may

result in high temperatures of around 110-130°C [37]. The SRP's of H_2O_2 (in acidic medium), and H_2SO_4 are 1.776V and 0.172V respectively[38]. The high oxidizing characteristics and high reaction temperatures can sometimes oxidize the silicon, silicon nitride and other components during device interconnect fabrication. The SRP of nitric acid (HNO_3) is 0.934V [38], which is a moderate one compared to other acids. Nitric acid oxidizes BCN into B_2O_3 . A good solvent is needed to dissolve B_2O_3 so as to increase the overall etching rate. Phosphoric acid (H_3PO_4) is good at dissolving B_2O_3 and acetic acid (CH_3COOH) provides a good buffer for wetting the substrate. Hence a common aluminum etchant comprising of HNO_3 , H_3PO_4 and CH_3COOH is used as a viable, safe, economic option and an effective etchant at various temperatures.

A basic aluminum etchant was used for the etching studies of BCN thin films. The etchant consisted of 16 parts of phosphoric acid (H_3PO_4), 1 part of nitric acid (HNO_3), 1 part of acetic acid (CH_3COOH) and 20 parts of DI water. 40ml of freshly prepared aluminum etch was filled into a small glass beaker of 100ml capacity. The glass beakers were submerged in a water bath to control the uniformity of the etching temperature. Etching was performed first at room temperature, but the etching was very slow. Hence the temperature was increased and etching was performed at three different temperatures, i.e. a) 50°C, b) 60°C and c) 70°C. The temperatures were monitored with the help of a glass thermometer. Duration of complete etching of the film was monitored by stopwatch. As BCN is hydrophilic in nature, the DI water was used to rinse the etched samples to check whether the sample would turn completely hydrophobic and silver-gray in color denoting the silicon surface.

CHAPTER 4: RESULTS AND DISCUSSION

4.1: Mechanical Properties of BCN thin films

Tables 4.1 and Table 4.2 show the X-ray reflectivity (XRR) mass densities (ρ) for the two sets of BCN films deposited with C/BN and B₄C /BN targets. For both sets of films, sputtering with pure Ar produced the densest films with densities of 2.4–2.5 g/cm³. These values are close to the theoretical density for B₄C of 2.52 g/cm³ (interestingly, the B/(C+O+N) ratio for the B₄C /BN sputter deposited film is 3.7 and also close to that for B₄C).

Table 4.1 summarizes the XPS data for a series of BCN films deposited at room temperature using various N₂/Ar ratios and the C and BN targets. For all films, XPS detected the presence of B, C, N and some oxygen (O) contamination (typically < 3%). The latter is attributed to background H₂O, CO, and CO₂ in the high vacuum sputtering system. Carbon nitride rich (> 95%) BCN films were obtained when sputtering with Ar gas only. However, the B content increased significantly from < 5% to ~ 34% with the addition of just 20% N₂. The B, C, and N content remained relatively fixed at ~ 34, 18, and 45%, respectively with increasing percentage of N₂ working gas [39].

Table 4.1: XPS elemental composition, mass density, and dielectric constant for BCN thin films sputter deposited using C and BN targets and different N₂/Ar gas flow ratios. NM = not measured due to high leakage currents.

% N ₂	% Ar	% B	% C	% N	% O	ρ (g/cm ³)	k
0%	100%	1.7	18.5	78.5	1.3	2.4±0.1	NM
22%	78%	34.2	18.9	45	1.9	2.1±0.1	NM
33%	67%	34.5	19.1	44.9	1.5	2.0±0.1	NM
50%	50%	34.5	16.6	46	2.9	2.1±0.1	4.3±0.1
70%	30%	29.1	14.8	46.2	9.9	2.0±0.1	NM
100%	0%	34.4	18.8	44.7	2	2.0±0.1	5.0±0.1

Table 4.2: XPS elemental composition, mass density, and dielectric constant for BCN thin films sputter deposited using B₄C and BN targets and different N₂/Ar gas flow ratios

% N ₂	% Ar	% B	% C	% N	% O	ρ (g/cm ³)	k
0%	100%	78.8	8.9	5.2	7.2	2.5±0.1	NM
20%	80%	46.5	10.1	32.9	10.5	2.1±0.1	3.9±0.1
33%	67%	45.5	14.4	37.4	2.7	2.1±0.1	4.5±0.1
40%	60%	45.5	14.4	37.4	2.7	2.0±0.1	3.9±0.1
50%	50%	46.1	11.6	32.8	9.6	2.1±0.1	4.6±0.1
100%	0%	44.7	10.6	24.7	20.0	2.2±0.1	4.3±0.1

Figure 4.1 shows a reflection Ge ATR-FTIR spectra for the same set of BCN films sputter deposited using the B₄C and BN targets. For the film deposited using only Ar, a single broad peak centered at ~ 1100 cm⁻¹ was observed. This band is attributed to B-B inter and intra-icosahedral vibrational modes consistent with the large B composition determined by XPS [29]. A faint absorption band at ~ 2500 cm⁻¹ is also observed and attributed to the B-H stretching mode (again consistent with the B rich composition).³⁶ With addition of N₂ sputtering gas, the 1100 cm⁻¹ absorption band shifted to 1400 cm⁻¹ consistent with the T-FTIR spectra collected for the C/BN

sputtered films. Due to the similarities, we similarly attribute this peak to mixed sp^2 BN and CN stretching modes. The intensity of this band increases with increasing % N₂ working gas and then decreases for 100% N₂. This is consistent with the XPS measurements where the N content was observed to increase and then decrease with increasing % N₂.

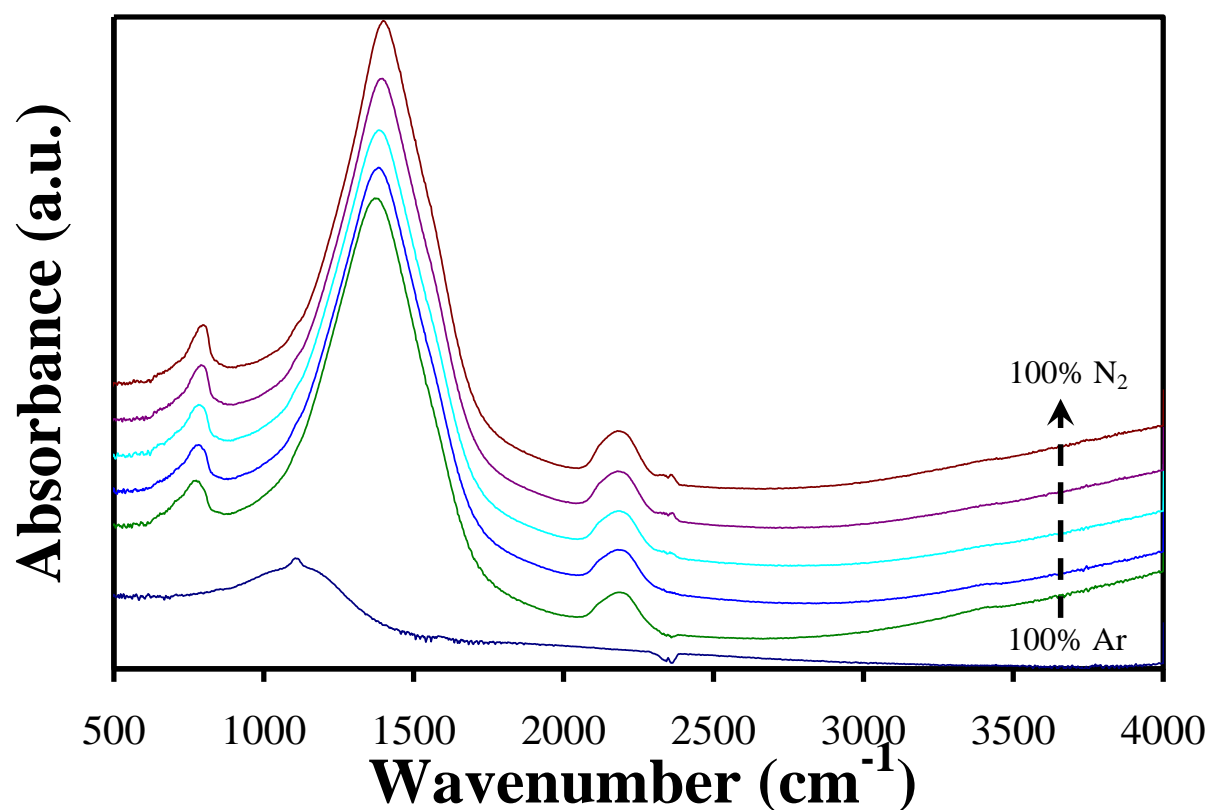


Figure 4.1: FTIR spectra for BCN films sputter deposited at room temperature using C and BN targets and various N₂/Ar gas ratios.

In Figure 4.2, small peaks at 2200 and 3350 cm⁻¹ are also observed. The former has been previously attributed to C≡N bonding. The latter is attributed to N-H bonding consistent with prior

observations of PECVD a-BN:H films. This suggests the presence of a significant amount of hydrogen ($\sim 10\text{-}15\%$) for the B_4C /BN sputter deposited films. Interestingly, the $\text{C}\equiv\text{N}$ and N-H peaks largely disappear for the 100% N_2 sputter deposited film.

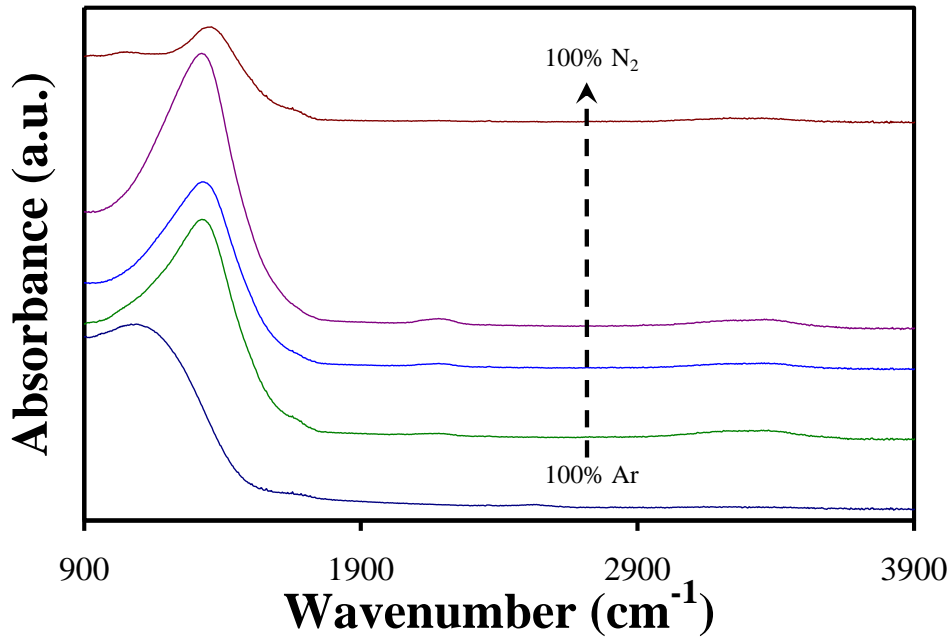


Figure 4.2: FTIR spectra for BCN films sputter deposited at room temperature using B_4C and BN targets and various N_2/Ar gas ratios.

For illustrative purposes, Figure 4.3 presents a plot of Young's modulus as a function of indentation depth (h_c) for two different BCN films sputter deposited using the C and BN targets with and without N_2 sputter gas. For the film sputter deposited using only Ar, Young's modulus increases significantly with indentation depth and then rolls off at ~ 20 nm due to the substantially lower modulus of the underlying Si (100) substrate. In this case, Young's modulus was taken as

the peak value. However, it should be noted that this may cause the value of Young's modulus for this film to be significantly underestimated due to the presence of the softer underlying substrate. The second BCN film shown in Figure 3 (sputter deposited using 20% N₂/ 80% Ar) does not show such a roll off in Young's modulus with indentation depth. In this case, the reported Young's modulus for this film was taken as the baseline value at an indentation depth of ~ 50 nm.

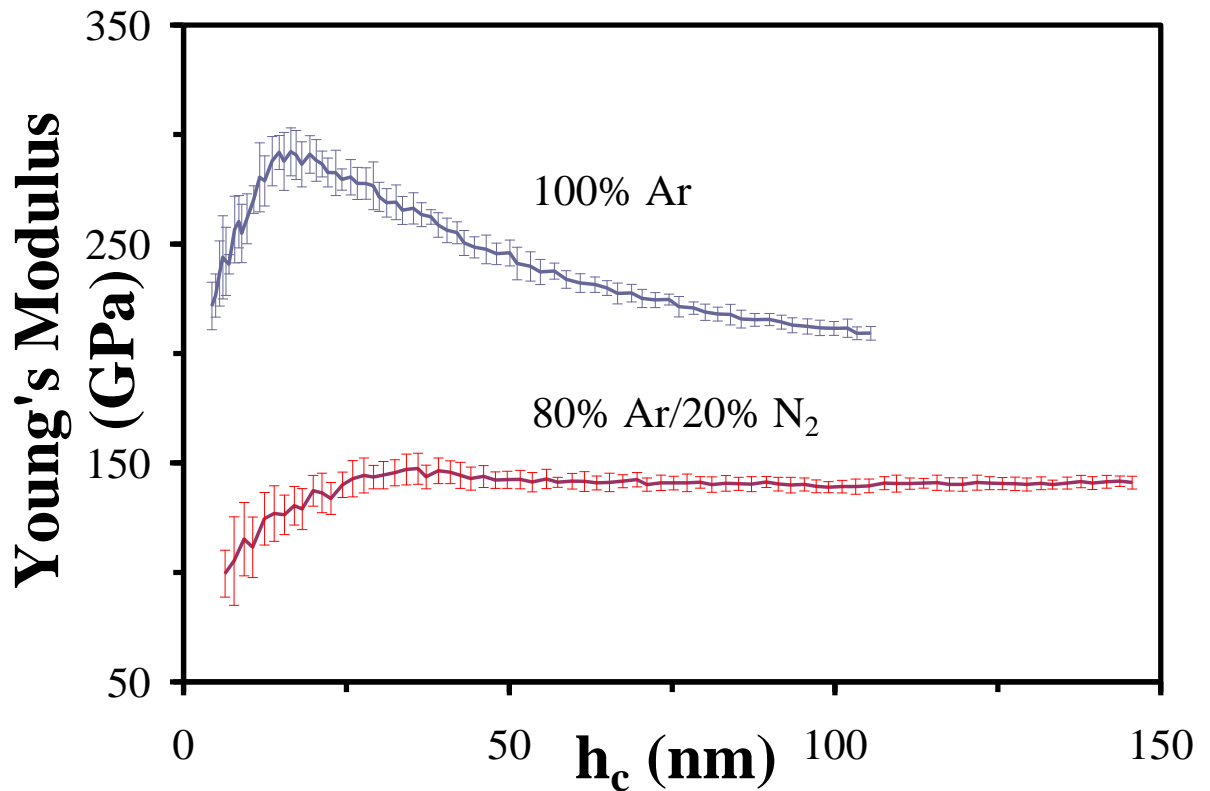


Figure 4.3: Nanoindentation Young's modulus as a function of indentation depth (h_c) for two BCN films sputter deposited using C and BN targets with and without N₂ working gas.

Figures 4.4 and 4.5 present nanoindentation Young's modulus (E) and hardness (H) results as a function of N₂/Ar gas ratio for the BCN films sputter deposited using the C/BN and B₄C/BN

targets, respectively. For films deposited using pure Ar and either set of targets, high values of Young's modulus (~ 285 GPa) and hardness ($30 - 40$ GPa) were observed. These values are consistent with the relatively high values of Young's modulus that have been previously reported for B_4C and sputter deposited amorphous carbon films [29]. However as both Figure 4.4 and 4.5 illustrate, these large values decreased significantly with the addition of N_2 and remained essentially invariant at $100 - 150$ GPa and $6 - 13$ GPa with further addition up to 100% N_2 . This is consistent with the significant decrease in mass density that was also observed when N_2 was added to the Ar sputtering gas.

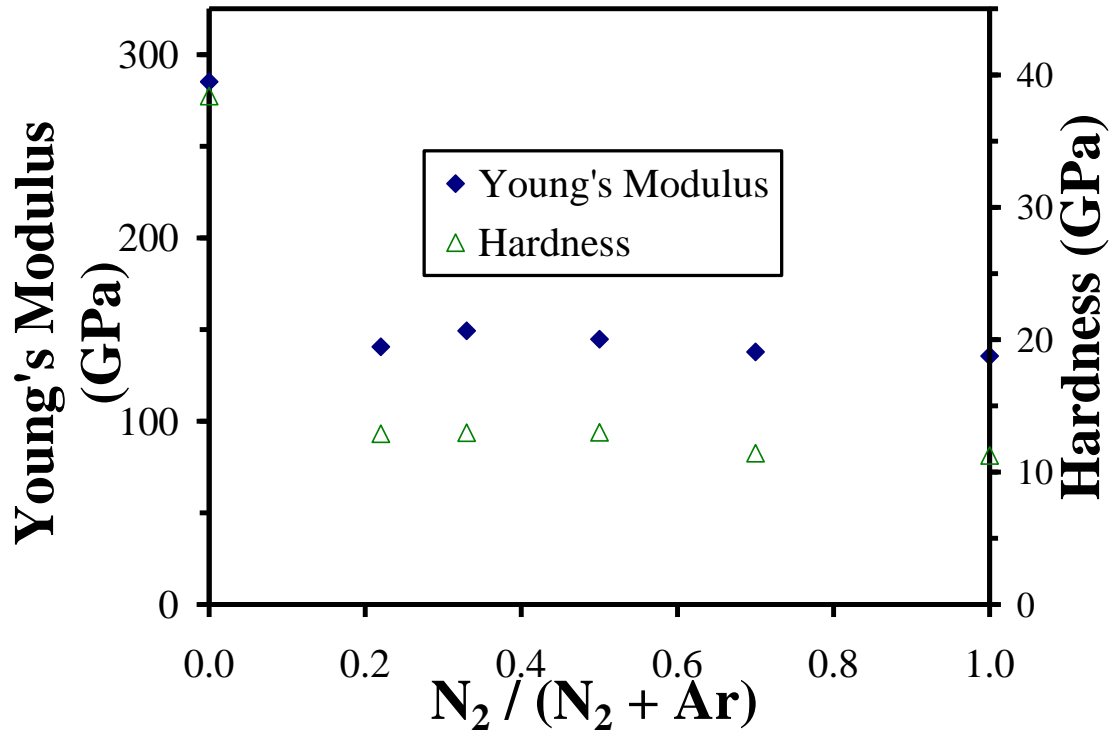


Figure 4.4: Nanoindentation Young's modulus and hardness as a function of $N_2/(N_2+Ar)$ gas ratio for BCN films sputter deposited using C and BN targets.

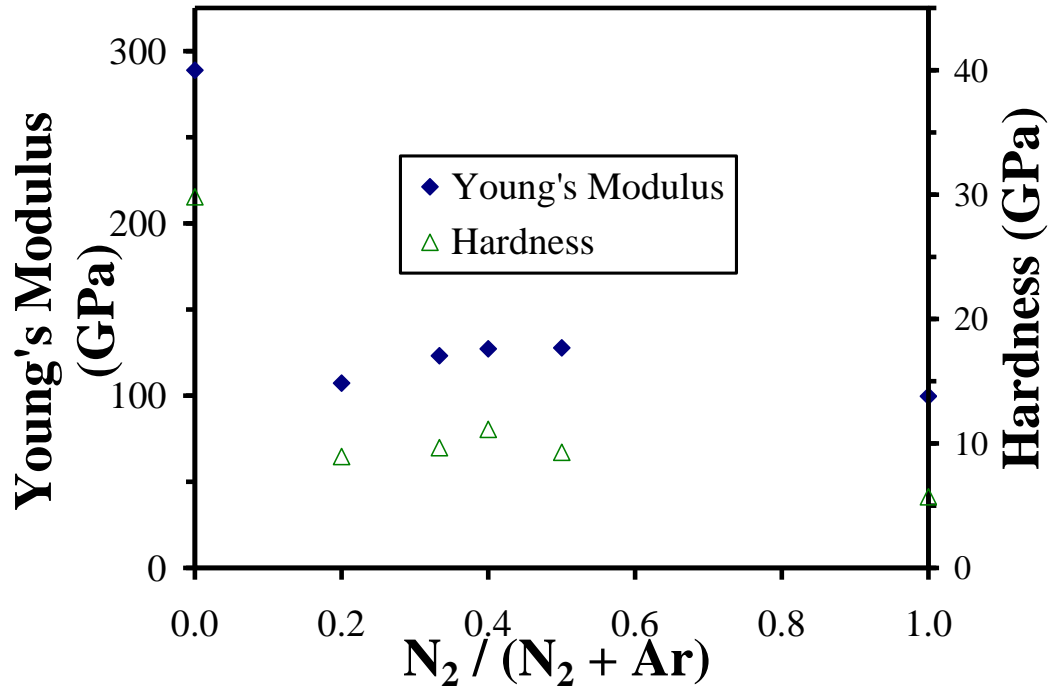


Figure 4.5: Nanoindentation Young's modulus and hardness as a function of $N_2/(N_2+Ar)$ gas ratio for BCN films sputter deposited using B_4C and BN targets.

The decrease in BCN mechanical properties with addition of N_2 sputtering gas is also consistent with the change in composition of the deposited films where the films sputtered in pure Ar were boron or carbon rich while those sputtered in Ar/ N_2 mixtures were closer to BN in composition and sp^2/h -BN in chemical structure. Reduced mechanical properties for BCN films have been previously reported. For example, Perrone et al. have reported microhardness values of ~ 2.9 GPa for BCN films deposited using pulsed laser ablation of graphite and hexagonal boron nitride (h-BN) targets[40]. Thus, the observed mechanical properties for the BCN films deposited here are consistent with the literature and the reduced mechanical properties for the Ar/ N_2 sputter deposited films can be attributed to the predominate BN composition and sp^2/h -BCN chemical

structure.

Included in Table 4.3 are the nanoindentation Young's modulus and hardness values for BCN films sputter deposited using B₄C and BN targets with various DC and RF biases. High modulus and hardness values exceeding 250 and 25 GPa, respectively, were observed in all cases. This is consistent with the high B content and BC structure exhibited by these films. Unfortunately, no clear trends were observable between the mechanical properties and the variation in DC and RF bias for the sample set investigated here. There are also no obvious correlations between the mechanical properties and the percentage or ratio of elements detected by XPS in these films.

Table 4.3: XPS elemental composition and nanoindentation Young's modulus and hardness for BCN thin films sputter deposited using B₄C and BN targets and varying DC and RF biases.

RF-BN (W)	DC- B ₄ C (W)	% B	% C	% N	% O	E (GPa)	H (GPa)
200	100	69.2	11.1	17.9	1.9	300	27.0
200	150	72.1	12.7	13.9	1.4	283	25.0
200	200	73.8	13.8	11.1	1.3	306	26.7
150	200	76.1	15.4	7.2	1.4	256	22.5
100	200	76.2	16.3	3.5	4.0	322	28.7

However, the mechanical properties for this last set of BCN films were all high with a maximum nitrogen content of only 18%. In comparison, the minimum nitrogen content for the previous BCN sample sets was 24% and the mechanical properties were greatly reduced. This observation is consistent with a prior study of BCN by Martinez et.al where the hardest films were those with the lowest nitrogen concentration and a minimum in hardness was observed at a nitrogen concentration of ~ 20%.¹³ Based on these observations, one may conclude that

maintaining nitrogen content to $< \sim 20\%$ may be ideal for achieving BCN films with the highest possible mechanical properties.

4.2: Deposition and XPS studies of dual sputtered BCN thin films

Figure 4.6.a) shows the plot of deposition rate as a function of various BN (RF) target powers while maintaining BC power at 100W. The deposition rate shows an increasing trend. This can be explained as follows. With the increase in BN power, there is a scope of increasing incorporation of nitrogen in the BCN film. The more the BN power, the more easily the nitrogen is incorporated. Hence this favors the formation of BCN with increase in BN power subsequently increasing the deposition rate. Figure 4.6.b) shows the plot of deposition rate as a function of B₄C (DC) target powers while maintaining BN power at 100W. The nitrogen gas flow ratio is kept at 0.25 of total gas flow, intentionally to allow the impact of DC/RF power variation on rate of deposition of BCN films. For this study, the films are deposited at room temperature conditions. In case of films deposited by varying B₄C DC power, the deposition rate shows a decreasing trend with increasing target power. This may be due to the fact that, the deposition rate of B₄C is greater than BN. The sputtering yields of B₄C and BN are 0.567 atoms/ion and 0.2 atoms/ion [41] respectively. While forming BCN, B bonds preferentially with nitrogen than carbon and with the increase in B₄C power, there is a lesser incorporation of nitrogen into the film. A majority of boron concentration remain as an elemental mixture without forming stable BCN compound. Hence the rate of formation or the deposition rate slows down by a small amount with increasing DC power.

a)

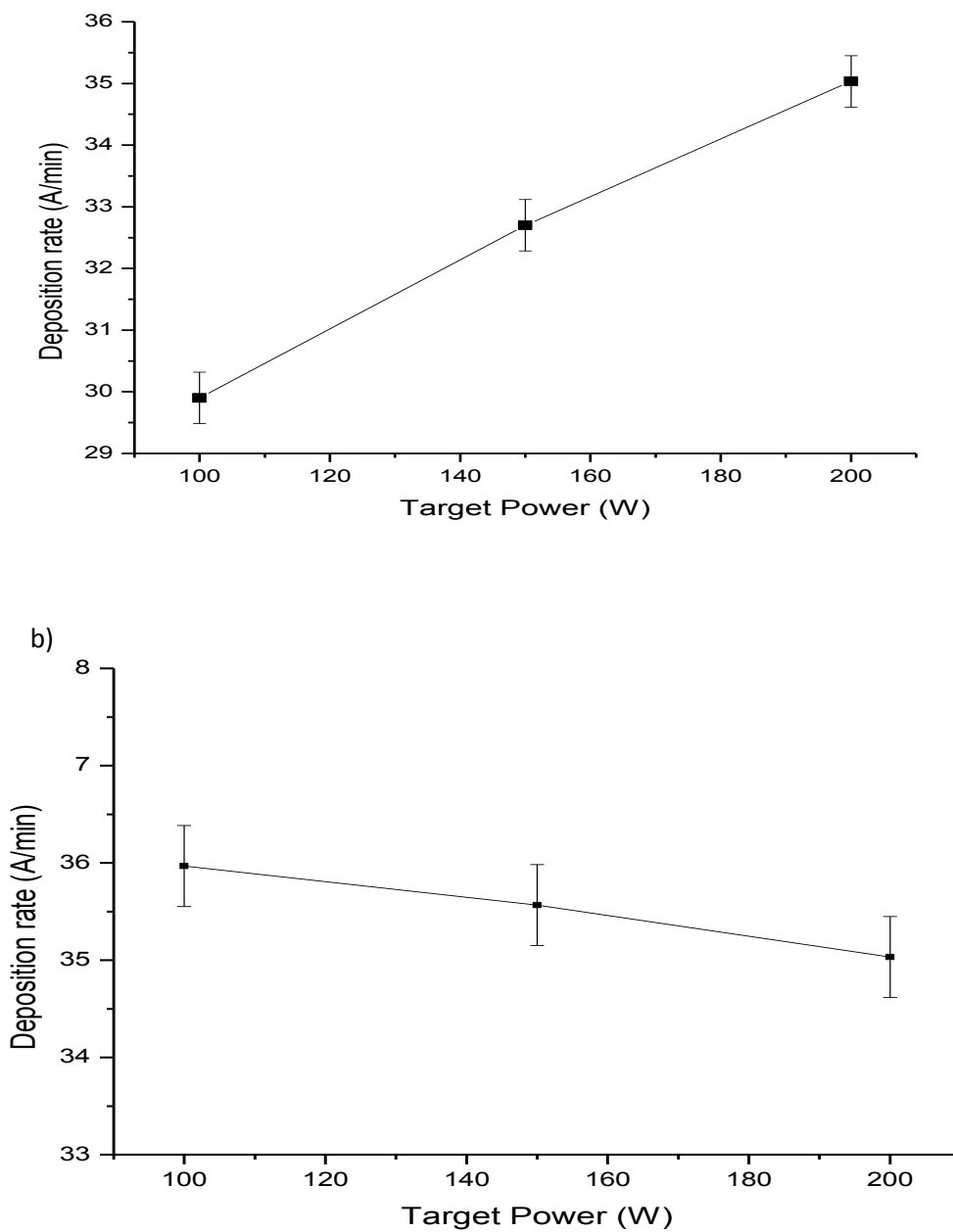


Figure 4.6: a) Deposition rate as a function of RF target power to BN target, 100W DC power to BC target and b) Deposition rate as a function of DC target power to B₄C target, 100W RF power to BN target.

Figure 4.7 shows plot of deposition rate as a function of various substrate deposition temperatures. The target powers of both B_4C and BN are maintained at 200W. The deposition rate shows a decrease in trend with increasing substrate deposition temperature and an increase in trend can be observed at 400°C. Our group had previously demonstrated similar trend during the deposition of BCN thin film using the single B_4C target using RF reactive magnetron sputtering and nitrogen as reactive gas [42]. The films deposited at 200W RF/DC and at 400°C shows the highest deposition rate.

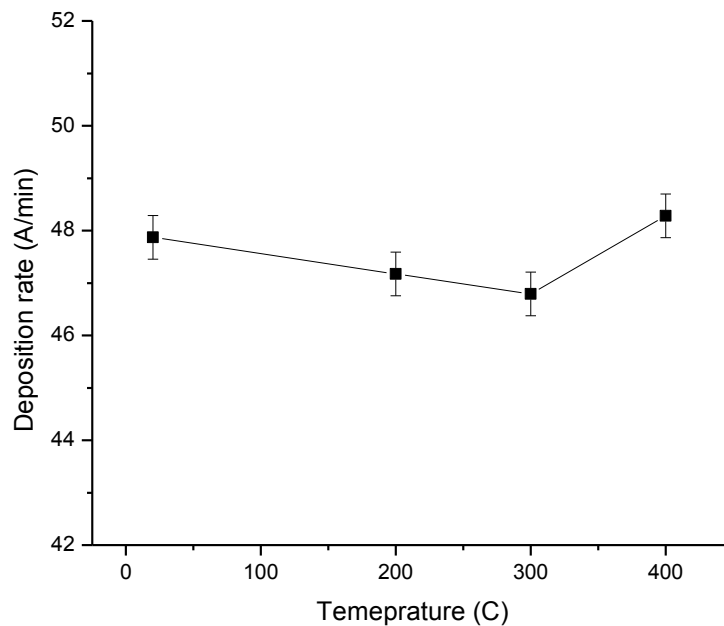


Figure 4.7: Deposition rate as a function of substrate deposition temperature at Ar = 20sccm and 200W power for both the targets.

In this section, as the main focus is on the effect of gas flow ratio on the deposition rate of BCN thin films, the BN target power has been kept constant at 250W and the B_4C target power is varied

at 20W and 40W. By maintaining a high BN target power and a low B₄C target power, an attempt has been made to keep both the targets' deposition rate similar, since the yield of BN target is very low as compared to B₄C target. This keeps the focus only on the deposition rate due to varying gas flow conditions rather than varying target power conditions. Table 4.4 provides the percentage composition of C, N and B in the BCN film deposited at various N₂/Ar gas flow ratio at 20W DC power and RF power of 250W. This is calculated from high resolution spectra of XPS for each element. The percentage compositions of carbon and boron show decreasing trend with increase in the N₂/Ar gas flow ratio in the range of 0.25 to 0.75, later increases with increase in gas flow. The concentration of nitrogen shows an increasing trend with increase in N₂/Ar gas flow ratio from 0.25 to 0.5. There is a significant loss in nitrogen concentration thereafter yielding to a lower composition nitrogen which remains constant from N₂/Ar gas flow ratio 0.75 to 1. The loss of carbon concentration and gain in nitrogen concentration shows that more BN like films are deposited at higher gas flow ratios and it favors more BN formation with increase in gas flow ratio. BCN films deposited at N₂/Ar = 1 has the highest concentration of carbon and the lowest concentration of nitrogen, hinting the formation of carbon rich BC like films. This can be explained as follows. The sputtering yield reduces with increase in nitrogen. So due to this, the overall yield coming from both the targets is reduced. As the sputter yield of B₄C is more compared to BN target, there is an increase in the carbon concentration in the films deposited at N₂/Ar gas flow ratio of 1.

Table 4.4: The percentage composition of B, C and N in the BCN thin film deposited at various N_2/Ar gas flow ratio at 20W DC power with constant RF power of 250W calculated from XPS data.

N_2/Ar gas flow ratio	%C	%N	%B
0.25	66.2	28.5	5.3
0.5	61.8	35.6	2.6
0.75	79.7	12.6	7.7
1	82.7	12.7	4.6

Figure 4.8 shows the deposition rates of BCN thin films for substrate deposition temperatures 200°C and 300°C as a function of various gas flow ratios at 20W DC keeping the RF power of BN constant at 250W. They show a decreasing trend with increasing N_2/Ar gas flow ratios till $N_2/Ar = 0.75$. Then it shows an increasing trend at $N_2/Ar = 1$. This can be attributed to the fact that increase in nitrogen gas in the sputtering ambience decreases the effective sputtering yield due to nitridation of the target [42]. Based on the XPS measurements from Table 4.4, it is observed that, initially BN formation is more favored with increase in gas flow ratio from $N_2/Ar = 0.25$ to 0.75 and BC is favored thereafter. As the deposition rate of BN is lower than that of BC and favorability of formation of BN is more with increase in gas flow ratio, the overall deposition rate decreases with increase in gas flow ratio. But at $N_2/Ar = 1$, as BC formation is more favored, hence increase in the deposition rate is observed.

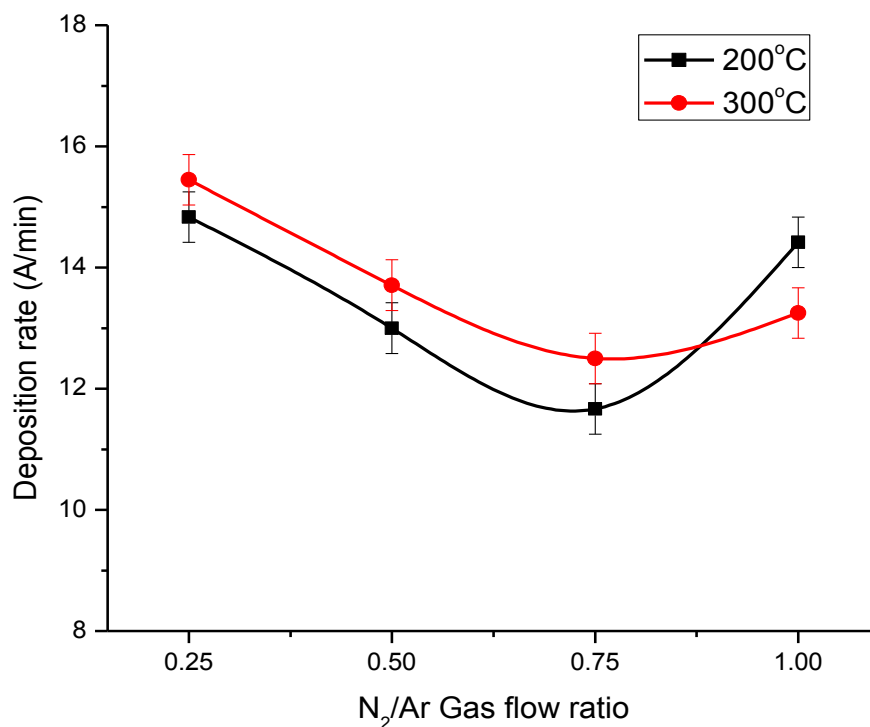


Figure 4.8: Deposition rate as a function of various gas flow ratios at 20W DC

Table 4.5 provides the percentage composition of C, N and B in the BCN thin film deposited at various N₂/Ar gas flow ratio at 40W DC power and RF power of 250W. The concentration of carbon and nitrogen both has an initial increasing trend when the N₂/Ar gas flow ratio is increased from 0.25 to 0.5. But subsequently it shows decreasing trend with increase in N₂/Ar gas flow ratio. Boron shows a decrease in its concentration with increase in N₂/Ar gas flow ratio from 0.25 to 0.75 but increases at N₂/Ar = 1.

Table 4.5: The percentage composition of B, C and N in the BCN thin film deposited at various N₂/Ar gas flow ratio at 40W DC power with constant RF power of 250W calculated by XPS

N ₂ /Ar Flow Ratio	%C	%N	%B
0.25	38.87	47.74	13.3
0.5	55.50	36.43	8.08
0.75	52.43	42.10	5.45
1	39.99	47.02	12.91

Figure 4.9 shows the deposition rate as a function of various gas flow ratios at 40W DC for BC target with a constant RF power of 250W to the BN target. The deposition rate characteristics can be explained from Table 3. The concentration of the carbon increases initially from N₂/Ar = 0.25 to 0.5 with decrease in concentration of nitrogen and boron. This explains the favorable formation of more BC rich film and hence this leads to greater deposition rate of BC target. Therefore, overall deposition rate increases. From N₂/Ar = 0.5 to 0.75, the deposition rate decreases, this can be explained due to decrease in the carbon concentration and subsequent increase in the nitrogen concentration. Hence the formation of BN rich film is favored and as deposition rate of BN is low, the overall deposition rate decreases. There is an increasing trend found in the end from N₂/Ar = 0.75 to 1. The concentration of carbon and boron has increased and the concentration of nitrogen has decreased. This increase in trend can be attributed to the fact that the rate of formation of BCN is favored more due to chemical reaction than the decreasing sputtering yield as a result nitridation of the target [42].

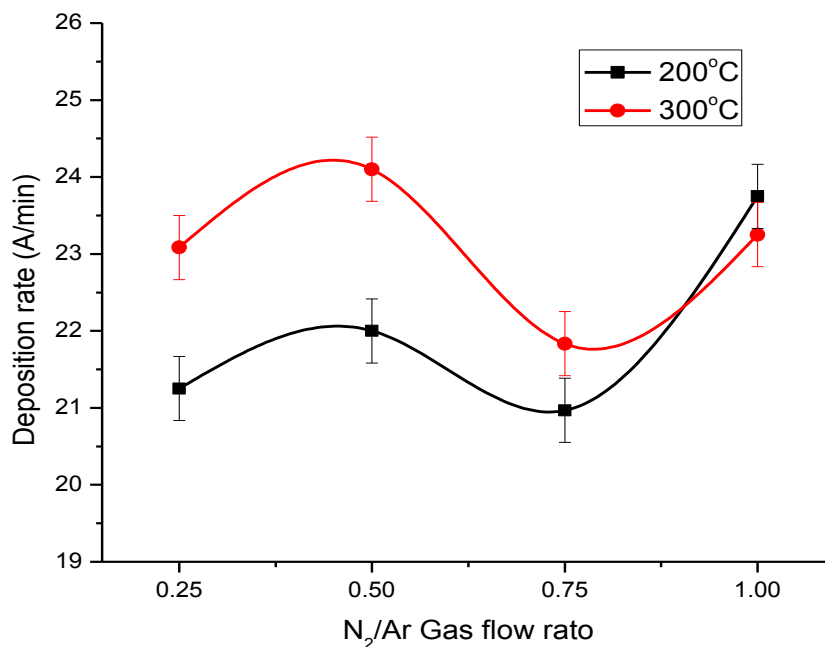


Figure 4.9: Deposition rate as a function of various gas flow ratios at 40W DC

Figure 4.10 shows the N1s high resolution scan for various gas flow ratios and target powers. The peaks between 397 and 397.5 are assigned to B-N bonds [43]. The peaks between 398 and 398.5 eV can be attributed to sp^3 N-C. According to the literature, the peaks between 399 and 399.5 eV are due to sp^2 N-C bonding [44, 45]. The peak between 400.5 and 401 eV can be attributed to the presence of N-O bonds formed as a result of contamination [46]. For films deposited at 20W DC for various gas flow ratios the BN peak remains fairly same throughout. The peak intensity of sp^3 -NC decreases from a) to b) and then an increase in trend is observed from c) to d). But the exact opposite trend is observed in case of sp^2 -NC formation for all samples deposited at 20W DC for various gas flow ratios. In case of films deposited at 40W DC, there is N1s peak shift towards higher binding energy, which indicates the higher concentration of carbon and more concentration

of sp^2 -NC bonds [47]. The BN peak intensity decreases from a) to b) with highest intensity at c) and it is either absent or very negligible at d). The N1s alone does not help much to find the bonding states because the difference between the binding energies of N-B and N-C bonds is relatively small. Therefore it is difficult to interpret [48].

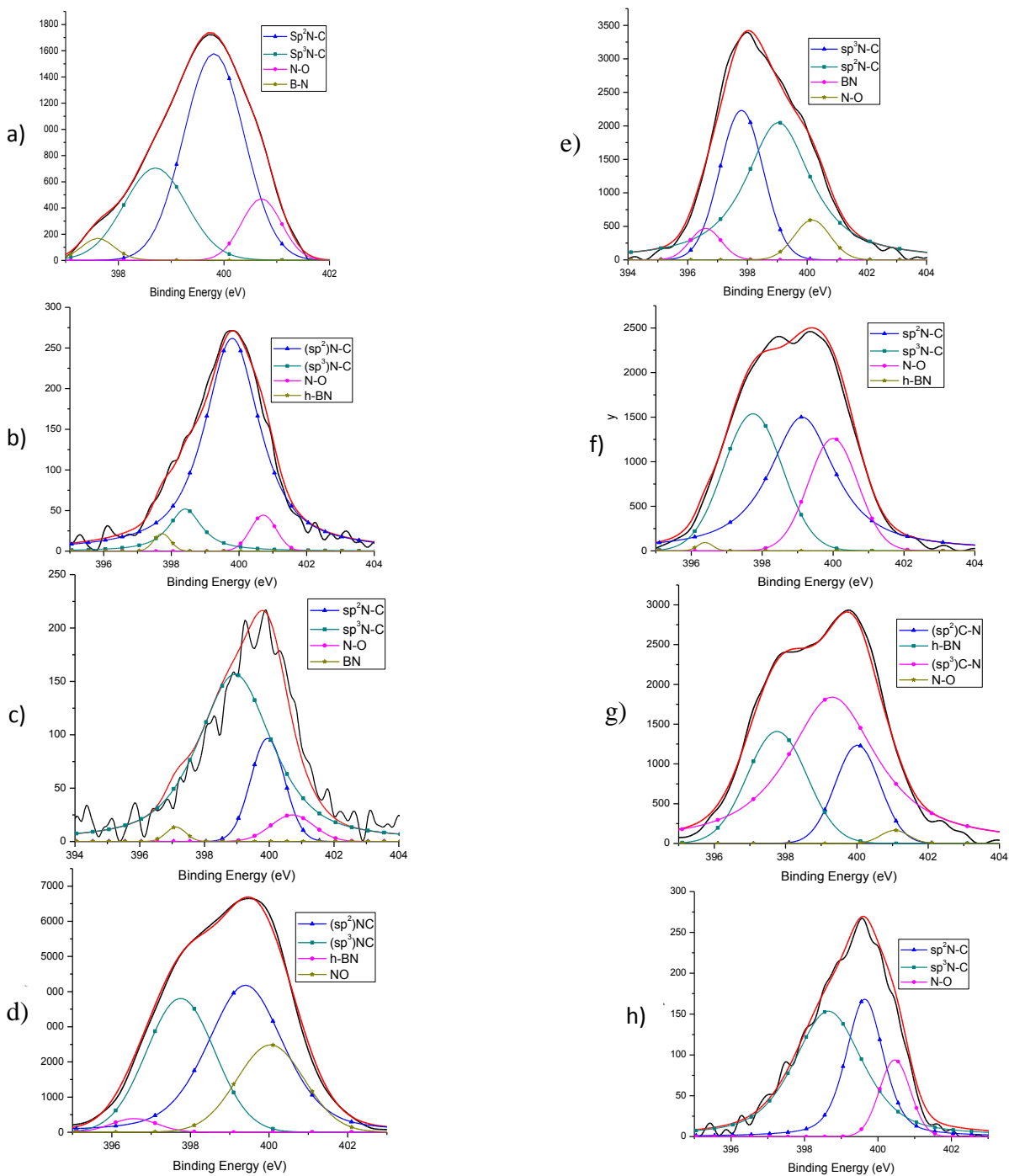


Figure 4.10: XPS narrow scan of N1s for BCN thin films deposited at 20W DC and $N_2/Ar =$ a) 0.25, b) 0.5, c) 0.75 d) 1; 40W DC and $N_2/Ar =$ e) 0.25, f) 0.5, g) 0.75, h) 1.

Figure 4.11 shows the high resolution scan of C1s for various gas flow ratio and target powers. The peak at 284.6 eV denotes the presence of adventitious carbon [49]. The peaks found at ~284.3 eV and 282.9 eV can be attributed to BC₃ and B₄C respectively [50, 51]. The C-N bonds can be found at ~286-286.9 eV [50, 52]. The second peak found at ~287.3 eV can be attributed to (sp³) C-N peak [53]. The peaks resulted from C-O contamination can be located at ~288-288.5 [43, 44]. According to Mannan et.al, the broader C=C peaks may or may not constitute a B-C-N hybrid and the prominent CN_x phase can be separated from the hybrid [47]. From Figure 6, for films deposited at 20W DC, BC peak intensity decreases from a) to c), but increases its intensity at d). The broadening of C-N peak is found towards films deposited at higher N₂/Ar gas flow ratio and becomes prominent at N₂/Ar gas flow ratio = 1. In case of films deposited at 40W DC, the peak intensity of BC fairly remains constant. The C=C peak intensity is observed to be relatively lower and narrower as compared to previous case. The C-N peak appears to slightly shift towards lower energy for f) to h), this may be due to lower concentration of C.

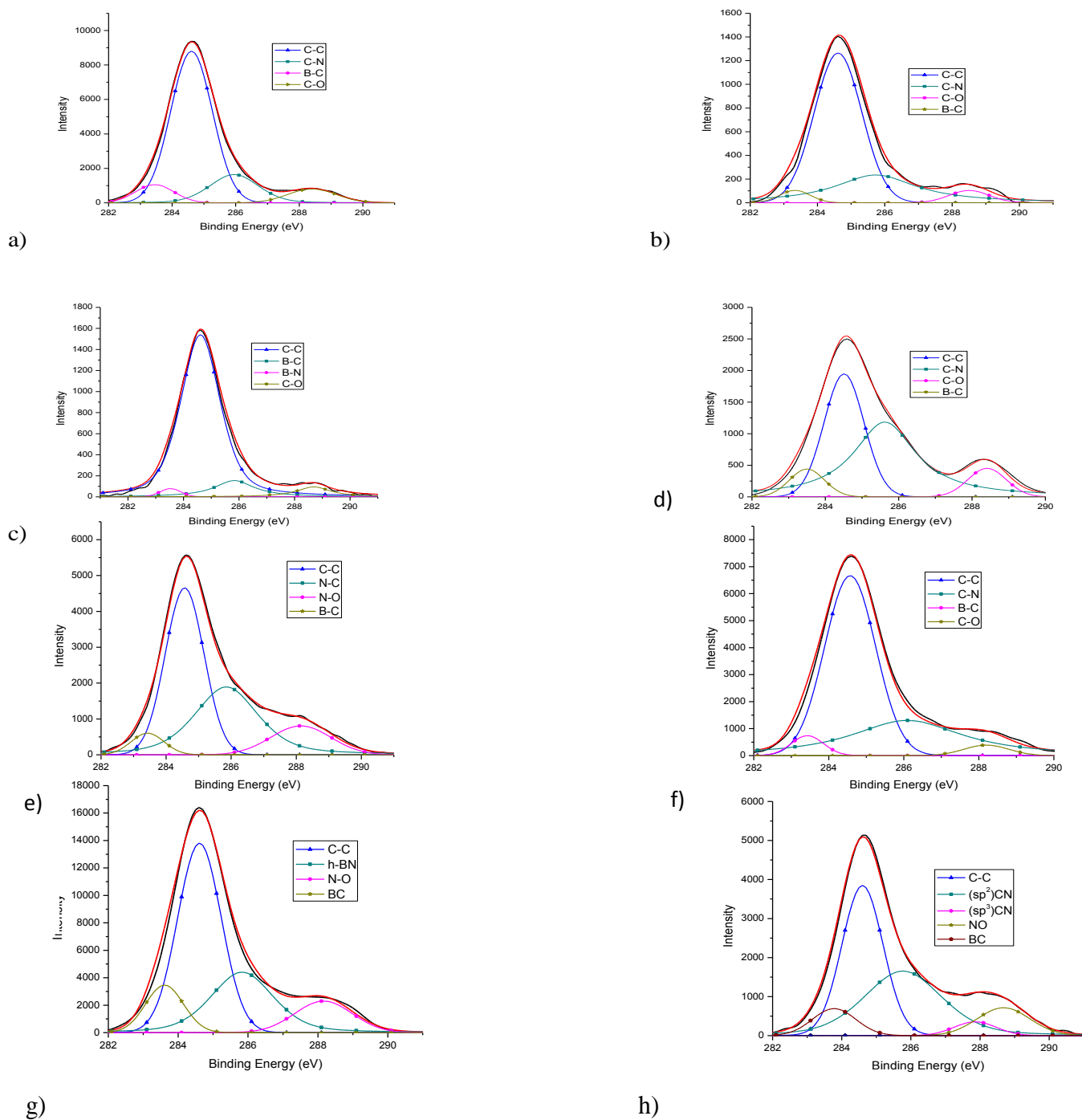


Figure 4.11: XPS narrow scan of N1s for BCN thin films deposited at 20W DC and $N_2/Ar =$ a) 0.25, b) 0.5, c) 0.75 d) 1; 40W DC and $N_2/Ar =$ e) 0.25, f) 0.5, g) 0.75, h) 1.

Figure 4.12, shows the high resolution peak of B1s for various gas flow ratios and target powers. The peaks found at ~188.4 eV , ~189.5 eV and 188 eV can be attributed to B₄C, BC₃ and a-BCN respectively [50]. The peak found at 190 eV can be attributed to h-BCN [47]. The hybrid bonds of B-C-N can be found at a diverse binding energies at ~188-191.0 eV [47] but more dominating peak at ~189.6 eV is found to be that of B-C-N atomic hybrids [54-57]. The peak at ~190.5 eV can be assigned to h-BN [58]. Lastly, the peaks at ~192 eV and ~193.2 eV can be assigned to BCO₂ and B₂O₃ respectively [59]. The peak shifts towards the higher binding energy is because of the various factors such as surface contamination and instrument sensitivity. An increase in the BC peak intensity can be observed in case of BCN films deposited at 20W DC and for N₂/Ar gas flow ratio from 0.25 to 0.75. BC peak is either absent or negligible for BCN film deposited at N₂/Ar gas flow ratio = 1. The peak intensity of BCN, is observed to be an increasing trend and the absence of BN peak in Figure 4.12.d) denotes the complete hybridization of BCN. BN peak intensity fairly remains same throughout. In case of BCN films deposited at 40W DC, BN peak is found to be completely absent for N₂/Ar gas flow ratio of 1. This is due to the complete hybridization of BC into BCN peak. This can be confirmed from the broadening of the BCN peak at higher gas flow ratio. Here the dominating center peak is BCN. As compared to BCN films deposited at 20W DC, clear broader peaks of BCN are found. The prominent BCN peak is observed at N₂/Ar gas flow ratio = 1.

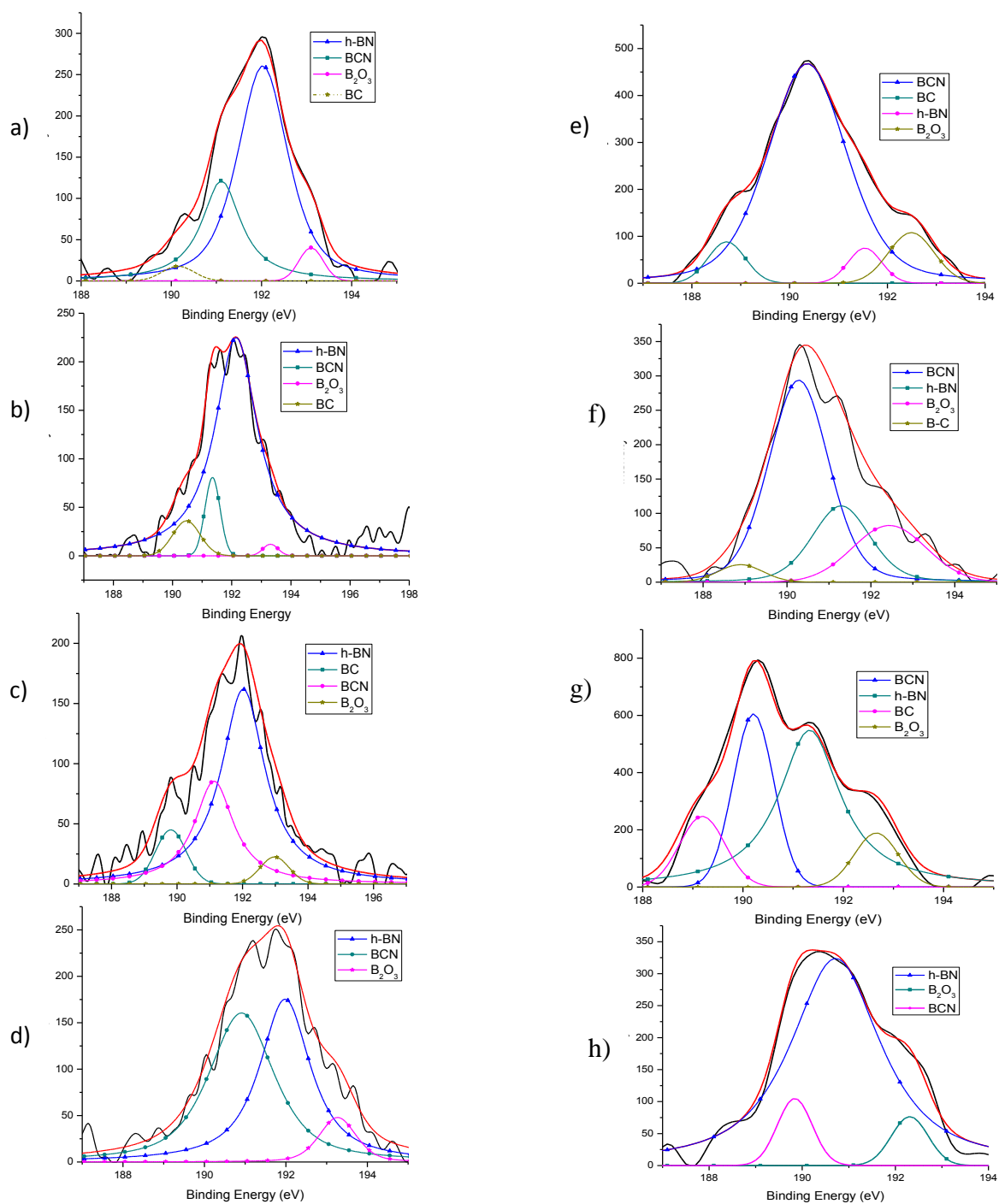


Figure 4.12: XPS narrow scan of B1s for BCN thin films deposited at 20W DC and N_2/Ar = a) 0.25, b) 0.5, c) 0.75 d) 1; 40W DC and N_2/Ar = e) 0.25, f) 0.5, g) 0.75, h) 1.

4.3: Feasibility of etching studies on BCN thin films

Investigation of wet chemical etching Boron carbon nitride (BCN) thin films deposited by dual magnetron sputtering of B₄C (DC) and BN (RF) targets was conducted. BCN, a low-k dielectric material, is a potential candidate as inter-layer dielectric (ILD) in VLSI process. A common aluminum etchant consisting of phosphoric acid (H₃PO₄), nitric acid (HNO₃) and acetic acid (CH₃COOH) was tested for its feasibility as a good etchant for BCN thin films. The etching studies were performed on BCN films that were deposited at room temperature, 200°C and 300°C as a function of various N₂/Ar gas flow ratios in an rf sputtering technique. It was found that the film deposited at higher temperatures shows lower etching rate trends. Activation energies (E_a) were calculated for each N₂/Ar gas flow ratio with the help of Arrhenius plots and compared with respect to elemental compositions of the films.

Table 4.6 shows the percentage elemental compositions of B, C, N, and O in BCN films that were deposited at various substrate temperatures and pressures. During the deposition process of the BCN films, B and C can form compounds reacting with N or with each other. Therefore, the process of N integration and the reciprocity among B, C and N during the deposition become the main factors, which affect the composition and properties BCN films [42]. According to the literature [48, 60], many XPS analyses report that, the BCN chemical composition can either be a stable ternary BCN and/or a mixture of CN and BN phases [61, 62]. Lei et.al reports that B-C can exist in two different phases namely, B₄C and BC₃ depending on the film's boron and carbon compositions [63]. The BCN films deposited at room temperature, in Table 4.6 show an overall carbon rich film with low boron concentration. Hence, we can deduce that the as-deposited BCN films may be dominated by a mixture of CN, BN and BC₃ phases. The films deposited at 200°C

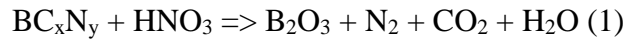
show boron rich films with low nitrogen concentration. These films can be assumed to consist of CN, BN, and B₄C phases. Comparable concentrations of carbon and nitrogen with a considerable amount of boron can be seen for films deposited at 300°C. CN phase may dominate in this condition. Traces of BCN or a considerable amount of it can also be found in all the process conditions.

Table 4.6: Percentage elemental compositions of B, C and N at various N₂/Ar gas flow ratios and substrate deposition temperatures.

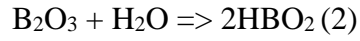
N ₂ /Ar	Percentage elemental composition											
	Room Temperature				200°C				300°C			
	B	C	N	O	B	C	N	O	B	C	N	O
0.25	3.1	74.2	19.3	3.4	63.2	27.2	5.1	4.5	12.2	43.2	40.0	4.6
0.5	13.1	48.1	31.2	7.6	59.6	34.3	2.5	3.7	12.0	42.5	40.1	5.4
1	8.8	53.7	27.2	10.3	74.2	10.9	4.6	7.3	19.6	25.3	50.3	4.8

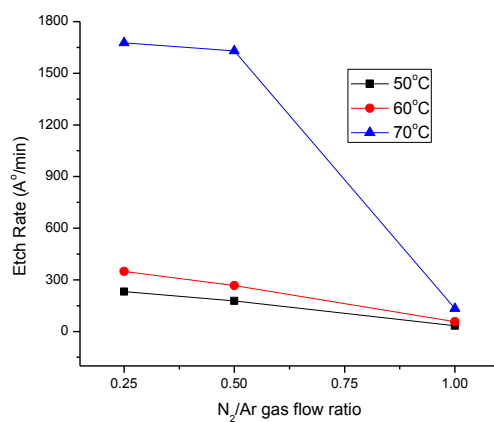
Usually, wet etching involves oxidation of the surface and dissolution of the resulting oxides [64]. The CH₃COOH helps in buffering and wetting. It is considered as a good industrial solvent. HNO₃ is a strong oxidizing agent which reduces BCN into B₂O₃. The proposed reaction is given in equation (1). According to literature, hot H₃PO₄ is said to dissolve BN [65]. Hence, it can be considered as an additional oxidizing agent to reduce BCN as well. DI water is used for dilution. It is also found that, hot water dissolves B₂O₃ into metaboric acid (HBO₂) [66] as shown in the equation (2). Films deposited by sputtering may result in BCN and parts of boron carbide (B₄C) and boron nitride (BN). According to the literature, B₄C is insoluble in acids but soluble in fused salts and alkaline hydroxides like potassium hydroxide (KOH) [67]. There is a limited solubility

of BN in hydrochloric acid (HCl), hydrofluoric acid (HF), sulfuric acid (H₂SO₄), phosphoric acid (H₃PO₄) and hydrogen peroxide (H₂O₂) [67]. Therefore, by choosing the combination of nitric acid and phosphoric acid with good wetting solvent like acetic acid, the BN part of BCN can be attacked to yield B₂O₃. Hence the above said etchant is chosen to perform the etch studies of the BCN films.

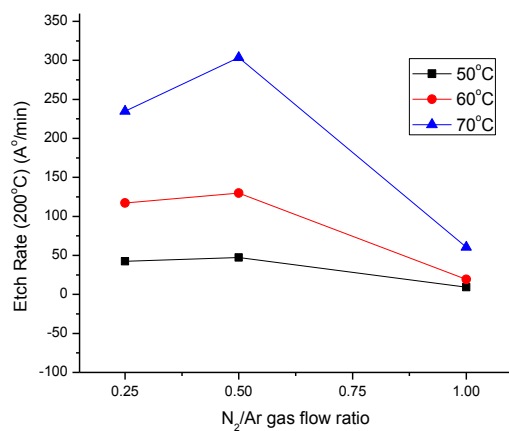


x and y denotes various possible compositions of carbon and nitrogen in BCN thin films.

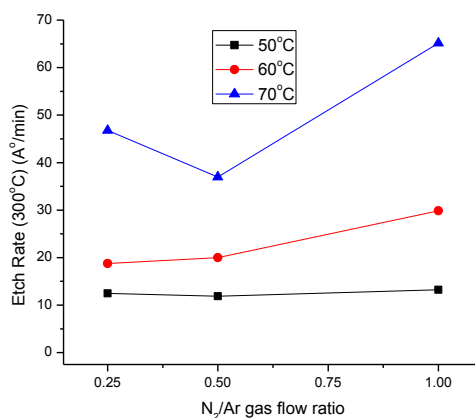




a.)



b.)



c.)

Figure 4.13: Etch rate as a function of N₂/Ar gas flow ratio at various etching temperatures for films deposited at a.) Room temperature, b.) 200°C, c.) 300°C.

Figure 4.13 shows the BCN etch rate as a function of N_2/Ar gas flow ratio at different etching temperatures. It is observed that the etch rate is lower for films deposited at higher temperatures. The X-ray diffraction (XRD) studies performed on the films indicated that, the films deposited at higher temperatures improved their grain sizes. Several literatures also report the increase in grain size with the increase in deposition temperature. Mannan et.al. reports significant increase in grain size for RF sputtered BCN films with increase in deposition temperatures[68]. Similar work by the same group on microwave plasma CVD deposition of BCN has deduced that, the BCN films can be found in crystalline forms of h-BCN in short-range order when deposited at 300 W and 400 W process power [69]. In this study, the BCN was deposited at 250W BN target power and 20W B_4C target power. This higher target power and increase in deposition temperatures might have assisted increase in grain size. Hence, lower temperature deposited films etched faster thereby having the highest etch rate.

For the room temperature deposited films, it shows an overall decreasing trend with respect to increase in N_2/Ar gas flow ratio. The films etched at 70°C show the highest overall etch rate. It is interesting to note that, the etch rate is lowest and similar for all the films deposited at $N_2/Ar = 1$. A similar trend can be found in the films deposited at 200°C. The etch rate remains almost same for films deposited at $N_2/Ar = 0.25$ and 0.5 but decreases by a great factor at $N_2/Ar = 1$. A carbon rich film is deposited at $N_2/Ar = 0.25$, with a low amount of boron. Hence, most of film might be comprised of elemental carbon with traces of BC_3 and CN phases. HNO_3 is known to dissolve carbon to form carbon dioxide (CO_2) and nitrous oxide (N_2O) [67]. Therefore, initially the etch rate is high. At $N_2/Ar = 0.5$, there is a decrease in carbon concentration and increase in both boron and nitrogen concentration, which gives rise to more BC_3 and C-N phases, thereby decreasing the

etching rate by a small factor. The etch rate slightly decreases further at $N_2/Ar = 1$. This is due to further increase in BC_3 and C-N phases as a result of small increase in the carbon composition. Hence, a marginal decrease in the etch rate is observed for films deposited at $N_2/Ar = 1$. The etch rates for films etched at $60^\circ C$ and $70^\circ C$, have similar trends with respect to increase in gas flow ratios but they have higher etch rates than films etched at $50^\circ C$. Increase in the reaction temperature, increases the frequency of collision of particles, thereby providing the necessary activation energy for successful collisions. This increases the rate of the reaction and such reaction follows the Arrhenius equation[70]. Further work on Arrhenius plots are discussed in the next subsection.

From Table 4.7, it can be observed that for films deposited at $200^\circ C$, the carbon composition is highest at $N_2/Ar = 0.5$ whereas the etch rate at $N_2/Ar = 1$ is the lowest. The overall nitrogen composition is low in films deposited at $200^\circ C$. From this it is assumed that the films deposited at $N_2/Ar = 1$ has more B-C phase in the films with B_4C being the dominant bonding characteristic. Literatures have reported that carbon forms stronger networks when singly bonded with elements compared to doubly or triply bonded cases [53, 71]. Hence the films in which carbon is found in B_4C forms are difficult to etch. B_4C is fairly insoluble in acids[67] and hence the etch rate further decreases for films deposited at $200^\circ C$ when compared to room temperature deposited film. As the film deposited at $N_2/Ar = 0.25$ has considerable amount of carbon and boron, it forms more B_4C phases. Hence, the etch rate is high. For films deposited at $N_2/Ar = 0.5$, the boron and carbon compositions do not vary much when compared to $N_2/Ar = 0.25$ deposited film, hence the etch rate does not seem to differ by a great amount. The $N_2/Ar = 1$ deposited film consists of significant amount of boron with considerable amount of carbon and traces of nitrogen. Hence, this film is

assumed to consist of phases of B₄C and traces of elemental boron. Boron can be etched effectively by concentrated HNO₃ [67]. As the aluminum etchant consists of dilute HNO₃ in lower quantity, the overall etch rate of the film decreases. Hence the films deposited at N₂/Ar = 1 has the overall lowest etch rate.

The films deposited at 300°C were observed to have constant etch rate from N₂/Ar = 0.25 to 0.5 but show an increase in etch rate at N₂/Ar = 1. From Table 4.6, the percentage compositions of B, C and N were similar for films deposited at N₂/Ar = 0.25 and 0.5. Hence their etch rates showed similar behavior. For films deposited at N₂/Ar = 1, the compositions of both boron and nitrogen increased significantly while the carbon composition decreased. As the boron bonds more preferentially with nitrogen than carbon, it was easier to etch away films with higher h-BN characteristics than B₄C or BC₃. Hence the overall etch rate becomes high for films deposited at N₂/Ar = 1.

Activation Energy

The activation energy (E_a) and high temperature limit of etch rate or pre-exponential factor (R₀) can be calculated according to the Arrhenius law: [72]

$$R = R_0 \exp (-E_a/kT) \quad (3)$$

Wherein, R = etch rate, k = Boltzmann's constant and T is temperature in Kelvin. Figure 2 shows the Arrhenius plot of BCN films deposited at different N₂/Ar gas flow ratios and substrate deposition temperatures.

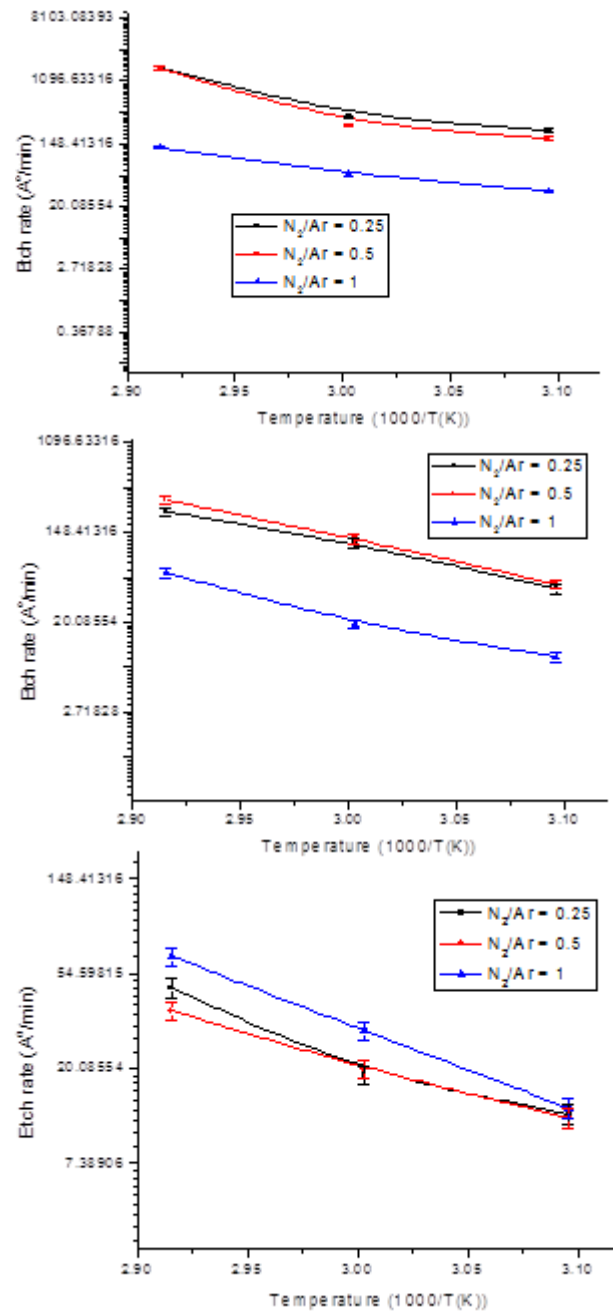


Figure 4.14: Arrhenius plot of films deposited at a.) Room temperature, b.) 200°C, c.) 300°C.

Table 4.7: Activation energy and pre-exponential factor of BCN thin films deposited at various gas flow ratios and substrate deposition temperatures.

N ₂ /Ar	Room Temperature		200°C		300°C	
	E _a (eV)	R ₀ (Å /min)	E _a (eV)	R ₀ (Å /min)	E _a (eV)	R ₀ (Å /min)
0.25	0.38	1.97e08	0.939	1.94e16	0.379	1.02e07
0.5	0.375	1.24e08	0.932	1.71e16	0.482	3.95e08
1	0.506	2.64e09	0.683	4.16e11	0.753	7.44e12

In Figure 4.14, the etch rates follow a linear Arrhenius plot as shown. Arrhenius plots can be used to find the activation energies (E_a) and their high temperature etch rate limit factor (R₀). Table 4.7 lists all the values of E_a and R₀. In case of room temperature deposited films, the etch rate is highest for films deposited at N₂/Ar = 0.25 and 0.5. The lesser the etch rate for a reaction, the higher will be the activation energy needed to complete the etching.

The E_a and R₀ are dependent on several reaction parameters like concentration of the solution, nature of etchant and substrate [73]. Activation energy of a reaction is a direct indicator to its high temperature etch limits. Hence, both these terms can be used interchangeably to explain the reaction kinetics. In this study, the activation energies obtained for BCN etching using aluminum etchant ranges from as low as 0.375 eV to 0.939 eV and their corresponding R₀ values range from 1.24 x 10⁸ Å /min to 1.94 x 10¹⁶ Å /min, respectively. Some literatures report on the activation energies of closely related ceramic high temperature materials such as silicon carbide (SiC) and silicon nitride (SiN). Gelder et.al reports the activation energy of 0.99 eV for silicon nitride, using phosphoric acid (94.5%) etchant [73]. D H van Dorp et.al conducted the anodic wet etching of SiC

using 0.1M KOH solution and were successful in achieving activation energy as low as 45.8 kJ mol⁻¹ (0.47 eV) [74]. In this present work it was possible to achieve lower activation energies in the range of 0.38 eV - 0.506 eV for room temperature deposited BCN films.

Films deposited at 200°C, yielded the highest activation energy range despite the fact that films deposited at 300°C had the slowest etching rates. Hence, the films deposited at 200°C were more temperature dependent than other films. The pre-exponential factors of as-deposited films and films deposited at 300°C are in the orders of 10⁷ to 10¹², whereas the films deposited at 200°C have pre-exponential factor in the range of 10¹⁶. From Table 4.6, it is noted that, the percentage compositions of boron and carbon are very high for films deposited at 0.25 and 0.5 N₂/Ar ratio and 200°C deposition temperature. The ratio of boron to carbon composition is around 2:1. Hence, we can deduce that the films rich in boron and carbon compositions in particular, yield B₄C rich films. As B₄C has a very limited solubility in acids, therefore it solely depends on the high temperatures and takes longer to break its bonds. This is the reason why the pre-exponential factor and its subsequent reaction activation energy is very high for the films deposited at 200°C. Figure 4.15 shows the activation energy of BCN films for various N₂/Ar gas flow ratios and substrate deposition temperatures. The films deposited at room temperature and 300°C show an increase in trend whereas the films deposited at 200°C show a decreasing trend. From Table 4.6, it can be observed that the percentage compositions of nitrogen in the as-deposited and 300°C deposited films, is considerably high when compared to films deposited at 200°C.

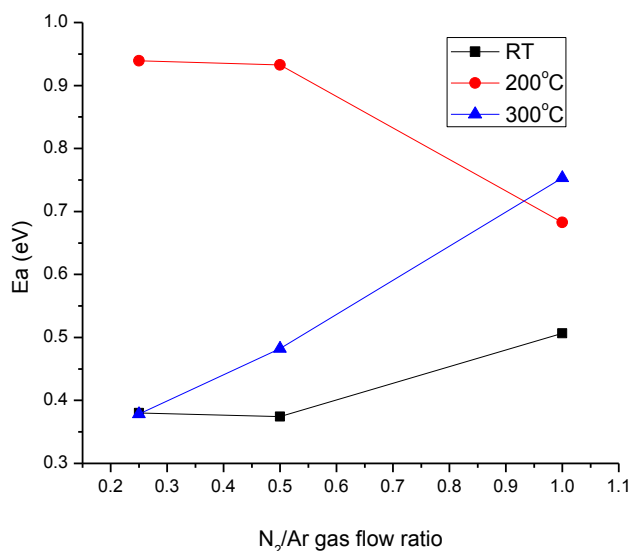


Figure 4.15: Activation energy as a function of N₂/Ar gas flow ratios at various substrate deposition temperatures.

The activation energies of BCN films of room temperature deposited and those deposited at 300°C show an increase in trend with increase in gas flow ratio. Their overall activation energy is lower than the 200°C deposited films. It is probably because of higher nitrogen and lower boron concentration in these films with significant carbon concentrations. According to the chemical properties of B, C and N during the deposition process, B and C can exist both as elements and as compounds reacting with N or each other, while N could exist in the films only as compound by reacting with either B or C. Therefore, the process of nitrogen integration and the reciprocity among B, C and N during the deposition become main factors, which affect the composition and properties of BCN films [75]. These films can be considered as carbon rich films with elemental carbon and traces of C-N, and B-N bonds. Hence, it is easy to dissolve these carbon rich films and therefore their subsequent activation energy for the reaction is less.

4.4: Study of Copper diffusion in RF magnetron sputtered BCN thin films

Secondary-ion-mass spectrometry (SIMS) analysis was conducted to study the copper (Cu) diffusion in boron carbon nitride (BCN) thin films. BCN being a dense low-k material, has a potential to be the Inter-layer dielectric (ILD) in ULSI processes. Hence study of Cu diffusion into BCN films is a major reliability factor to be considered. SIMS analysis performed on BCN films at different annealing temperatures confirmed very low degree of copper diffusion. Copper diffusion increased with increase in boron concentration in BCN film.

In Figure 4.16, the as-deposited films show no peak overlapping between the peaks of B, C and N. These peak overlapping are caused by various factors like ion mixing, matrix effect at metal-film interface which in turn may promote inter-diffusion. These effects are owed to anomalies like surface roughness, localized concentration variations as a result of impurities and segregation arising from sputtering. Also the expansion of the interfacial region (BCN-Cu) is very less when compared to many oxide/aluminum based systems as reported by Sundaram et.al [76]. They report an expansion of 2.5 times during the interface formation but in Figure 1, little or no expansion is noticed. Therefore it proves that, BCN is robust to all the above effects and hence its composition profile seldom changes. The diffusion of B, C and N into copper did not happen in any considerable way in case of BCN films deposited at $N_2/Ar = 0.25$ and 0.5 . This is because of the comparable atomic radius of copper with respect to radii of B, C and N ions. As-deposited films have very low thermal energies to initiate any substitutional diffusion, hence there is a scope for marginal interstitial diffusion to take place in a dense copper layer. In the entire depth of the BCN film, very low counts of the copper was observed when compared to B, C and N in films

deposited at $N_2/Ar = 0.25$ and 0.5 gas flow ratios.

Table 4.8. Percentage composition of B, C and N at various N_2/Ar gas flow ratios.

N_2/Ar gas flow ratio	%B	%C	%N
0.25	3.2	76.8	20
0.5	14.1	52.3	33.6

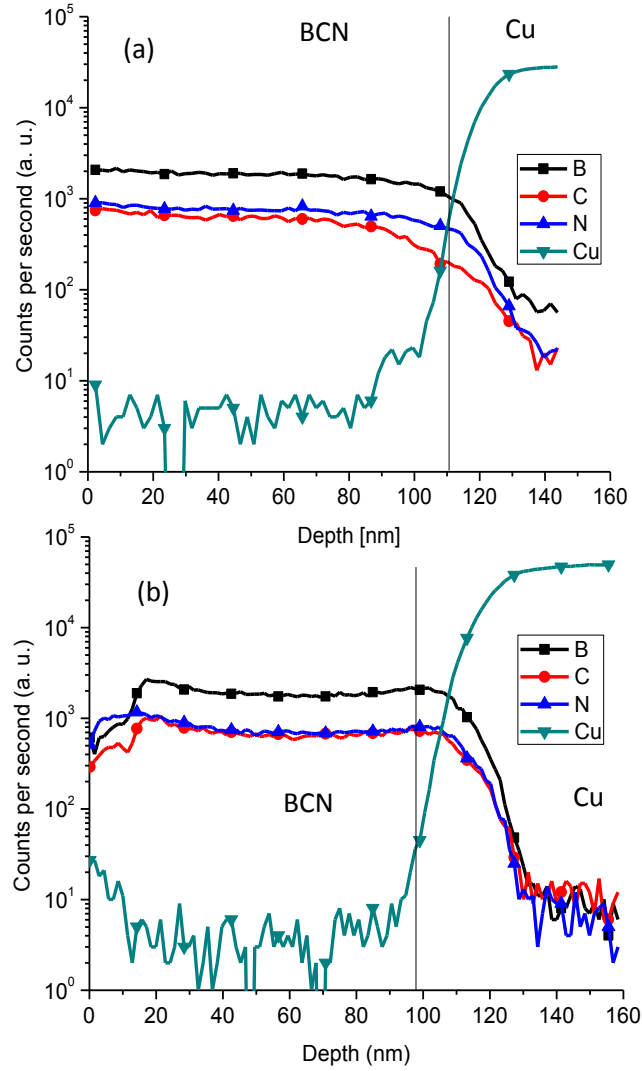


Figure 4.16. SIMS data plot showing inter-diffusion of B, C, N and Cu at (a) $N_2/Ar = 0.25$ and (b) $N_2/Ar = 0.5$ for as-deposited BCN films on copper.

Most of the back-end-of-the-line (BEOL) processes are performed around 350°C. Hence it is necessary to lower the unit process temperatures to 200°C. This is to minimize the degradation of reliability and optimize other process parameters [77]. Therefore the annealing temperatures in this study is kept at 200°C and 300°C. Figure 4.17 shows the effects of annealing at 200°C and

300°C at various time periods. It is observed that the boundary profile for un-annealed films is steep and did not show any considerable counts of copper ions into the BCN films. Further it can be seen that, even after annealing at 300° C for 30 minutes, copper has seldom diffused. The copper forms covalent bonds more readily with boron than nitrogen or oxygen while forming Cu-B complexes leading to substitutional diffusion[78]. Therefore during annealing, the copper might have either precipitated or formed a stable complex thereby accumulating at the surface. From Table 4.8, the concentration of boron is significantly higher in the films deposited at $N_2/Ar = 0.5$ as compared to 0.25. Interstitial diffusion is not a major factor in terms of Cu^+ in BCN since the radii of boron, carbon and nitrogen are similar to that of copper ion. Interstitial diffusion is enhanced in both the cases only with the help of higher annealing temperatures. In Figure 4.16.a), copper concentration in the BCN film tends to be higher for higher annealing temperatures and duration. The highest copper diffusion for the films deposited at $N_2/Ar = 0.25$ and 0.5 was found to be for samples annealed at 200°C even though higher temperature should have assisted diffusion. This can be explained in terms of substitutional diffusion. Higher annealing temperatures favor formation of stable complexes or precipitates such as Cu-B. This decreases the point defects or other reaction sites for further diffusion of copper into the BCN bulk. Hence we can assume that temperatures till 200°C assists diffusion and beyond that it helps in the formation of stable complexes like Cu-B thereby decreasing further diffusion. This holds good for both the cases in Figure 4.17.a) and b).

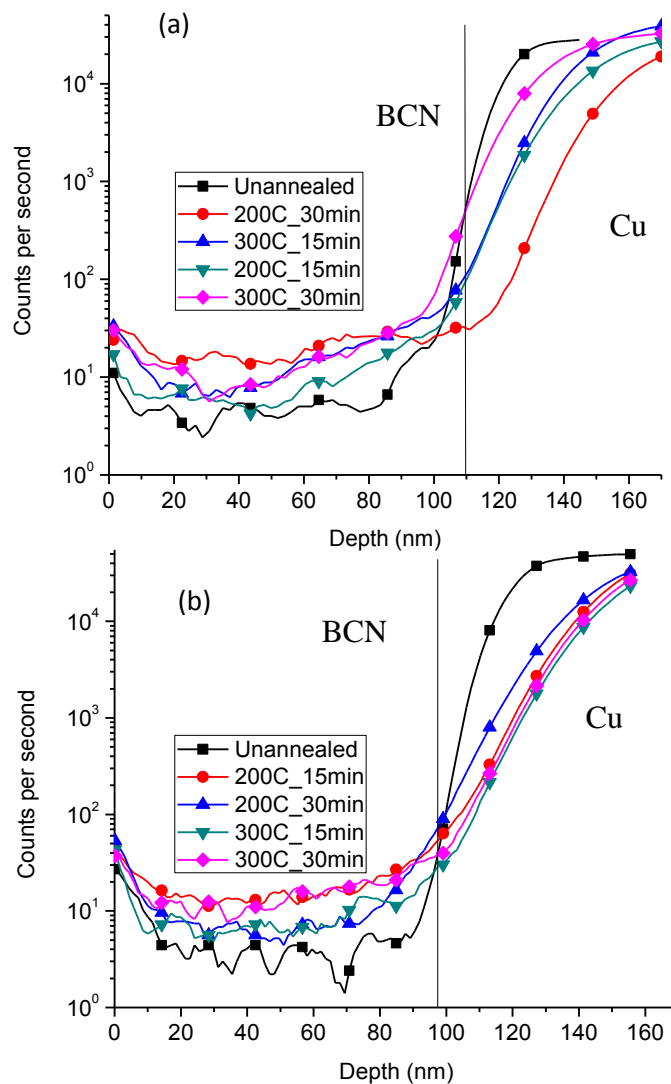


Figure. 4.17 SIMS data plotted for Cu diffusion in the BCN deposited at (a) $N_2/Ar = 0.25$, (b) $N_2/Ar = 0.5$ at different annealing periods at 200°C and 300°C.

In Figure 4.17, the concentration of copper in the BCN surface increases at ~30nm towards the surface. This is because of increasing accumulation of copper on to the surface. The Cu-B pairs are unstable even at room temperatures unlike other 3d transition metals like Fe [79]. Hence the

concentration increases towards the surface, as unstable Cu-B dissociates easily and Cu⁺ accumulates near the surface. Surface defects also provide a stable sink for copper ions. Many literatures have reported regarding point defects and many copper-acceptor pairs like Cu-B, Cu-In etc. [80-82] showing similar trends. The higher boron concentration in Figure 4.1.b) can explain the increased accumulation of copper. Higher the boron concentration, higher is the formation of Cu-B complexes in the bulk and as the complexes are unstable in the bulk they accumulate readily to the surface with more defect sites. Hence it can be deduced that a significant copper concentration is found on the surface of BCN at higher N₂/Ar ratios. The increased copper concentration at the surface can also be due to copper getting trapped in the native oxides at the surface[78]. BCN scarcely forms native oxides of boron and carbon or a complex of both due to prolonged exposure to atmospheric oxygen, hence there is a great possibility of copper getting trapped in the native oxides at the surface as well. Similar works on trapped copper ions in the native oxides of silicon has been reported in the literature[83, 84].

In a multi-level interconnect system, the conducting metal layer can be either on top or bottom side of the dielectric layer. In order to find the diffusion effects of copper being on top of the dielectric layer, the following experiment was conducted. For this study a copper layer was deposited on the top of the BCN film and annealed at 400 °C for 30 minutes. After the annealing is completed, the copper is stripped off with the help of dilute nitric acid (HNO₃) at room temperature. Subsequently SIMS analysis is performed. This method also helps us to obtain a clear and sharp demarcation between deposited copper and BCN films.

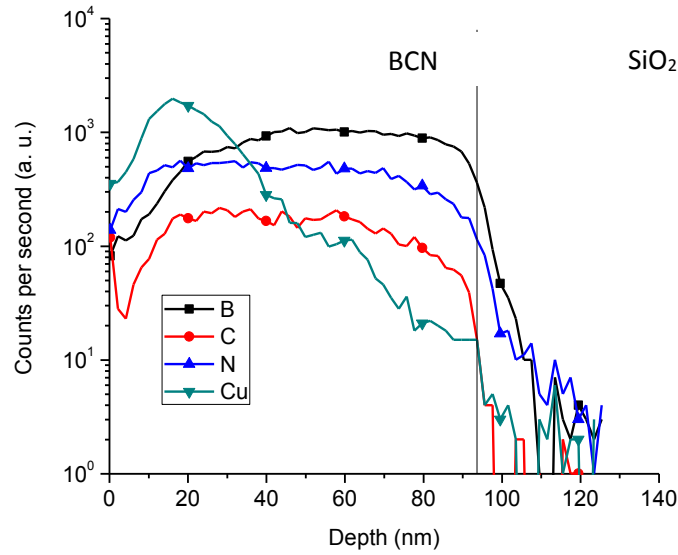


Figure 4.18 SIMS data plot showing inter-diffusion of B, C, N and Cu at $N_2/Ar = 0.25$, for copper deposited on the as-deposited BCN films and annealed at $400^\circ C$ for 30 minutes.

In the Figure 4.18, the count of copper has increased for the first 20 nm and then decreases by over two orders of magnitude gradually towards the end of the BCN film. As the SIMS measurements are done ex-situ, there is a tendency for BCN films to form native oxides from the interaction with atmosphere. In the literature it is found that the copper diffuses faster in oxide based thin films [85]. Therefore there is an increased accumulation of copper below the surface. Similar trend is observed for the copper counts below the surface for the films annealed at 200 and $300^\circ C$ as shown in Figure 4.16.

BCN being a low-k material with high density can be a potential inter dielectric layer with copper interconnects. This work shows that even annealing the film in the range of $200-400^\circ C$ has minimal copper diffusion effects in the BCN films. Films deposited at higher N_2/Ar ratio yielded higher boron concentration. Films with higher boron concentration showed marginal increase in

copper diffusion compared to lower concentration films. BCN being a low-k material with high density can be a potential inter dielectric layer with copper interconnects. This work shows that even annealing the film in the range of 200-400°C has minimal copper diffusion effects in the BCN films. Films deposited at higher N₂/Ar ratio yielded higher boron concentration. Films with higher boron concentration showed marginal increase in copper diffusion compared to lower concentration films.

4.5: Optical studies of BCN thin films by co-sputtering of B₄C and BN targets

Boron carbon nitride (BCN) thin films are investigated for their optical properties. BCN, is the unanimous choice for inter-dielectric layer (IDL) in very large scale integration (VLSI) because of its low-k dielectric constant. Optical properties can be tailored as a function of elemental composition, which makes BCN a prospective material in UV-filters and mirrors. Films are deposited by reactive co-sputtering of boroncarbide (B₄C) and boronnitride (BN) with varying N₂/Ar gas flow ratio by DC and RF sputtering respectively. XPS studies are performed to deduce the bonding and chemical properties of the BCN film. Optical band gap (E_g) studies are performed as a result of varying target powers, gas ratios and deposition temperatures. E_g is found to increase with N₂/Ar flow ratios and deposition temperatures. BCN deposited at 20W DC exhibited higher band gap range and the highest achieved is 3.7 eV at N₂/Ar = 0.75. Lowest value achieved is 1.9 eV at N₂/Ar = 0.25 for as-deposited films.

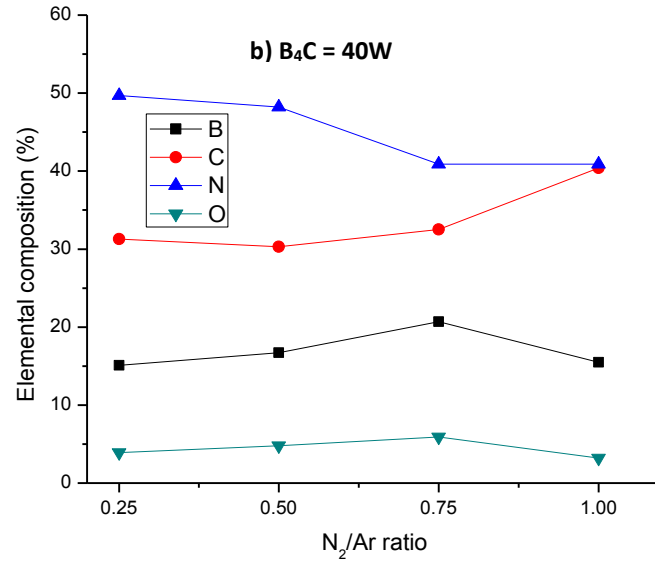
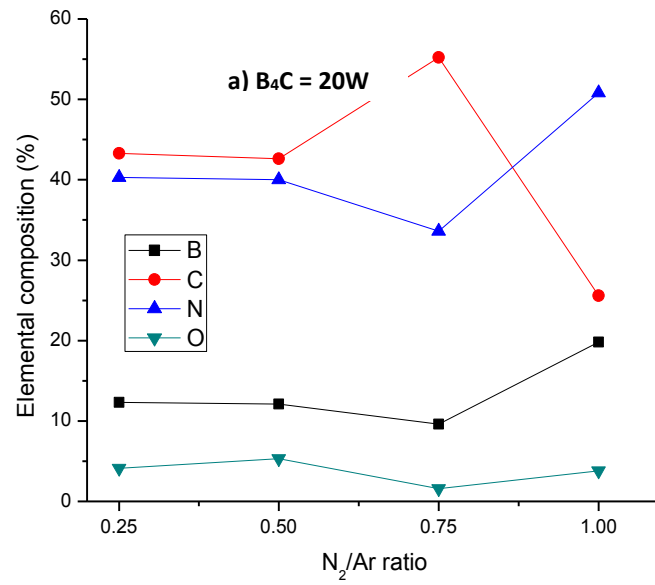


Figure 4.19: Percentage elemental compositions of B, C and N for BCN thin films deposited at a) 20W B₄C and b) 40W B₄C

Figure 4.20, shows the B1s high resolution scan in which a) and b) show the B1s spectra for BCN deposited at $N_2/Ar = 0.25$ and 1 respectively at 20W B_4C power. The peak at ~ 189.5 eV is attributed to B-C bonding [56], the peak at ~ 190 eV is attributed to h-BCN and the peak at ~ 191.5 eV is attributed to h-BN bond [86]. Finally, the BCO_2 and B_2O_3 bonds are attributed to peaks at ~ 192 eV and ~ 193.2 eV respectively [87]. In Figure 4.20 a) and b), the B-C peak shifts towards lower binding energy with higher gas flow ratio. The h-BCN peak broadens and increases in intensity with the increase in N_2/Ar gas flow ratio, whereas a smaller and shifted h-BN peak is observed. According to the Figure 4.19, the concentration of the nitrogen increases and carbon concentration decreases. Hence, this supports the fact that h-BCN is more favorably formed at higher N_2/Ar gas flow ratio. Figure 4.20, c) and d) shows the B1s spectra for BCN films deposited at $N_2/Ar = 0.25$ and 1 respectively at 40W DC power. From Figure 4.19, the concentration of boron does not change significantly with higher N_2/Ar gas flows. But the concentration of nitrogen decreases and the concentration of carbon increases. From the Figure 4.20, it can be observed that the B-C peak shifts towards lower energy indicating increased stability. The intensity of h-BCN peak more or less remains the same but a shift towards lower energy with broadening can be observed whereas the h-BN peak intensity decreases with increase in gas flow ratio. This may be due to higher B_4C (higher yield than BN target) DC target power of 40W, that produces carbon rich BCN films unlike those deposited at 20W. Thereby incorporating higher B-C related characteristics in these films.

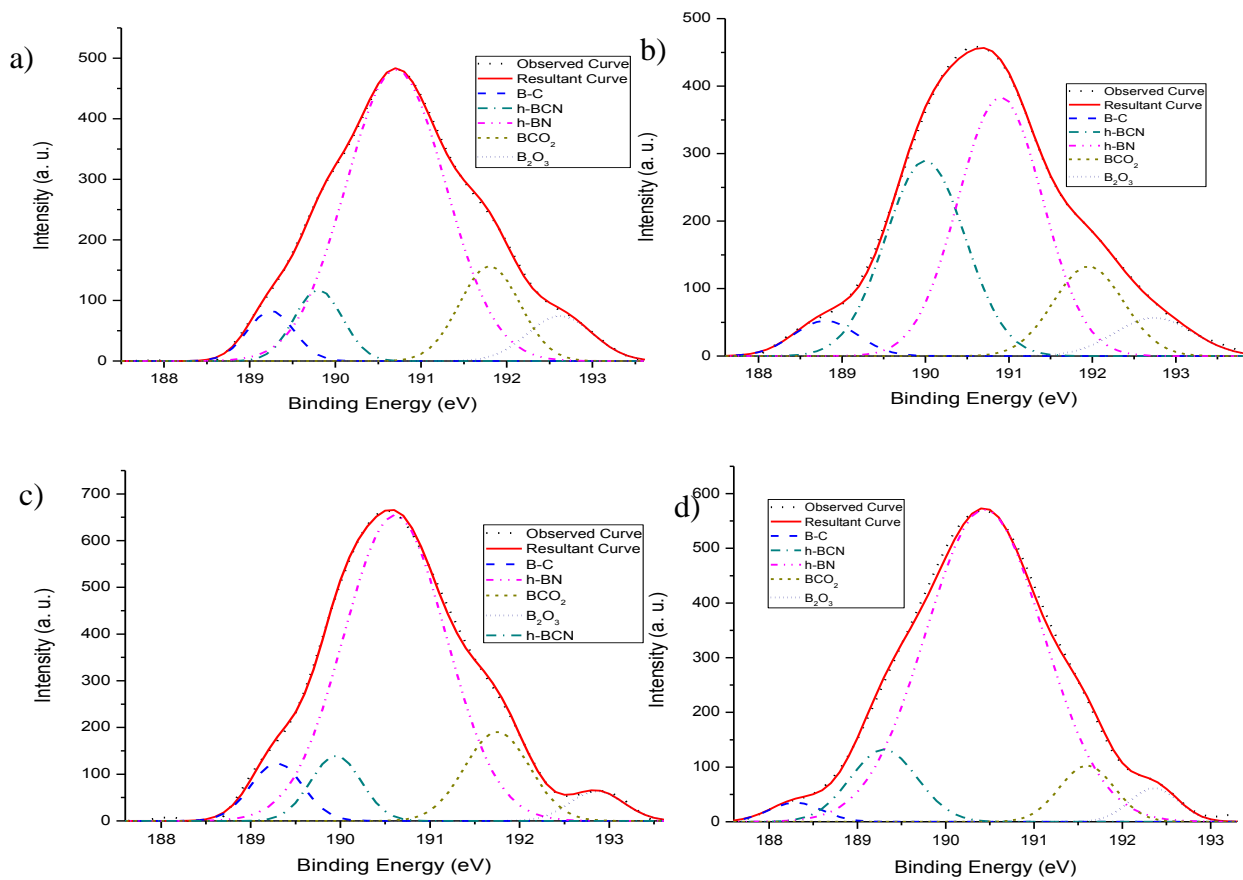


Figure 4.20: B1s spectra of BCN thin films deposited at a) 20W B₄C and N₂/Ar = 0.25, b) 20W B₄C and N₂/Ar = 1, c) 40W B₄C and N₂/Ar = 0.25, d) 40W B₄C and N₂/Ar = 1

Figure 4.21 shows the N1s high resolution scan in which a) and b) shows the N1s spectra for BCN deposited at $N_2/Ar = 0.25$ and 1 respectively at 20W B₄C power. According to Yang et.al, the peaks between 397.3 and 398 eV can be attributed to B-N bond[50]. The peaks at ~400 eV can be attributed to N=C double bond [88-90]. According to Bhattacharya et al. (sp) N-C peak can be found at 398.8 eV. The peak between 398 eV and 398.3 eV can be attributed to N-C bond formation [88, 91]. The peak between 400.5 eV and 401 eV is due to the presence of N-O contamination bonds [92]. In Figure 4.21 b), the B-N peak has a peak shift towards lower binding energy as well as increase in peak intensity. This shows a distinct and separate phase of B-N than its counterpart in Figure 4.21 a). From Figure 2, it can be observed that, the compositions of nitrogen and boron have increased, but the carbon concentration has nearly halved. This denotes that more B-N bonds can be found in the film deposited at higher N_2/Ar gas flow ratios. This also shows an increase in the peak intensities of (sp³) C-N and (sp²) C-N, whereas a slight decrease in (sp) C-N can be observed with increase in N_2/Ar gas flow ratio indicating that higher gas flow ratio favors the formation of more stable B-N or BCN rich films. Figure 4.21, c) and d) shows the N1s spectra for BCN films deposited at $N_2/Ar = 0.25$ and 1 respectively at 40W DC power. In Figure 4.21 c) and d), the B-N peak intensity increases for higher gas flow ratio. The peak intensity of (sp³) C-N and (sp²) C-N decreases marginally with increase in N_2/Ar gas flow but the intensity of (sp) C-N fairly remains same at higher N_2/Ar gas flow. A slight shift towards the lower binding energy is observed for these peaks but for (sp) C-N peak. This favors the formation of more stable (sp³) C-N, (sp²) C-N and B-N at higher gas flow ratios for BCN film deposited at 40W DC.

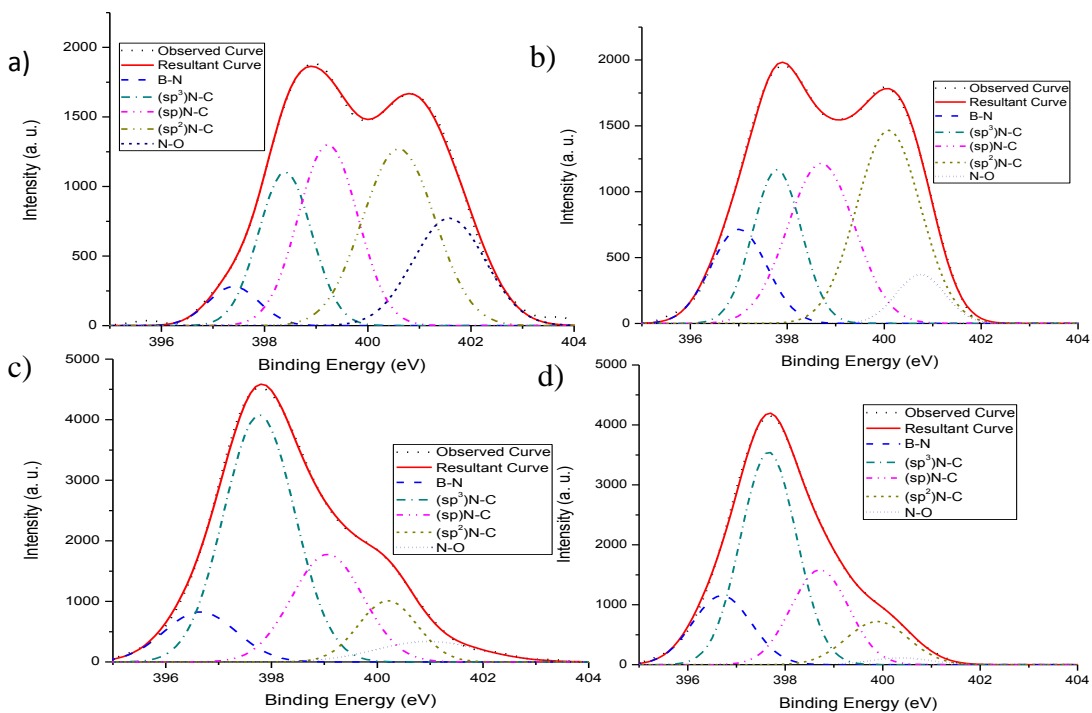


Figure 4.21: N1s spectra of BCN thin films deposited at a) 20W B₄C and N₂/Ar = 0.25, b) 20W B₄C and N₂/Ar = 1, c) 40W B₄C and N₂/Ar = 0.25, d) 40W B₄C and N₂/Ar =

Figure 4.22 shows the C1s high resolution scan in which a) and b) depicts the C1s spectra for BCN deposited at $N_2/Ar = 0.25$ and 1 respectively at 20W B_4C power. The C1s binding energies for BC_3 and B_4C have been reported to be 284.3 and 283.0 eV respectively [47, 54]. The peaks around 285.6 to 286.5 eV are attributed to $(sp^2)C-N$ [50] and the peaks around 287.3 eV are attributed to $(sp^3)C-N$ [53]. Hence the peak at 283.9 eV in a) can be attributed to either BC_3 or B_4C . This peak in b) is fairly narrower and smaller in intensity than its counterpart in a). A small peak shift in C-N towards higher binding energies can be noticed. The higher binding energy peaks located at >288 eV are due to the presence of C-O bonds which are considered as contamination [8, 93]. In Figure 4.19, the compositions of boron and nitrogen increase whereas the composition of carbon is halved at higher N_2/Ar flow ratio. There is a decrease in B-C peak intensity for films deposited at higher N_2/Ar flow ratios and the overall intensities of all the other peaks tend to decrease due to decrease in carbon concentration in the film and hardly any peak shifts are noticed for $(sp^3)C-N$ and $(sp^2)C-N$. Figure 5 c) and d) show the C1s spectra for BCN films deposited at $N_2/Ar = 0.25$ and 1 respectively at 40W DC power. But from the Figure 4.19, we can see that the composition of the boron remains constant but there is an increase in carbon concentration and decrease in nitrogen concentration. From this we can deduce that, BCN films deposited at higher B_4C power will create more carbon rich films. When inspecting the $(sp^2)C-N$ peaks in Figure 4.22 a) and b) there is a small peak shift towards lower binding energy side. In Figure 4.19, as we can see that the composition of carbon reduces considerably at higher N_2/Ar gas flow ratio whereas the boron concentration nearly doubles. This shows that the $(sp^2)C-N$ peak intensity decreases, paving way to more stable nitrogen bonding to boron. In Figure 4.22 c) and d) it can be observed that both $(sp^2)C-N$ and $(sp^3)C-N$ has a peak shift towards lower binding energy as well as decrease in their

respective intensities, whereas the intensity of C-C peak has increased considerably. It is known that carbon can also exist as a standalone element in a BCN film as well as compound [42]. Hence it is deduced that, BCN films with marginal increase in B_4C target power yields carbon rich films, which plays a major role in bandgap engineering.

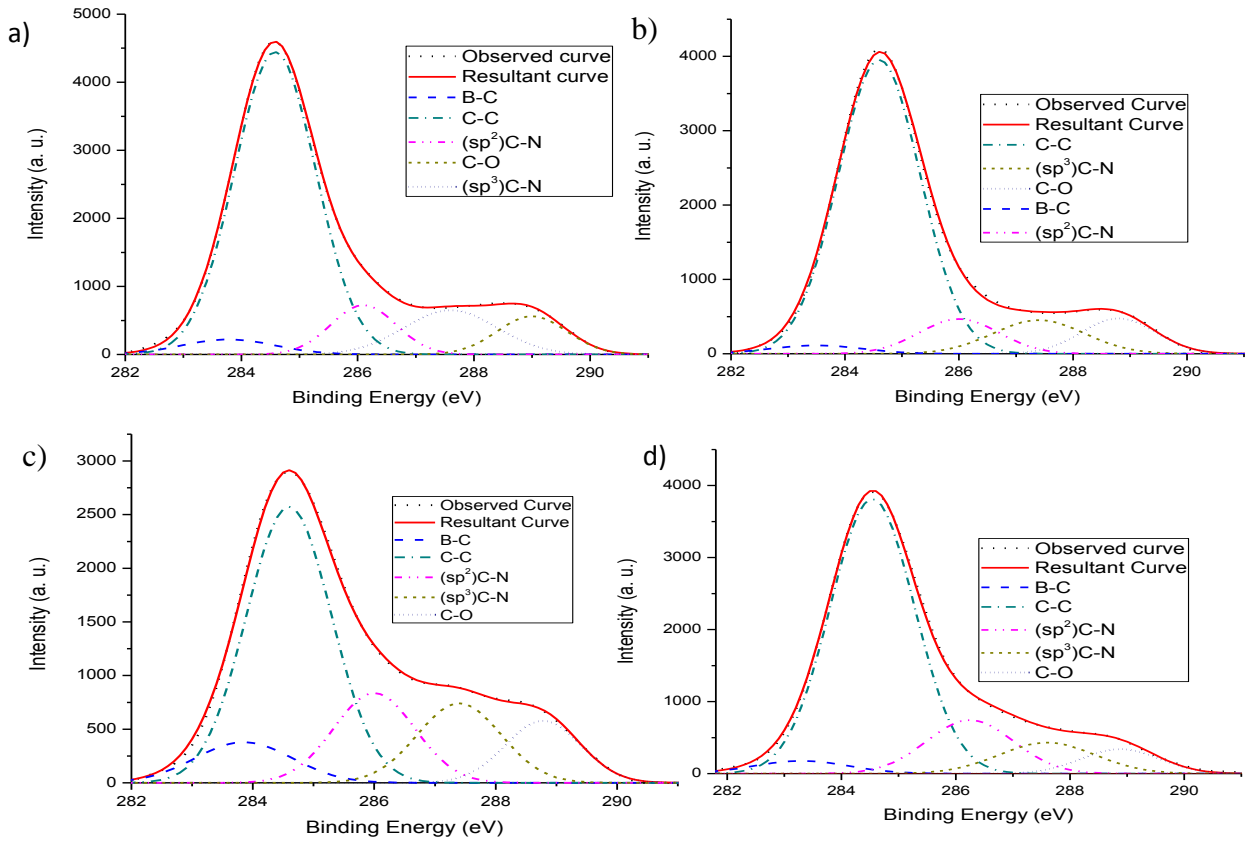


Figure 4.22: C1s spectra of BCN thin films deposited at a) 20W B_4C and $N_2/Ar = 0.25$, b) 20W B_4C and $N_2/Ar = 1$, c) 40W B_4C and $N_2/Ar = 0.25$, d) 40W B_4C and $N_2/Ar = 1$

Figure 4.23 a) shows the transmission spectra for the BCN films deposited at various gas flow ratios for 20W DC power applied to B₄C target. The highest and least transmissions are observed for N₂/Ar = 0.75 and N₂/Ar = 1 gas flow ratio respectively. The highest transmission achieved is around 90% in the visible region. Figure 4.23 b) shows the transmission spectra for various gas flow ratios at 40W DC power to B₄C. The highest transmission is found to be at N₂/Ar = 1 for the visible light range but the absorption edge is not as sharp as indicated for the film deposited at 20W power. The transmission tail decreases smoothly below 600 nm all the way to 200 nm in the UV region. The films deposited at N₂/Ar = 0.75 ratio shows better transmission in that range and the least transmission is found at N₂/Ar = 1 gas flow ratio. The highest transmission is found to be around 85% for N₂/Ar = 0.75.

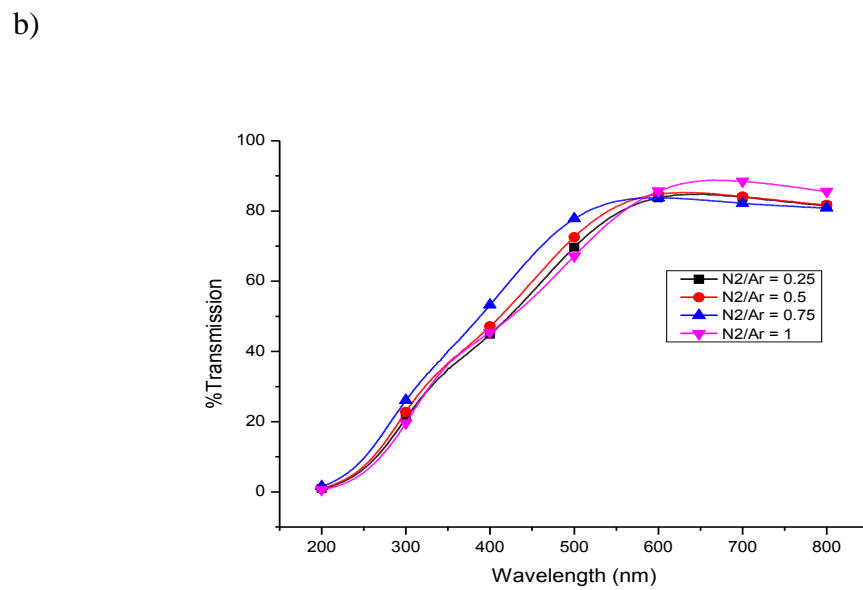
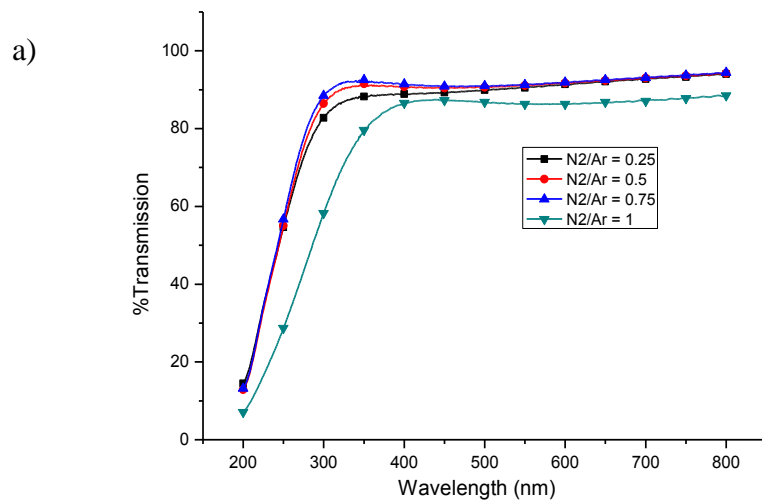


Figure 4.23: a) % Transmission for various gas ratios at 20W DC power to B_4C ; b) % Transmission for various gas ratios at 40W DC power to B_4C .

The Optical density (OD) is calculated first with the help of percentage transmission values and then the absorption coefficient for each of those OD is calculated by using the equation 1.

$$\alpha = 2.303 \times \text{OD} = \frac{-2.303}{t} \log_{10}(\%T) \quad (1) \quad [94]$$

Where, α = absorption coefficient and t = thickness of the film

The absorption coefficient is plotted against photon energy.

Using the Tauc's plot by fitting the data into following equation, the optical band gap is calculated [94].

$$(\alpha * hv)^{\frac{1}{2}} = B(hv - E_{opt}) \quad (2)$$

Where, B = Constant factor, hv = Photon Energy, E_g = Optical band gap.

Figure 4.24 shows the Tauc plot for the absorption coefficient values extracted from the Figure 4.23

a). The optical band gap is found by extrapolating linear region of the Tauc curve to x-axis. The X-intercept values gives the optical band gap values for corresponding curves.

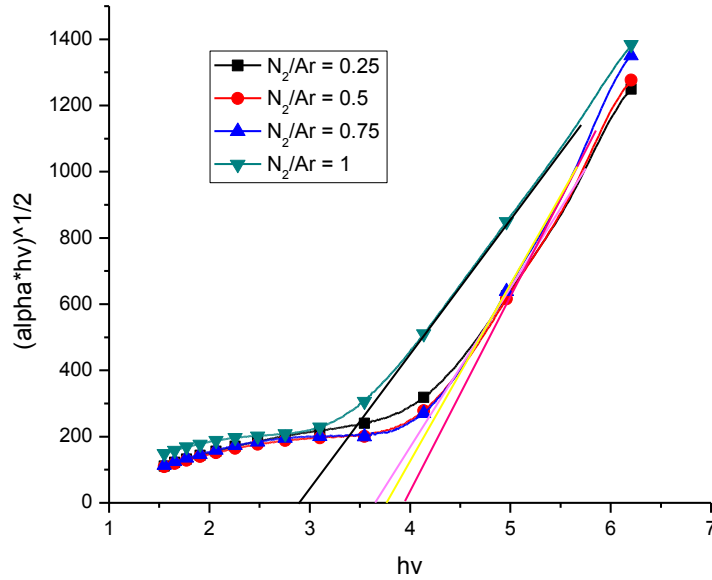
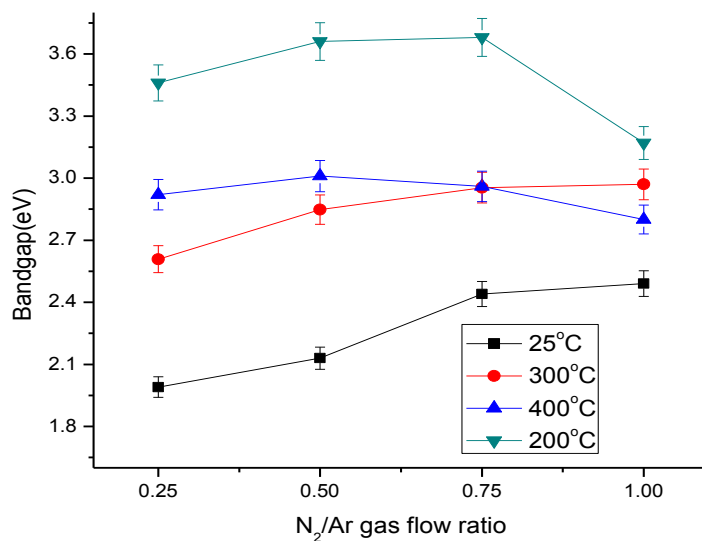


Figure 4.24: Tauc plot of BCN thin films deposited at 20W power to B₄C

Figure 4.25 a) shows plot of optical band gap versus gas flow ratios for various deposition temperatures. For these studies, the target power used is 20W DC power to B₄C target keeping a constant BN target power of 250W. The optical band gap increases with increase in N₂/Ar gas flow ratios for all the temperature ranges but a decreasing trend at N₂/Ar = 1 for 200 and 400 °C is observed. Similar trend for SiCBN is observed by Vijayakumar et al [95]. The increase in band gap with increase in N₂/Ar gas flow ratio is due to the increase in composition of nitrogen and decrease in carbon concentration as shown in Figure 4.19. Similar trend is observed in the work performed by Tado et al and Todi et al [96, 97]. The band gap is reported to increase with increase in deposition temperature as reported by Lei et al [63]. The BCN films deposited at 200°C showed

the highest band gap range and the films deposited at room temperature showed least optical band gap range. The highest band gap achieved is 3.7 eV for BCN film deposited at $N_2/Ar = 0.75$ and lowest band gap achieved is 1.9 eV for BCN film which is as-deposited at $N_2/Ar = 0.25$.

a)



b)

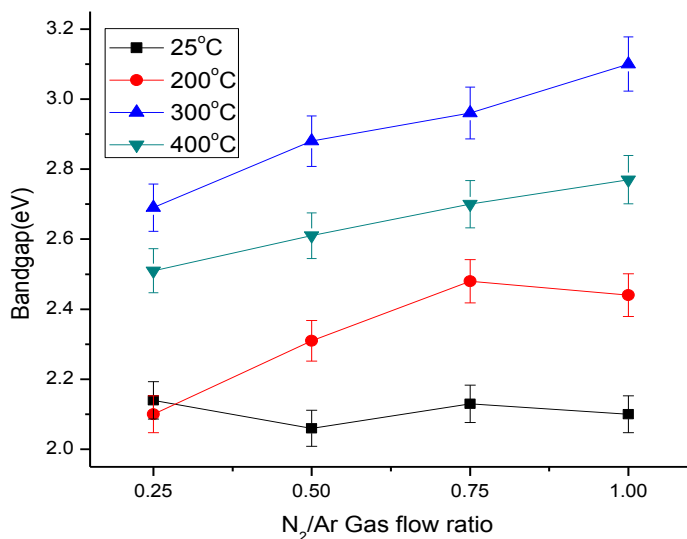


Figure 4.25: a) Optical band gap as a function of gas flow ratio at 20W DC; b) Optical band gap as a function of gas flow ratio at 40W DC.

Figure 4.25 b) shows plot of optical band gap versus gas flow ratios for various deposition temperatures. For these studies, the target power used is 40W DC power to B_4C target keeping a

constant BN target power of 250W. The optical band gap increases with increase in N_2/Ar gas flow ratios except for a couple of decreasing trend at $N_2/Ar = 1$ for as-deposited and 200°C. The BCN films deposited at 300 °C showed the highest band gap range and as-deposited films showed lowest band gap range. The increase in optical band gap can be attributed to the increase in nitrogen concentration as shown in Figure 4.19. As the increase in nitrogen composition is not significant, the band gap increase is also not drastic as compared to the films deposited at 20W. The highest band gap achieved is 3.1 eV for film deposited at 300 °C at $N_2/Ar = 1$ and the lowest band gap of 2.06 eV is achieved for film deposited at room temperature at $N_2/Ar = 0.5$. From these observations it can be deduced that films deposited at 20W have more scope for band gap engineering because of its wide range of possible band gap values.

4.6: Photoluminescence studies on BCN thin films synthesized by RF magnetron sputtering

Photoluminescence (PL) studies on boron carbon nitride (BCN) thin films deposited at various temperatures were conducted. Two sharp PL peaks in the visible region were identified at 498 nm and 599 nm for the BCN films with variable peak intensities. Low temperature PL study was conducted at 77K for the films. It was found that, the PL intensity tend to decrease significantly with decrease in the substrate temperature during the measurement. The phenomenon of negative thermal quenching (NTQ) was observed for the first time in BCN thin films.

Figure 4.26 shows various peaks found in BCN thin films deposited at various substrate deposition temperatures. The peaks at $2\theta = 44^\circ$ can be assigned to BN (101) phase[98, 99]. A more distinct and high intensity peak can be observed for film deposited at 200°C substrate deposition

temperature. Whereas, this peak is absent for the film deposited at 400°C. The B_8C (21, 3, 0) phase is assigned to the peak at $2\theta = 55.95^\circ$ as per the JCPDS convention. The B_8C peak gets narrower and distinct, with increase in substrate deposition temperatures. The peak around $2\theta = 62^\circ$ can be attributed to silicon peak resulting from the substrate background[100, 101]. From the XRD analysis, it can be deduced that, the BCN films deposited at various temperatures has crystallinity of very short range order.

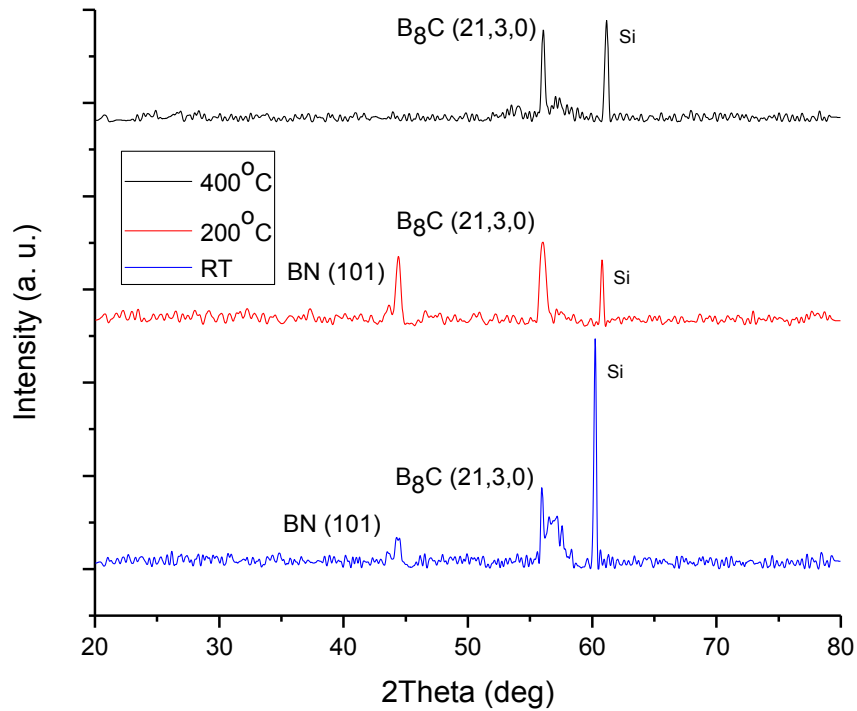


Figure 4.26: X-ray diffraction patterns for BCN thin films deposited at (a) room temperature, (b) 200°C, and (c) 400°C.

One of the most prominent absorption peaks is observed at 1080 cm^{-1} , which corresponds to reststrahlen band of cubic boron nitride (c-BN) [51] and/ or cubic BCN (c-BCN) due to increase

in carbon content in the films [102]. As seen from the Figure 4.27, for the as-deposited films, the peak broadens to a higher wavenumber. This may include the peak absorption caused by icosahedral vibrations due to B_4C peak around 1100 cm^{-1} [103],[104]. The absorption peaks found at 780 cm^{-1} and 1400 cm^{-1} correspond to out-of-plane bending of (sp^2) B-N-B bond and (sp^2) B=N bond respectively. Among these, the (sp^2) B=N bond is found to be prominent and distinct in all the specimens. This peak becomes narrower with increase in substrate deposition temperatures. Hence, this shows the existence of hexagonal BN (h-BN) and/or hexagonal BCN (h-BCN)[51]. The C(sp^2)-N peak and C(sp)-N peaks are found at 1600 cm^{-1} and 2200 cm^{-1} respectively [105, 106]. The C(sp)-N peak broadens and becomes distinct with increase in substrate deposition temperature.

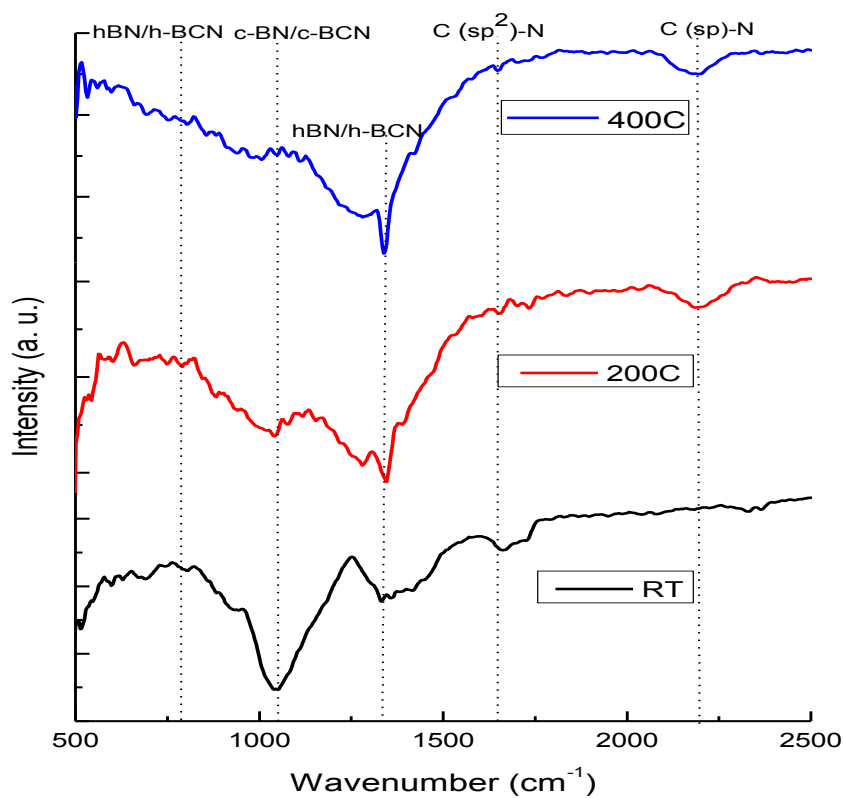


Figure 4.27: FTIR transmission spectra of BCN thin films deposited at room temperature, 200°C and 400°C.

Table 4.9 shows the percentage compositions of B, C and N in the BCN thin films deposited at different temperatures extracted from XPS. The composition table will help to gain better understanding on the different trends of PL for films deposited at various temperatures.

Table 4.9: XPS percentage compositions of B, C and N of BCN thin films deposited at various substrate deposition temperatures.

Deposition temperature	%B	%C	%N
As-deposited	3.2	76.8	20
200°C	66.2	28.5	5.3
400°C	12.8	45.2	42.0

Two distinct photoluminescence (PL) peaks were observed at 498 nm (2.49 eV) and 599 nm (2.07 eV) respectively for an ultraviolet (UV) excitation of 365 nm. Similar strong PL peak at 600 nm was found in BC₂N thin films as reported by Watanabe et.al [107]. Jian et.al reported strong PL peaks at 370 nm and 700 nm at an excitation of 310 nm for B₃CN₃ fibers [108]. Such huge differences in the PL peak positions are due to quantum confinement effect in fibers and other structures like quantum dots, nano-rods. In this work, the highest PL peak intensity was observed in the BCN films deposited at 400°C and the lowest intensity PL in the films deposited at 200°C. This is due to the fact that samples grown at higher temperatures tend to have improved crystalline quality. This in turn will have a reduction in the non-radiative recombination for the electron-hole pairs [109]. The BCN films grown at higher temperature also has the lower deposition rate when compared to its lower temperature counterparts, as reported in one of our previous works [75]. Hence, this lower surface to volume ratio of films have lesser defects than the bulkier ones. From Fig. 1, the XRD peaks of films deposited at 400°C are narrower and distinct, suggesting larger crystallites when compared to as-deposited films. All these factors influence greatly towards increase in PL intensity for 400°C deposited films. The 200°C deposited BCN film

is supposed to show increase in PL intensity when compared to as-deposited BCN film, but it has the lowest PL intensity. This peculiar trend is explained as follows. The XRD peak for 200°C deposited film shows a well-defined BN peak as compared to as-deposited film. BN is an anisotropic material and polar like many other III-V semiconductors [110]. Therefore, it could be highly polarization anisotropic in luminescence i.e. the emission peak profile changes with parallel and perpendicular incidences [111]. Li et.al. and other groups have reported similar decrease in PL intensity with increased alignment of hBN particles [110]. Table 4.8 shows the percentage compositions of boron, carbon and nitrogen for BCN films deposited at different deposition temperatures. The films deposited at 200°C has a high percentage of boron. During the BCN deposition process, B and C can exist both as standalone elements and as compounds reacting with N or each other, while N could exist in the films only as compound by reacting with either B or/and C[75]. Therefore, the 200°C deposited film may contain traces of elemental boron. Boron is known to be detrimental to photoluminescence as it acts as a PL quencher in many solids like silicon nanocrystals [112]. This is attributed to increase in nonradiative Auger recombination[113, 114]. All these factors result in the decreased PL activity of 200 °C deposited BCN films.

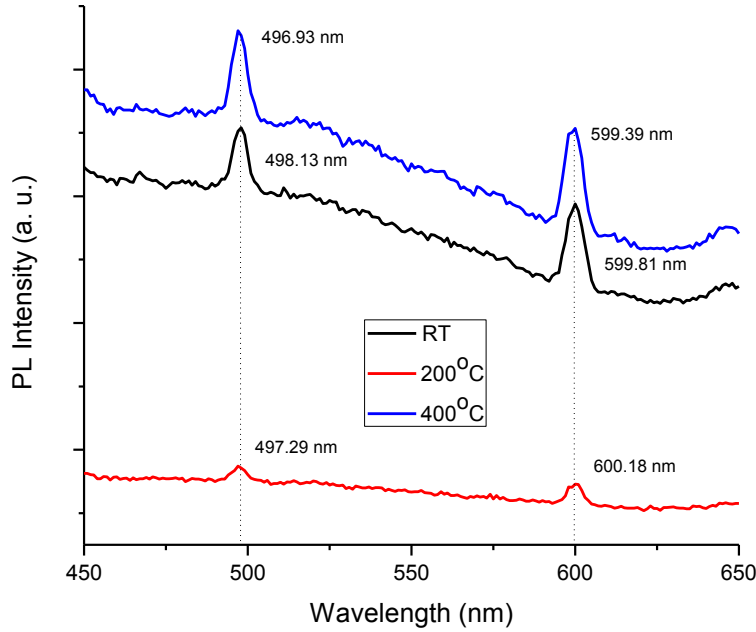


Figure 4.28. Photoluminescence measurements of BCN thin films deposited at different substrate deposition temperatures.

Usually, the PL intensity has a tendency to increase with decrease in temperature as a result of thermal quenching (TQ) phenomenon. This phenomenon is attributed to the increase in nonradiative recombination of electrons and holes with increase in temperatures. All the groups who have investigated on BCN PL, report TQ phenomenon. A peculiar behavior of negative thermal quenching is observed as shown in Figure 4.29, NTQ was observed for BCN films deposited at all temperatures. There are reports about NTQ found in materials such as ZnS, GaAs, ZnO [115-117]. The explanation for NTQ phenomenon is as follows. Shibata et.al proposed a simple model for TQ and NTQ [115]. A material with only two states i.e. initial and final state is most likely to show TQ if the energy separation between the initial and final state is sufficiently

large compared to the temperature of the system as the thermal excitation is negligible. But due to defects or unintentional donors, a system may have a number of multilevel states between initial and final state. Hence, when the energy difference between the initial states and some middle states is comparable to the temperature of the system, thermal excitation of electrons between these states are not negligible. Therefore, increase in temperature increases the PL intensity. BCN is known to be direct band gap semiconductor in the literature [107, 118]. The low temperature measurements might have introduced intermediate states or unintentional donors that might have resulted in the NTQ phenomenon in RF sputtered BCN thin films.

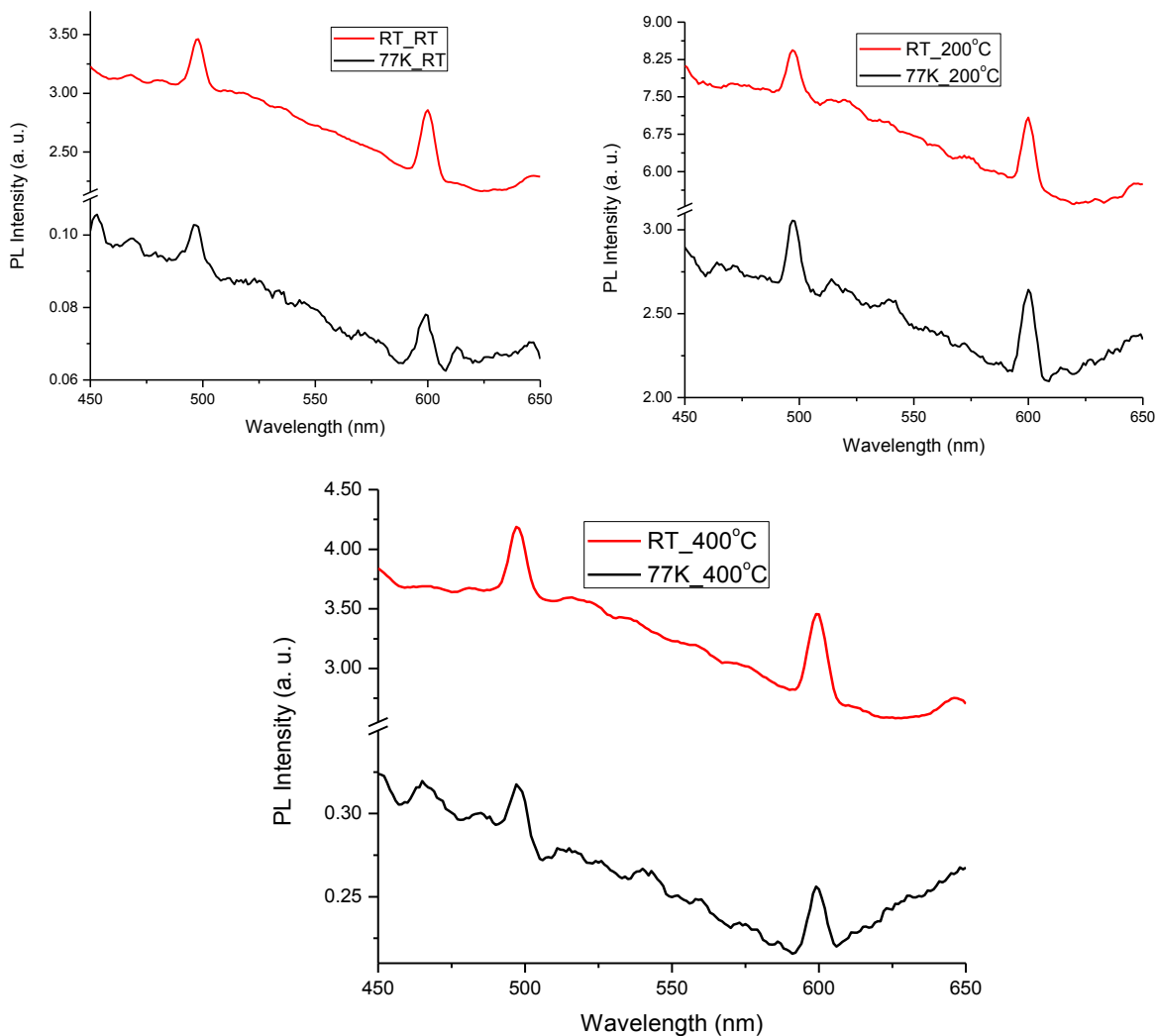


Figure 4.29. Photoluminescence at room temperature and 77K, for BCN thin films deposited at different substrate deposition temperatures.

A systematic PL study of RF sputtered BCN thin was performed. Two sharp PL peaks were observed in the visible region. The films deposited at 400°C showed the highest PL peak intensity.

This was attributed to the larger crystallites and high surface-to-volumes ratio with less defects in

the 400°C deposited films. For the first time, NTQ was observed in the BCN thin films deposited at all the substrate deposition temperatures. This may be due to the introduction of intermediate states or unintentional donors during low temperature measurements and whose energy difference between the initial and middle states was comparable to temperature of the system. Thermal excitation of electrons was deemed negligible in this case, resulting in NTQ property.

4.7: Boron carbon nitride based Metal-Insulator-Metal UV detectors for harsh environment applications

A metal-insulator-metal (MIM) structures using Boron carbon nitride (BCN) was tested for its UV detection capability. BCN being one of the hardest material and chemically robust, it is expected to be a potential choice for UV detector in extreme and harsh conditions. The BCN thin films were deposited using dual target RF magnetron sputtering process. The optoelectronic performance of the BCN MIM devices were examined through UV photocurrent measurements. A UV photocurrent two orders of magnitude higher with respect to dark current was achieved in the range of -3V to 3V

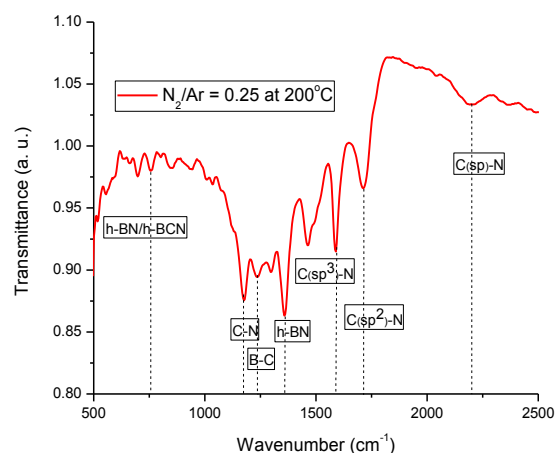


Figure 4.30: FTIR spectra of BCN thin films deposited at gas flow ratio of $N_2/Ar = 1$ and at $200^\circ C$ deposition temperature.

The most prominent peaks found are out-of-plane sp^2 bonded B-N-B bending mode at 780 cm^{-1} as reported by Hasegawa et.al [51]. This peak may also denote the occurrence of either hexagonal boron nitride (h-BN) and/or hexagonal BCN (h-BCN). There are two peaks found near 1250 cm^{-1} and 1220 cm^{-1} . Chien et al. attribute those peaks to carbon rich B-C bond and the sp^3 bonded C-N ($1212\text{--}1265\text{ cm}^{-1}$) respectively [53]. In-plane B-N stretching bond can be seen at $\sim 1370\text{ cm}^{-1}$ [119]. Tempez et al. and other groups have reported significant peaks of $C(sp^2)\text{-N}$ peak at $\sim 1600\text{ cm}^{-1}$ and $C(sp)\text{-N}$ peak at $\sim 2200\text{ cm}^{-1}$. Similar peaks can be found in the Figure 4.30. The peak, which is found in the BCN film as a result of surface contamination due to atmospheric exposure can be attributed to $C=O$ peak at $\sim 1700\text{ cm}^{-1}$. The h-BN, $C(sp^3)\text{-N}$ and C-N peaks are found to be in considerable intensity and amongst them $C(sp^3)\text{-N}$ is dominant. Hence the properties of these films are significantly dependent on these peak. The deposited BCN film showed several phases related to h-BCN, $(sp^3)\text{-CN}$, B-C, h-BN, $C(sp^3)\text{-N}$, $C(sp^2)\text{-N}$ and $C(sp)\text{-N}$. Similar multiple phases of BCN films were reported in our earlier XPS studies [75].

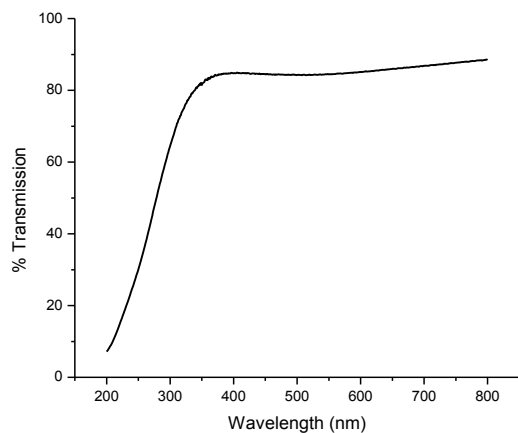


Figure 4.31: UV-Vis transmission spectra of BCN thin film deposited at 200°C.

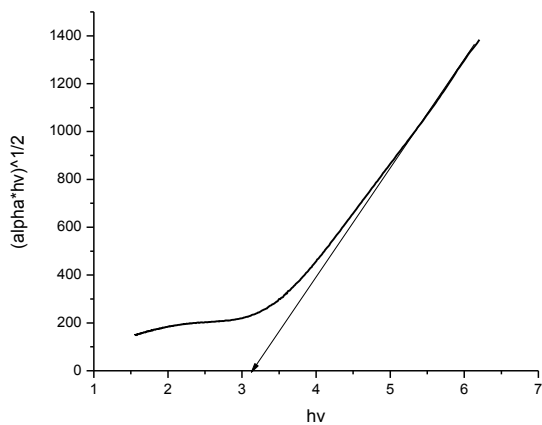


Figure 4.32: Tauc plot for bandgap extraction.

Figure 4.31 shows the transmission spectra for BCN thin film in visible and UV region. The film is fairly transparent in the visible region till the near UV region. It starts to absorb around 350 nm wavelength range with a sharp slope till 200 nm wavelength. This denotes that BCN film is a good

absorber only towards UV region. The absorption coefficient was calculated using the equation 1.

$$\alpha = 2.303 \times \text{OD} = \frac{-2.303}{t} \log_{10}(\%T) \quad (1)$$

where, α = absorption coefficient and t = thickness of the film. The optical bandgap is calculated using the Tauc plot by fitting the data into following equation [94].

$$(\alpha \times hv)^{\frac{1}{2}} = B(hv - E_g) \quad (2)$$

Where, B = Constant factor, hv = Photon Energy, E_g = Optical band gap. Figure 4.32, shows the Tauc plot for the absorption coefficient values extracted from the Figure 4.31. The optical band gap is extracted by extrapolating linear region of the Tauc curve to x-axis. The x-intercept gives the optical band gap of the BCN film. The bandgap obtained was found to be 3.2 eV (~380 nm).

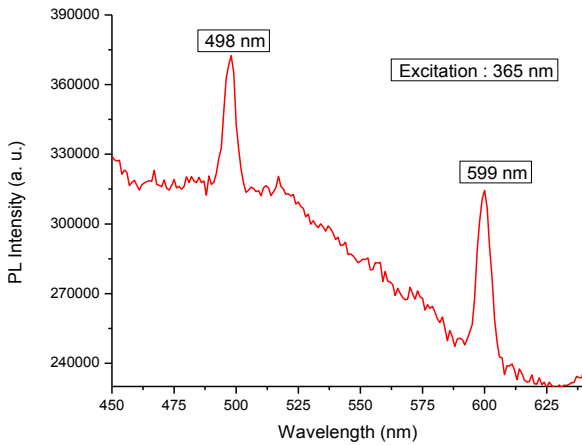


Figure 4.33. PL spectra of BCN thin films deposited at gas flow ratio of $N_2/Ar = 1$ and at 200°C deposition temperature

Two strong photoluminescence peaks are identified at 498 nm (2.49 eV) and 599 nm (2.07 eV) respectively for an excitation of 365 nm. The peak at 498 nm belongs to blue-green spectrum and 599 nm belongs to orange-red spectrum. Similar peak can be found for BCN related compounds

like SiCBN thin film, which shows a blue spectrum at 465 nm (2.67 eV) [120]. Watanabe et.al reported a strong photoluminescence spectra at 2.06 eV (600 nm) corresponds to BC2N p-type semiconductor [107]. Jian et.al reported PL phenomenon of BCN fibers in both strong UV and visible light luminescence at 370nm and 700nm for an excitation of 310 nm (4.0 eV) [108]. PL peaks obtained in this study are narrow and distinct, which signifies that BCN deposited by sputtering has less impurities or defects. Therefore less non-radiative recombination occurs, which further leads to desirable PL properties. The BCN film in this study was amorphous in nature and from literatures it is observed that BCN in fiber and nanotubes form will have an added advantage of quantum confinement effect, which increases the PL peak energies by a great factor. We can possibly deduce that BCN films synthesized with variable elemental composition is a good candidate for a wide range of PL and photo detection capabilities.

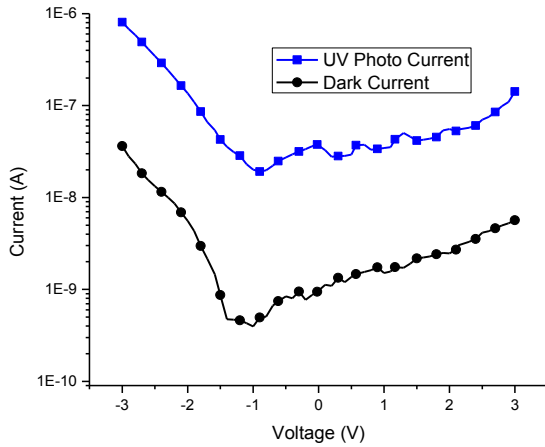


Figure 4.34: IV characteristics of Al-BCN-Au MIM devices showing dark and UV photocurrent

Figure 4.34 shows the dark and UV photo current at room temperature for Au-BCN-Al photodetector measured as a function of bias voltage in the range of -3V to 3V. A UV photo

response of two orders of magnitude higher with respect to dark current response is achieved. Nesladek et.al reported similar photo responses for BCN films by measuring the photocurrent [121]. When illuminated under the UV source with increasing device voltage, the photocurrent increases. This is because with increasing voltage, the electric field between the electrodes increases gradually, as a result the carrier drift rate rises, which shortens the transit time, therefore the probability of carrier recombination decreases and the photocurrent increases [122]. The photo responsivity (R) of the detector is given by [123].

$$R = \frac{I_p}{P_{in}} = \frac{\eta q}{hf} \approx \frac{\eta \lambda (\mu m)}{1.24} A/W$$

Where I_p is photocurrent, P_{in} is power due to light irradiation, η is quantum efficiency of the detector, q is electric charge, h is Planck's constant, f and λ are frequency and wavelength of the optical signal respectively. Under 365nm illumination and 3V applied bias, the maximum photo responsivity of the device was found to be 6 mA/W. The dark current for the Al-BCN diode was found to be about two orders higher in magnitude as compared to the BCN-Au diode. Its corresponding UV responsivity also reduced from 6 mA/W to 70.8 μ A/W since Au has a higher work function (5.1 eV) as compared to Al (4.28 eV) [124, 125].

CONCLUSION

BCN thin films were deposited successfully by RF magnetron sputtering from B₄C target in argon and nitrogen gas ambient. BCN thin films were deposited successfully by dual magnetron DC and RF sputtering from B₄C /BN and C/BN targets in an N₂/Ar ambient. Variations in BCN chemical composition and chemical bonding produced by sputtering with different N₂/Ar ratios and DC/RF bias were investigated using XPS and FTIR and correlated to other physical, dielectric and mechanical properties such as mass density, dielectric constant, Young's modulus and hardness. Depending on the specific targets utilized, sputtering in pure Ar was observed to produce either carbon rich (C/BN targets) or boron rich (B₄C /BN targets) BCN films with mass densities of 2.4–2.5 g/cm³ that approached the theoretical mass density for B₄C (2.5 g/cm³). In nano-indentation Measurements, these same films exhibited high values of Young's modulus and hardness of ~285 GPa and 30–40 GPa, respectively. The addition of N₂ to the Ar working gas lead to the incorporation of significantly more N (20–45%) and the formation of predominantly sp²/h-BCN structured films. The higher nitrogen content films exhibited reduced mass densities (2.0–2.1 g/cm³), low dielectric constants (3.9–4.6) and reduced values of Young's modulus (100–150 GPa) and hardness (6–13 GPa). Based on additional experiments varying the DC and RF biases, it was concluded that ~ 20% nitrogen is a possible threshold for achieving BCN films with either high mechanical properties or electrically insulating properties with a low dielectric constant. The deposition rate tends to show an increasing trend with an increase in RF power to BN target while keeping DC power to the BC target constant but maintains a constant trend with an increase in DC power to BC target keeping RF power to BN target constant. The BCN films deposited at various

substrate deposition temperatures show a decreasing trend and tends to increase at 400 °C. The deposition rate of BCN films deposited at various N₂/Ar gas flow ratios and 20 W DC power tends to show a decreasing trend for N₂/Ar gas ratio of 0.25 to 0.75 but shows an increasing trend towards the end. For the BCN films deposited at 40W DC, no clear trend is observed. XPS analyses reveal a distinct BCN phase formation for the BCN films deposited at both 20 W and 40 W B₄C and various N₂/Ar gas flow ratios and temperatures. From N1s peak it can be deduced that BCN films deposited at 20 W DC power have a constant BN peak with an increase in N₂/Ar gas flow ratio whereas in BCN films deposited at 40WDC, N1s peak shift towards higher binding energy, indicating a higher concentration in carbon. Higher concentration of sp²-NC bonds can be seen. In the case of C1s peak, the BCN films deposited at 20 W DC power; it shows an overall decreasing trend for B–C peak but remains fairly constant for BCN films deposited at 40 W DC power. The broadening of C–N peak is found towards the higher N₂/Ar gas flow ratio deposited films and becomes prominent at N₂/Ar gas flow ratio = 1 for films deposited at 20 W DC power whereas the C–N peak slightly shifts towards lower energy for higher gas flow ratio hinting lower concentration of C. B1s narrow spectra provide a good understanding on BCN characteristics. A clear BCN peak formation can be observed in the BCN films deposited all the parameters. The BCN peak is observed to show an increasing trend for 20W DC deposition while the BN peak remains fairly constant. For the films deposited at 40 W DC power, the BCN peak broadens with an increase in N₂/Ar gas flow ratio being a prominent peak at N₂/Ar gas ratio of 1. Clearer BCN peaks can be observed for films deposited at 40 W as compared with films deposited at 20W. Optical characteristics are moderately dependent on the N₂/Ar gas flow ratio and various other parameters like deposition temperatures and target power. The transmission increases with

increase in N_2/Ar gas flow ratio from 0.25 to 0.75 with $N_2/Ar = 1$ showing least transmission. The optical band gap increases with increase in N_2/Ar gas flow ratios for all the temperature ranges but a decreasing trend at $N_2/Ar = 1$ for 200 and 400 °C is observed. The BCN films deposited at 200 °C showed the highest band gap range and the films deposited at room temperature showed least optical band gap range. The films deposited at 20W DC resulted in higher band gap values than 40W DC target power. The highest band gap achieved is 3.7 eV for BCN films deposited at $N_2/Ar = 0.75$ and lowest band gap achieved is 1.9 eV for BCN film which is as-deposited at $N_2/Ar = 0.25$. The increase in optical band gap can be attributed to the increase in nitrogen concentration. BCN being a low-k material with a high density can be a potential inter-dielectric layer with copper interconnects. This work shows that even annealing the film in the range of 200–400°C has minimal copper diffusion effects in the BCN films. The films deposited at higher N_2/Ar ratio yielded higher boron concentration. The films with higher boron concentration showed marginal increase in copper diffusion compared to lower concentration films. A common aluminum etchant was used to etch these samples at different temperature conditions and their subsequent activation energies (E_a) and pre-exponential factors (R_o) were calculated using Arrhenius plots. Room temperature deposited BCN film at $N_2/Ar = 0.25$ was found to have the highest etch rate of 231.6 Å/min. Boron rich films with significant amount of carbon showed B_4C like characteristics, hence the overall etch rate decreased drastically and they became more temperature dependent reactions yielding very high values of R_o and E_a . BCN films deposited at 200°C showed the highest temperature dependent reaction among others, and they have a high E_a (~0.9 eV) and R_o (1016 Å/min). Films deposited at 300°C showed the lowest etch rate in the range of (~11–13 Å/min). BCN has a wide range of reaction kinetics with respect to different elemental compositions due to

the various deposition parameters involved. This work accounts for workability of common aluminum etchant as an economic, effective reagent for BCN etching and cleaning in a fabrication process. BCN MIM structure as a potential UV photo detector for harsh environment applications was studied. The optoelectronic performance of the BCN MIM device was examined through UV photocurrent measurements. A good UV photocurrent response of two orders of magnitude higher with respect to dark current was achieved for the MIM detector using an LED UV source. The maximum photo responsivity of this photodetector was found to be 6 mA/W. A systematic PL study of RF sputtered BCN thin was performed. Two sharp PL peaks were observed in the visible region. The films deposited at 400°C showed the highest PL peak intensity. This was attributed to the larger crystallites and high surface-to-volumes ratio with less defects in the 400°C deposited films. For the first time, NTQ was observed in the BCN thin films deposited at all the substrate deposition temperatures. This may be due to the introduction of intermediate states or unintentional donors during low temperature measurements and whose energy difference between the initial and middle states was comparable to temperature of the system. Thermal excitation of electrons was deemed negligible in this case, resulting in NTQ property.

FUTURE WORK

Hydrogen doping studies on dielectric properties of BCN thin films is a good prospective investigation to begin with. Various groups have shown decrease in the dielectric constants of many low-k materials with very minimal effects on the material's surface, electrical, mechanical and optical properties. It will be interesting and highly significant for the industrial point of view to reach the absolute low-k dielectric limit of a dense, hard, wideband gap material like BCN. Numerous surface characterization techniques are required to be performed on hydrogen doped BCN to assess its capability as a versatile low-k dielectric material. This could prove economical in the many places such as optics, hard coating industry, aerospace by large and fabrication industry in particular, as it can fit into different scheme of things. It could be a one stop solution to various problems such as RC time delay and undesired power dissipation in ULSI circuits.

LIST OF REFERENCES

- [1] S.P. Muraka, M. Eizenberg, A.K. Sinha, Interlayer dielectrics for semiconductor technologies, Academic Press 2003.
- [2] B. Zhao, M. Brongo, Integration of Low Dielectric Constant Materials in Advanced Aluminum and Copper Interconnects, MRS Proceedings, Cambridge Univ Press, 1999, pp. 485.
- [3] R.H. Fowler, L. Nordheim, Electron emission in intense electric fields, Proceedings of the Royal Society of London A: Mathematical, Physical and Engineering Sciences, The Royal Society, 1928, pp. 173-181.
- [4] X. Wu, S. Soss, E. Rymaszewski, T.-M. Lu, Dielectric constant dependence of Poole-Frenkel potential in tantalum oxide thin films, Materials chemistry and physics, 38 (1994) 297-300.
- [5] R. Prioli, D. Reigada, F. Freire Jr, The role of capillary condensation of water in the nanoscale friction and wear properties of boron carbide films, Journal of Applied Physics, 88 (2000) 679-682.
- [6] M. Kawaguchi, B/C/N materials based on the graphite network, Advanced Materials, 9 (1997) 615-625.
- [7] S. Umeda, T. Yuki, T. Sugiyama, T. Sugino, Boron carbon nitride film with low dielectric constant as passivation film for high speed electronic devices, Diamond and related materials, 13 (2004) 1135-1138.
- [8] W. Pan, J. Sun, H. Ling, N. Xu, Z. Ying, J. Wu, Preparation of thin films of carbon-based compounds, Applied surface science, 218 (2003) 298-305.
- [9] O. Conde, A. Silvestre, J. Oliveira, Influence of carbon content on the crystallographic structure of boron carbide films, Surface and Coatings Technology, 125 (2000) 141-146.

- [10] V. Domnich, S. Reynaud, R.A. Haber, M. Chhowalla, Boron carbide: structure, properties, and stability under stress, *Journal of the American Ceramic Society*, 94 (2011) 3605-3628.
- [11] H.O. Pierson, *Handbook of Refractory Carbides & Nitrides: Properties, Characteristics, Processing and Apps*, William Andrew 1996.
- [12] A.A. Ahmad, N.J. Ianno, S.-D. Hwang, P.A. Dowben, Sputter deposition of high resistivity boron carbide, *Thin Solid Films*, 335 (1998) 174-177.
- [13] S. Lee, J. Mazurowski, G. Ramseyer, P.A. Dowben, Characterization of boron carbide thin films fabricated by plasma enhanced chemical vapor deposition from boranes, *Journal of applied physics*, 72 (1992) 4925-4933.
- [14] F. Thevenot, Boron carbide—a comprehensive review, *Journal of the European Ceramic society*, 6 (1990) 205-225.
- [15] O. Mishima, J. Tanaka, S. Yamaoka, O. Fukunaga, High-temperature cubic boron nitride pn junction diode made at high pressure, *Science*, 238 (1987) 181-183.
- [16] R.F. Davis, III-V nitrides for electronic and optoelectronic applications, *Proceedings of the IEEE*, 79 (1991) 702-712.
- [17] A.O. Sezer, J. Brand, Chemical vapor deposition of boron carbide, *Materials Science and Engineering: B*, 79 (2001) 191-202.
- [18] M. Watanabe, S. Itoh, K. Mizushima, T. Sasaki, Electrical properties of BC₂N thin films prepared by chemical vapor deposition, *Journal of applied physics*, 78 (1995) 2880-2882.
- [19] J. Yue, W. Cheng, X. Zhang, D. He, G. Chen, Ternary BCN thin films deposited by reactive sputtering, *Thin Solid Films*, 375 (2000) 247-250.
- [20] L. Liu, Y. Wang, K. Feng, Y. Li, W. Li, C. Zhao, Y. Zhao, Preparation of boron carbon

nitride thin films by radio frequency magnetron sputtering, *Applied surface science*, 252 (2006) 4185-4189.

[21] E. Martí, A. Lousa, J. Esteve, Micromechanical and microtribological properties of BCN thin films near the B 4 C composition deposited by rf magnetron sputtering, *Diamond and related materials*, 10 (2001) 1892-1896.

[22] A.Y. Liu, M.L. Cohen, Prediction of new low compressibility solids, *Science*, 245 (1989) 841-842.

[23] J. Kouvetakis, M. Todd, B. Wilkens, A. Bandari, N. Cave, Novel synthetic routes to carbon-nitrogen thin films, *Chemistry of materials*, 6 (1994) 811-814.

[24] N. Nakayama, Y. Tsuchiya, S. Tamada, K. Kosuge, S. Nagata, K. Takahiro, S. Yamaguchi, Structural properties of amorphous carbon nitride films prepared by reactive RF-magnetron sputtering, *Japanese journal of applied physics*, 32 (1993) L1465.

[25] B.C. Daly, S.T. Bailey, R. Sooryakumar, S.W. King, Noncontact optical metrologies for Young's modulus measurements of nanoporous low-k dielectric thin films, *Journal of Nanophotonics*, 7 (2013) 073094-073094.

[26] Y. Lin, Y. Xiang, T.Y. Tsui, J.J. Vlassak, PECVD low-permittivity organosilicate glass coatings: Adhesion, fracture and mechanical properties, *Acta Materialia*, 56 (2008) 4932-4943.

[27] P.R. Griffiths, J.A. De Haseth, *Fourier transform infrared spectrometry*, John Wiley & Sons 2007.

[28] Y. Matsuda, S.W. King, R.H. Dauskardt, Tailored amorphous silicon carbide barrier dielectrics by nitrogen and oxygen doping, *Thin Solid Films*, 531 (2013) 552-558.

[29] S.W. King, M. French, G. Xu, B. French, M. Jaehnig, J. Bielefeld, J. Brockman, M. Kuhn,

Valence band offset and Schottky barrier at amorphous boron and boron carbide interfaces with silicon and copper, *Applied Surface Science*, 285 (2013) 545-551.

[30] S.W. King, Plasma enhanced atomic layer deposition of SiNx: H and SiO₂, *Journal of Vacuum Science & Technology A*, 29 (2011) 041501.

[31] H. Aoki, M. Hara, T. Masuzumi, F. Ahmed, C. Kimura, T. Sugino, Dry etching properties of methyl-BCN film with C₄F₈ gas for Cu/low-K interconnection, *Diamond and Related Materials*, 19 (2010) 507-509.

[32] S. Grenadier, J. Li, J. Lin, H. Jiang, Dry etching techniques for active devices based on hexagonal boron nitride epilayers, *Journal of Vacuum Science & Technology A*, 31 (2013) 061517.

[33] S. Nguyen, T. Nguyen, H. Treichel, O. Spindler, Plasma-Assisted Chemical Vapor Deposition and Characterization of Boron Nitride Films, *Journal of The Electrochemical Society*, 141 (1994) 1633-1638.

[34] E.D. Haberer, C.-H. Chen, A. Abare, M. Hansen, S. Denbaars, L. Coldren, U. Mishra, E.L. Hu, Channeling as a mechanism for dry etch damage in GaN, *Applied Physics Letters*, 76 (2000) 3941-3943.

[35] R. Dimitrov, V. Tilak, W. Yeo, B. Green, H. Kim, J. Smart, E. Chumbes, J. Shealy, W. Schaff, L. Eastman, Influence of oxygen and methane plasma on the electrical properties of undoped AlGaIn/GaN heterostructures for high power transistors, *Solid-State Electronics*, 44 (2000) 1361-1365.

[36] D. Watanabe, H. Aoki, R. Moriyama, M. Mazumder, C. Kimura, T. Sugino, Characterization of BCN film after wet process for interconnection integration, *Diamond and Related Materials*,

17 (2008) 669-672.

[37] P. Van Zant, Chapman, Microchip fabrication: a practical guide to semiconductor processing, McGraw-Hill New York 2000.

[38] W.M. Haynes, CRC handbook of chemistry and physics, CRC press 2014.

[39] I. Caretti, I. Jimenez, J. Albella, BCN films with controlled composition obtained by the interaction between molecular beams of B and C with nitrogen ion beams, Diamond and related materials, 12 (2003) 1079-1083.

[40] H.c. Tsai, D. Bogy, Characterization of diamondlike carbon films and their application as overcoats on thin-film media for magnetic recording, Journal of Vacuum Science & Technology A, 5 (1987) 3287-3312.

[41] M. Gamero-Castaño, M. Mahadevan, Sputtering yields of Si, SiC, and B₄C under nanodroplet bombardment at normal incidence, Journal of Applied Physics, 106 (2009) 054305.

[42] A. Prakash, K.B. Sundaram, Studies on Electrical Properties of RF Sputtered Deposited Boron Carbon Nitride Thin Films, ECS Journal of Solid State Science and Technology, 4 (2015) N25-N29.

[43] R. Trehan, Y. Lifshitz, J. Rabalais, Auger and x-ray electron spectroscopy studies of hBN, cBN, and N⁺ 2 ion irradiation of boron and boron nitride, Journal of Vacuum Science & Technology A, 8 (1990) 4026-4032.

[44] T. Ichiki, T. Momose, T. Yoshida, Effects of the substrate bias on the formation of cubic boron nitride by inductively coupled plasma enhanced chemical vapor deposition, Journal of applied physics, 75 (1994) 1330-1334.

[45] H. Sjöström, W. Lanford, B. Hjörvarson, K. Xing, J. Sundgren, Growth of CN_x H_y films

by reactive magnetron sputtering of carbon in Ar/NH₃ discharges, *Journal of materials research*, 11 (1996) 981-988.

[46] Y. Aoi, K. Ono, E. Kamijo, Preparation of amorphous CN_x thin films by pulsed laser deposition using a radio frequency radical beam source, *Journal of applied physics*, 86 (1999) 2318-2322.

[47] M.A. Mannan, M. Nagano, K. Shigezumi, T. Kida, N. Hirao, Y. Baba, Characterization of boron carbonitride (BCN) thin films deposited by radiofrequency and microwave plasma enhanced chemical vapor deposition, *Am. J. Appl. Sci*, 5 (2007) 736-741.

[48] V. Linss, S. Rodil, P. Reinke, M. Garnier, P. Oelhafen, U. Kreissig, F. Richter, Bonding characteristics of DC magnetron sputtered B–C–N thin films investigated by Fourier-transformed infrared spectroscopy and X-ray photoelectron spectroscopy, *Thin Solid Films*, 467 (2004) 76-87.

[49] T.L. Barr, S. Seal, Nature of the use of adventitious carbon as a binding energy standard, *Journal of Vacuum Science & Technology A*, 13 (1995) 1239-1246.

[50] Q. Yang, C. Wang, S. Zhang, D. Zhang, Q. Shen, L. Zhang, Effect of nitrogen pressure on structure and optical properties of pulsed laser deposited BCN thin films, *Surface and Coatings Technology*, 204 (2010) 1863-1867.

[51] T. Hasegawa, K. Yamamoto, Y. Kakudate, Influence of raw gases on B–C–N films prepared by electron beam excited plasma CVD, *Diamond and related materials*, 12 (2003) 1045-1048.

[52] Z. Zhou, I. Bello, M. Lei, K. Li, C. Lee, S. Lee, Synthesis and characterization of boron carbon nitride films by radio frequency magnetron sputtering, *Surface and Coatings Technology*, 128 (2000) 334-340.

- [53] S. Chien, S. Chattopadhyay, L. Chen, S. Lin, K. Chen, Mechanical properties of amorphous boron carbon nitride films produced by dual gun sputtering, *Diamond and Related materials*, 12 (2003) 1463-1471.
- [54] M. Watanabe, S. Itoh, K. Mizushima, T. Sasaki, Bonding characterization of BC₂N thin films, *Applied physics letters*, 68 (1996) 2962-2964.
- [55] M.N. Uddin, I. Shimoyama, Y. Baba, T. Sekiguchi, M. Nagano, X-ray photoelectron spectroscopic observation on B–C–N hybrids synthesized by ion beam deposition of borazine, *Journal of Vacuum Science & Technology A*, 23 (2005) 497-502.
- [56] A. Perrone, A. Caricato, A. Luches, M. Dinescu, C. Ghica, V. Sandu, A. Andrei, Boron carbonitride films deposited by pulsed laser ablation, *Applied surface science*, 133 (1998) 239-242.
- [57] M. Dinescu, A. Perrone, A. Caricato, L. Mirengi, C. Gerardi, C. Ghica, L. Frunza, Boron carbon nitride films deposited by sequential pulses laser deposition, *Applied surface science*, 127 (1998) 692-696.
- [58] C. Guimon, D. Gonbeau, G. Pfister-Guillouzo, O. Dugne, A. Guette, R. Naslain, M. Lahaye, XPS study of BN thin films deposited by CVD on SiC plane substrates, *Surface and Interface Analysis*, 16 (1990) 440-445.
- [59] L. Jacobsohn, R. Schulze, M.M. da Costa, M. Nastasi, X-ray photoelectron spectroscopy investigation of boron carbide films deposited by sputtering, *Surface Science*, 572 (2004) 418-424.
- [60] S. Ray, H. Tsai, C. Bao, J. Chiou, J. Jan, K.K. Kumar, W. Pong, M. Tsai, S. Chattopadhyay, L. Chen, Electronic and bonding structures of BCN thin films investigated by x-ray absorption

and photoemission spectroscopy, *Journal of applied physics*, 96 (2004) 208-211.

[61] S. Ulrich, H. Ehrhardt, T. Theel, J. Schwan, S. Westermeyr, M. Scheib, P. Becker, H. Oechsner, G. Dollinger, A. Bergmaier, Phase separation in magnetron sputtered superhard BCN thin films, *Diamond and related materials*, 7 (1998) 839-844.

[62] Y. Yap, Y. Wada, M. Yamaoka, M. Yoshimura, Y. Mori, T. Sasaki, Bond modification of BCN films on Ni substrate, *Diamond and related materials*, 10 (2001) 1137-1141.

[63] M. Lei, Q. Li, Z. Zhou, I. Bello, C. Lee, S. Lee, Characterization and optical investigation of BCN film deposited by RF magnetron sputtering, *Thin Solid Films*, 389 (2001) 194-199.

[64] D. Zhuang, J. Edgar, Wet etching of GaN, AlN, and SiC: a review, *Materials Science and Engineering: R: Reports*, 48 (2005) 1-46.

[65] C. Kim, B.K. Sohn, K. Shono, Chemical Vapor-Deposited Boron Nitride Film on Silicon as a Boron Diffusion Source, *Journal of The Electrochemical Society*, 131 (1984) 1384-1388.

[66] N. Ditrick, M. Bae, AN IMPROVED BORON-NITRIDE GLASS TRANSFER PROCESS, *Solid state technology*, 23 (1980) 69-73.

[67] P. Walker, W.H. Tarn, *CRC handbook of metal etchants*, CRC press 1990.

[68] M.A. Mannan, M. Nagano, K. Shigezumi, T. Kida, N. Hirao, Y. Baba, Characterization of boron carbonitride (BCN) thin films deposited by radiofrequency and microwave plasma enhanced chemical vapor deposition, *American Journal of Applied Sciences*, 5 (2008) 736-741.

[69] M.A. Mannan, H. Noguchi, T. Kida, M. Nagano, N. Hirao, Y. Baba, Chemical bonding states and local structures of the oriented hexagonal BCN films synthesized by microwave plasma CVD, *Materials Science in Semiconductor Processing*, 11 (2008) 100-105.

[70] K.A. Connors, *Chemical kinetics: the study of reaction rates in solution*, John Wiley &

Sons1990.

[71] V. Linss, I. Hermann, N. Schwarzer, U. Kreissig, F. Richter, Mechanical properties of thin films in the ternary triangle B–C–N, *Surface and Coatings Technology*, 163 (2003) 220-226.

[72] A. Guinier, G. Fournet, C. Walker, G.H. Vineyard, *Small-Angle Scattering of X-Rays*, *Physics Today*, 9 (2009) 38-39.

[73] K.R. Williams, R.S. Muller, Etch rates for micromachining processing, *Microelectromechanical Systems, Journal of*, 5 (1996) 256-269.

[74] D. Van Dorp, J. Weyher, J. Kelly, Anodic etching of SiC in alkaline solutions, *Journal of micromechanics and microengineering*, 17 (2007) S50.

[75] A. Prakash, K.B. Sundaram, Deposition and XPS studies of dual sputtered BCN thin films, *Diamond and Related Materials*, DOI (2016).

[76] K. Sundaram, A. Grogan Jr, S. Seshan, Auger electron spectroscopy and secondary-ion mass spectroscopy study of interdiffusion in gold-bismuth oxide and aluminium-bismuth oxide thin films, *Journal of Materials Science: Materials in Electronics*, 3 (1992) 257-262.

[77] M. Motoyoshi, Through-silicon via (TSV), *Proceedings of the IEEE*, 97 (2009) 43-48.

[78] A.A. Istratov, E.R. Weber, Physics of copper in silicon, *Journal of The Electrochemical Society*, 149 (2002) G21-G30.

[79] G. Zoth, W. Bergholz, A fast, preparation-free method to detect iron in silicon, *Journal of Applied Physics*, 67 (1990) 6764-6771.

[80] R. Hall, J.H. Racette, Diffusion and solubility of copper in extrinsic and intrinsic germanium, silicon, and gallium arsenide, *Journal of Applied Physics*, 35 (1964) 379-397.

[81] S. Estreicher, Rich chemistry of copper in crystalline silicon, *Physical Review B*, 60 (1999)

5375.

[82] R. Keller, M. Deicher, W. Pfeiffer, H. Skudlik, D. Steiner, T. Wichert, Copper in silicon, *Physical review letters*, 65 (1990) 2023.

[83] J. Harper, A. Charai, L. Stolt, F. d'Heurle, P. Fryer, Room-temperature oxidation of silicon catalyzed by Cu₃Si, *Applied physics letters*, 56 (1990) 2519-2521.

[84] L. Stolt, A. Charai, F. d'Heurle, P. Fryer, J. Harper, Formation of Cu₃Si and its catalytic effect on silicon oxidation at room temperature, *Journal of Vacuum Science & Technology A*, 9 (1991) 1501-1505.

[85] Y. Li, J. Hunter, T.J. Tate, SIMS study of Cu trapping and migration in low-k dielectric films, *Applied surface science*, 231 (2004) 791-795.

[86] M.A. Mannan, M. Nagano, T. Kida, N. Hirao, Y. Baba, Characterization of BCN films synthesized by radiofrequency plasma enhanced chemical vapor deposition, *Journal of Physics and Chemistry of Solids*, 70 (2009) 20-25.

[87] C. Zhang, X. Zhong, J. Wang, G. Yang, Room-temperature growth of cubic nitride boron film by RF plasma enhanced pulsed laser deposition, *Chemical physics letters*, 370 (2003) 522-527.

[88] F. Zhou, K. Adachi, K. Kato, Influence of deposition parameters on surface roughness and mechanical properties of boron carbon nitride coatings synthesized by ion beam assisted deposition, *Thin Solid Films*, 497 (2006) 210-217.

[89] T. Scharf, R. Ott, D. Yang, J. Barnard, Structural and tribological characterization of protective amorphous diamond-like carbon and amorphous CN_x overcoats for next generation hard disks, *Journal of Applied Physics*, 85 (1999) 3142-3154.

- [90] E. D'anna, M. De Giorgi, A. Luches, M. Martino, A. Perrone, A. Zocco, Study of C \square N binding states in carbon nitride films deposited by reactive XeCl laser ablation, *Thin Solid Films*, 347 (1999) 72-77.
- [91] P. Petrov, D. Dimitrov, D. Papadimitriou, G. Beshkov, V. Krastev, C. Georgiev, Raman and X-ray photoelectron spectroscopy study of carbon nitride thin films, *Applied surface science*, 151 (1999) 233-238.
- [92] V.O. Todi, B.P. Shantheyanda, K.B. Sundaram, Influence of annealing on the optical properties of reactively sputtered BCN thin films, *Materials Chemistry and Physics*, 141 (2013) 596-601.
- [93] I.F. Husein, Y. Zhou, F. Li, R.C. Allen, C. Chan, J.I. Kleiman, Y. Gudimenko, C.V. Cooper, Synthesis of carbon nitride thin films by vacuum arcs, *Materials Science and Engineering: A*, 209 (1996) 10-15.
- [94] J. Tauc, R. Grigorovici, A. Vancu, Optical properties and electronic structure of amorphous germanium, *physica status solidi (b)*, 15 (1966) 627-637.
- [95] A. Vijayakumar, R.M. Todi, A.P. Warren, K.B. Sundaram, Influence of N₂/Ar gas mixture ratio and annealing on optical properties of SiCBN thin films prepared by rf sputtering, *Diamond and Related Materials*, 17 (2008) 944-948.
- [96] T. Yuki, S. Umeda, T. Sugino, Electrical and optical characteristics of boron carbon nitride films synthesized by plasma-assisted chemical vapor deposition, *Diamond and related materials*, 13 (2004) 1130-1134.
- [97] V.O. Todi, B.P. Shantheyanda, R.M. Todi, K.B. Sundaram, K. Coffey, Optical characterization of BCN films deposited at various N₂/Ar gas flow ratios by RF magnetron

sputtering, *Materials Science and Engineering: B*, 176 (2011) 878-882.

[98] S. Bernard, P. Miele, Polymer-derived boron nitride: a review on the chemistry, shaping and ceramic conversion of borazine derivatives, *Materials*, 7 (2014) 7436-7459.

[99] S. Yuan, B. Toury, C. Journet, A. Brioude, Synthesis of hexagonal boron nitride graphene-like few layers, *Nanoscale*, 6 (2014) 7838-7841.

[100] M. Nieminen, T. Sajavaara, E. Rauhala, M. Putkonen, L. Niinistö, Surface-controlled growth of LaAlO₃ thin films by atomic layer epitaxy, *Journal of Materials Chemistry*, 11 (2001) 2340-2345.

[101] M. Nieminen, S. Lehto, L. Niinistö, Atomic layer epitaxy growth of LaGaO₃ thin films, *Journal of Materials Chemistry*, 11 (2001) 3148-3153.

[102] E. Knittle, R. Kaner, R. Jeanloz, M. Cohen, High-pressure synthesis, characterization, and equation of state of cubic C-BN solid solutions, *Physical Review B*, 51 (1995) 12149.

[103] Y. Wada, Y. Yap, M. Yoshimura, Y. Mori, T. Sasaki, The control of B-N and B-C bonds in BCN films synthesized using pulsed laser deposition, *Diamond and Related Materials*, 9 (2000) 620-624.

[104] A. Lousa, J. Esteve, S. Muhl, E. Martí, BCN thin films near the B₄C composition deposited by radio frequency magnetron sputtering, *Diamond and Related Materials*, 9 (2000) 502-505.

[105] A. Tempez, N. Badi, A. Bensaoula, J. Kulik, Surface composition of BN, CN, and BCN thin films, *Journal of Vacuum Science & Technology A*, 16 (1998) 2896-2900.

[106] G. Viera, J. Andujar, S. Sharma, E. Bertran, Si-C-N nanometric powder produced in square-wave modulated RF glow discharges, *Diamond and related materials*, 7 (1998) 407-411.

[107] M. Watanabe, S. Itoh, T. Sasaki, K. Mizushima, Visible-Light-Emitting Layered B₂C₂N₂

Semiconductor, Physical review letters, 77 (1996) 187.

[108] Y. Jian, Q. Tai, S. Chun-Ying, New BCN fibres for strong ultraviolet and visible light luminescence, Chinese Physics Letters, 23 (2006) 2573.

[109] Z. Cao, L. Liu, H. Oechsner, Plasma assisted deposition of nanocrystalline BCN thin films and property characterization, Journal of Vacuum Science & Technology B, 20 (2002) 2275-2280.

[110] L.H. Li, Y. Chen, B.-M. Cheng, M.-Y. Lin, S.-L. Chou, Y.-C. Peng, Photoluminescence of boron nitride nanosheets exfoliated by ball milling, Applied Physics Letters, 100 (2012) 261108.

[111] K. Watanabe, T. Taniguchi, Jahn-Teller effect on exciton states in hexagonal boron nitride single crystal, Physical Review B, 79 (2009) 193104.

[112] N. Salivati, N. Shuall, J.M. McCrate, J.G. Ekerdt, Effect of subsurface boron on photoluminescence from silicon nanocrystals, Surface Science, 605 (2011) 799-801.

[113] A. Mimura, M. Fujii, S. Hayashi, K. Yamamoto, Quenching of photoluminescence from Si nanocrystals caused by boron doping, Solid state communications, 109 (1999) 561-565.

[114] M. Fujii, S. Hayashi, K. Yamamoto, Photoluminescence from B-doped Si nanocrystals, Journal of Applied Physics, 83 (1998) 7953-7957.

[115] H. Shibata, Negative thermal quenching curves in photoluminescence of solids, Japanese journal of applied physics, 37 (1998) 550.

[116] H. He, Z. Ye, S. Lin, B. Zhao, J. Huang, H. Tang, Negative thermal quenching behavior and long luminescence lifetime of surface-state related green emission in ZnO nanorods, The Journal of Physical Chemistry C, 112 (2008) 14262-14265.

[117] Y. Wu, J. Li, H. Ding, Z. Gao, Y. Wu, N. Pan, X. Wang, Negative thermal quenching of

photoluminescence in annealed ZnO–Al₂O₃ core–shell nanorods, *Physical Chemistry Chemical Physics*, 17 (2015) 5360-5365.

[118] X. Bai, E. Wang, J. Yu, H. Yang, Blue–violet photoluminescence from large-scale highly aligned boron carbonitride nanofibers, *Applied Physics Letters*, 77 (2000) 67-69.

[119] J. Yu, E. Wang, J. Ahn, S. Yoon, Q. Zhang, J. Cui, M. Yu, Turbostratic boron carbonitride films produced by bias-assisted hot filament chemical vapor deposition, *Journal of Applied Physics*, 87 (2000) 4022-4025.

[120] A. Vijayakumar, K. Sundaram, R. Todi, Amorphous-SiCBN-based metal–semiconductor–metal photodetector for high-temperature applications, *Electron Device Letters, IEEE*, 28 (2007) 713-715.

[121] M. Nesládek, M. Vaněček, K. Meykens, K. Haenen, J. Manca, L. De Schepper, E. Pace, A. Pini, G. Verona Rinati, C. Kimura, Study of UV and subgap photocurrent response in diamond and BCN thin films for detector applications, *Physica status solidi (a)*, 185 (2001) 107-113.

[122] C. Yiren, S. Hang, L. Dabing, S. Xiaojuan, L. Zhiming, J. Hong, M. Guoqing, GaN-based MSM photovoltaic ultraviolet detector structure modeling and its simulation, *Journal of Semiconductors*, 32 (2011) 034005.

[123] K.W. Busch, M.A. Busch, *Multielement detection systems for spectrochemical analysis*, John Wiley & Sons 1990.

[124] M. Green, *Solid state surface science*, M. Dekker 1969.

[125] J. Hölzl, F. Schulte, *Work function of metals*, *Solid Surface Physics*, Springer 1979, pp. 1-150.